Draft version 11 November 2025
Typeset using LaTeX **twocolumn** style in AASTeX631



# GW231123: a Binary Black Hole Merger with Total Mass 190-265 $M_\odot$

A. G. Abac,[1] I. Abouelfettouh,[2] F. Acernese,[3,4] K. Ackley,[5] C. Adamcewicz,[6] S. Adhicary,[7] D. Adhikari,[8,9] N. Adhikari,[10] R. X. Adhikari,[11] V. K. Adkins,[12] S. Afroz,[13] A. Agapito,[14] D. Agarwal,[15] M. Agathos,[16] N. Aggarwal,[17] S. Aggarwal,[18] O. D. Aguiar,[19] I.-L. Ahrend,[20] L. Aiello,[21,22] A. Ain,[23] P. Ajith,[24] T. Akutsu,[25,26] S. Albanesi,[27,28] W. Ali,[29,30] S. Al-Kershi,[8,9] C. Alléné,[31] A. Allocca,[32,4] S. Al-Shammari,[33] P. A. Altin,[34] S. Alvarez-Lopez,[35] W. Amar,[31] O. Amarasinghe,[33] A. Amato,[36,37] F. Amicucci,[38,39] C. Amra,[40] A. Ananyeva,[11] S. B. Anderson,[11] W. G. Anderson,[11] M. Andia,[41] M. Ando,[42] M. Andrés-Carcasona,[43] T. Andrić,[44,45,8,9] J. Anglin,[46] S. Ansoldi,[47,48] J. M. Antelis,[49] S. Antier,[41] M. Aoumi,[50] E. Z. Appavuravther,[51,52] S. Appert,[11] S. K. Apple,[53] K. Arai,[11] C. Araujo Alvarez,[54] A. Araya,[42] M. C. Araya,[11] M. Arca Sedda,[44,45] J. S. Areeda,[55] N. Aritomi,[2] F. Armato,[29,30] S. Armstrong,[56] N. Arnaud,[57] M. Arogeti,[58] S. M. Aronson,[12] K. G. Arun,[59] G. Ashton,[60] Y. Aso,[25,61] L. Asprea,[28] M. Assiduo,[62,63] S. Assis de Souza Melo,[64] S. M. Aston,[65] P. Astone,[38] F. Attadio,[39,38] F. Aubin,[66] K. AultONeal,[67] G. Avallone,[68] E. A. Avila,[49] S. Babak,[20] C. Badger,[69] S. Bae,[70] S. Bagnasco,[28] L. Baiotti,[71] R. Bajpai,[72] T. Baka,[73,37] A. M. Baker,[6] K. A. Baker,[74] T. Baker,[75] G. Baldi,[76,77] N. Baldicchi,[78,51] M. Ball,[79] G. Ballardin,[64] S. W. Ballmer,[80] S. Banagiri,[6] B. Banerjee,[44] D. Bankar,[81] T. M. Baptiste,[12] P. Baral,[10] M. Baratti,[82,83] J. C. Barayoga,[11] B. C. Barish,[11] D. Barker,[2] N. Barman,[81] P. Barneo,[84,85,86] F. Barone,[87,4] B. Barr,[88] L. Barsotti,[35] M. Barsuglia,[20] D. Barta,[89] A. M. Bartoletti,[90] M. A. Barton,[88] I. Bartos,[46] A. Basalaev,[8,9] R. Bassiri,[91] A. Basti,[83,82] M. Bawaj,[78,51] P. Baxi,[92] J. C. Bayley,[88] A. C. Baylor,[10] P. A. Baynard II,[58] M. Bazzan,[93,94] V. M. Bedakihale,[95] F. Beirnaert,[96] M. Bejger,[97] D. Belardinelli,[22] A. S. Bell,[88] D. S. Bellie,[98] L. Bellizzi,[82,83] W. Benoit,[18] I. Bentara,[57] J. D. Bentley,[99] M. Ben Yaala,[56] S. Bera,[100,101] F. Bergamin,[33] B. K. Berger,[91] S. Bernuzzi,[27] M. Beroiz,[11] C. P. L. Berry,[88] D. Bersanetti,[29] T. Bertheas,[102] A. Bertolini,[37,36] J. Betzwieser,[65] D. Beveridge,[74] G. Bevilacqua,[103] N. Bevins,[104] R. Bhandare,[105] R. Bhatt,[11] D. Bhattacharjee,[106,107] S. Bhattacharyya,[108] S. Bhaumik,[46] S. Bhagwat,[109] V. Biancalana,[103] A. Bianchi,[37,110] I. A. Bilenko,[111] G. Billingsley,[11] A. Binetti,[112] S. Bini,[11,76,77] C. Binu,[113] S. Biot,[114] O. Birnholtz,[115] S. Biscoveanu,[98] A. Bisht,[9] M. Bitossi,[64,82] M.-A. Bizouard,[116] S. Blaber,[117] J. K. Blackburn,[11] L. A. Blagg,[79] C. D. Blair,[74,65] D. G. Blair,[74] N. Bode,[8,9] N. Boettner,[99] G. Boileau,[116] M. Boldrini,[38] G. N. Bolingbroke,[118] A. Bolliand,[119,40] L. D. Bonavena,[46] R. Bondarescu,[84] F. Bondu,[120] E. Bonilla,[91] M. S. Bonilla,[55] A. Bonino,[109] R. Bonnand,[31,119] A. Borchers,[8,9] S. Borhanian,[7] V. Boschi,[82] S. Bose,[121] V. Bossilkov,[65] Y. Bothra,[37,110] A. Boudon,[57] L. Bourg,[58] M. Boyle,[122] A. Bozzi,[64] C. Bradaschia,[82] P. R. Brady,[10] A. Branch,[65] M. Branchesi,[44,45] I. Braun,[106] T. Briant,[123] A. Brillet,[116] M. Brinkmann,[8,9] P. Brockill,[10] E. Brockmueller,[8,9] A. F. Brooks,[11] B. C. Brown,[46] D. D. Brown,[118] M. L. Brozzetti,[78,51] S. Brunett,[11] G. Bruno,[15] R. Bruntz,[124] J. Bryant,[109] Y. Bu,[125] F. Bucci,[63] J. Buchanan,[124] O. Bulashenko,[84,85] T. Bulik,[126] H. J. Bulten,[37] A. Buonanno,[127,1] K. Burtnyk,[2] R. Buscicchio,[128,129] D. Buskulic,[31] C. Buy,[102] R. L. Byer,[91] G. S. Cabourn Davies,[75] R. Cabrita,[15] V. Cáceres-Barbosa,[7] L. Cadonati,[58] G. Cagnoli,[130] C. Cahillane,[80] A. Calafat,[100] J. Calderón Bustillo,[54] T. A. Callister,[131] E. Calloni,[32,4] S. R. Callos,[79] M. Canepa,[30,29] G. Caneva Santoro,[43] K. C. Cannon,[42] H. Cao,[35] L. A. Capistran,[132] E. Capocasa,[20] E. Capote,[2,11] G. Capurri,[83,82] G. Carapella,[68,133] F. Carbognani,[64] M. Carlassara,[8,9] J. B. Carlin,[125] T. K. Carlson,[134] M. F. Carney,[106] M. Carpinelli,[128,64] G. Carrillo,[79] J. J. Carter,[8,9] G. Carullo,[109,135] A. Casallas-Lagos,[136] J. Casanueva Diaz,[64] C. Casentini,[137,22] S. Y. Castro-Lucas,[138] S. Caudill,[134] M. Cavaglià,[107] R. Cavalieri,[64] A. Ceja,[55] G. Cella,[82] P. Cerdá-Durán,[139,140] E. Cesarini,[22] N. Chabbra,[34] W. Chaibi,[116] A. Chakraborty,[13] P. Chakraborty,[8,9] S. Chakraborty,[105] S. Chalathadka Subrahmanya,[99] J. C. L. Chan,[141] M. Chan,[117] K. Chandra,[7] K. Chang,[142] S. Chao,[143,142] P. Charlton,[144] E. Chassande-Mottin,[20] C. Chatterjee,[145] Debarati Chatterjee,[81] Deep Chatterjee,[35] M. Chaturvedi,[105] S. Chaty,[20] K. Chatziioannou,[11] A. Chen,[146] A. H.-Y. Chen,[147] D. Chen,[148] H. Chen,[143] H. Y. Chen,[149] S. Chen,[145] Yanbei Chen,[150] Yitian Chen,[122] H. P. Cheng,[151] P. Chessa,[78,51] H. T. Cheung,[92] S. Y. Cheung,[6] F. Chiadini,[152,133] G. Chiarini,[8,9,94] A. Chiba,[153] A. Chincarini,[29] M. L. Chiofalo,[83,82] A. Chiummo,[4,64] C. Chou,[147] S. Choudhary,[74] N. Christensen,[116,154] S. S. Y. Chua,[34] G. Ciani,[76,77] P. Ciecielag,[97] M. Cieślar,[126] M. Cifaldi,[22] B. Cirok,[155] F. Clara,[2] J. A. Clark,[11,58] T. A. Clarke,[6] P. Clearwater,[156] S. Clesse,[114] F. Cleva,[116,119] E. Coccia,[44,45,43] E. Codazzo,[157,158] P.-F. Cohadon,[123] S. Colace,[30] E. Colangeli,[75] M. Colleoni,[100] C. G. Collette,[159] J. Collins,[65] S. Colloms,[88] A. Colombo,[160,129] C. M. Compton,[2] G. Connolly,[79] L. Conti,[94] T. R. Corbitt,[12] I. Cordero-Carrión,[161] S. Corezzi,[78,51] N. J. Cornish,[162] I. Coronado,[163] A. Corsi,[164] R. Cottingham,[65] M. W. Coughlin,[18] A. Couineaux,[38] P. Couvares,[11,58] D. M. Coward,[74] R. Coyne,[165] A. Cozzumbo,[44] J. D. E. Creighton,[10] T. D. Creighton,[166] P. Cremonese,[100] S. Crook,[65] R. Crouch,[2] J. Csizmazia,[2] J. R. Cudell,[167] T. J. Cullen,[11] A. Cumming,[88] E. Cuoco,[168,169] M. Cusinato,[139] L. V. Da Conceição,[170] T. Dal Canton,[41] S. Dal Pra,[171] G. Dálya,[102] B. D'Angelo,[29] S. Danilishin,[36,37] S. D'Antonio,[38] K. Danzmann,[9,8,9] K. E. Darroch,[124] L. P. Dartez,[65] R. Das,[108] A. Dasgupta,[95] V. Dattilo,[64] A. Daumas,[20] N. Davari,[172,173] I. Dave,[105] A. Davenport,[138] M. Davier,[41] T. F. Davies,[74] D. Davis,[11] L. Davis,[74] M. C. Davis,[18] P. Davis,[174,175] E. J. Daw,[176] M. Dax,[1] J. De Bolle,[96] M. Deenadayalan,[81] J. Degallaix,[177]

M. De Laurentis,[32,4] F. De Lillo,[23] S. Della Torre,[129] W. Del Pozzo,[83,82] A. Demagny,[31] F. De Marco,[39,38] G. Demasi,[178,63] F. De Matteis,[21,22] N. Demos,[35] T. Dent,[54] A. Depasse,[15] N. DePergola,[104] R. De Pietri,[179,180] R. De Rosa,[32,4] C. De Rossi,[64] M. Desai,[35] R. DeSalvo,[181] A. DeSimone,[182] R. De Simone,[152,133] A. Dhani,[1] R. Diab,[46] M. C. Díaz,[166] M. Di Cesare,[32,4] G. Dideron,[183] T. Dietrich,[1] L. Di Fiore,[4] C. Di Fronzo,[74] M. Di Giovanni,[39,38] T. Di Girolamo,[32,4] D. Diksha,[37,36] J. Ding,[20,184] S. Di Pace,[39,38] I. Di Palma,[39,38] D. Di Piero,[185,48] F. Di Renzo,[57] Divyajyoti,[33] A. Dmitriev,[109] J. P. Docherty,[88] Z. Doctor,[98] N. Doerksen,[170] E. Dohmen,[2] A. Doke,[134] A. Domiciano De Souza,[186] L. D'Onofrio,[38] F. Donovan,[35] K. L. Dooley,[33] T. Dooney,[73] S. Doravari,[81] O. Dorosh,[187] W. J. D. Doyle,[124] M. Drago,[39,38] J. C. Driggers,[2] L. Dunn,[125] U. Dupletsa,[44] P.-A. Duverne,[20] D. D'Urso,[172,157] P. Dutta Roy,[46] H. Duval,[188] S. E. Dwyer,[2] C. Eassa,[2] M. Ebersold,[189,31] T. Eckhardt,[99] G. Eddolls,[80] A. Effler,[65] J. Eichholz,[34] H. Einsle,[116] M. Eisenmann,[25] M. Emma,[60] K. Endo,[153] R. Enficiaud,[1] L. Errico,[32,4] R. Espinosa,[166] M. Esposito,[4,32] R. C. Essick,[190] H. Estellés,[1] T. Etzel,[11] M. Evans,[35] T. Evstafyeva,[183] B. E. Ewing,[7] J. M. Ezquiaga,[141] F. Fabrizi,[62,63] V. Fafone,[21,22] S. Fairhurst,[33] A. M. Farah,[131] B. Farr,[79] W. M. Farr,[191,192] G. Favaro,[93] M. Favata,[193] M. Fays,[167] M. Fazio,[56] J. Feicht,[11] M. M. Fejer,[91] R. Felicetti,[185,48] E. Fenyvesi,[89,194] J. Fernandes,[195] T. Fernandes,[196,139] D. Fernando,[113] S. Ferraiuolo,[197,39,38] T. A. Ferreira,[12] F. Fidecaro,[83,82] P. Figura,[97] A. Fiori,[82,83] I. Fiori,[64] R. P. Fisher,[124] R. Fittipaldi,[198,133] V. Fiumara,[199,133] R. Flaminio,[31] S. M. Fleischer,[200] L. S. Fleming,[201] E. Floden,[18] H. Fong,[117] J. A. Font,[139,140] F. Fontinele-Nunes,[18] C. Foo,[1] B. Fornal,[202] K. Franceschetti,[179] N. Franchini,[203] F. Frappez,[31] S. Frasca,[39,38] F. Frasconi,[82] J. P. Freed,[67] Z. Frei,[204] A. Freise,[37,110] O. Freitas,[196,139] R. Frey,[79] W. Frischhertz,[65] P. Fritschel,[35] V. V. Frolov,[65] G. G. Fronzé,[28] M. Fuentes-Garcia,[11] S. Fujii,[205] T. Fujimori,[206] P. Fulda,[46] M. Fyffe,[65] B. Gadre,[73] J. R. Gair,[1] S. Galaudage,[186] V. Galdi,[207] R. Gamba,[7] A. Gamboa,[1] S. Gamoji,[181] D. Ganapathy,[208] A. Ganguly,[81] B. Garaventa,[29] J. García-Bellido,[209] C. García-Quirós,[189] J. W. Gardner,[34] K. A. Gardner,[117] S. Garg,[42] J. Gargiulo,[64] X. Garrido,[41] A. Garron,[100] F. Garufi,[32,4] P. A. Garver,[91] C. Gasbarra,[21,22] B. Gateley,[2] F. Gautier,[210] V. Gayathri,[10] T. Gayer,[80] G. Gemme,[29] A. Gennai,[82] V. Gennari,[102] J. George,[105] R. George,[149] O. Gerberding,[99] L. Gergely,[155] Sayantan Ghosh,[195] Shaon Ghosh,[193] Shrobana Ghosh,[8,9] Suprovo Ghosh,[211] Tathagata Ghosh,[81] J. A. Giaime,[12,65] K. D. Giardina,[65] D. R. Gibson,[201] C. Gier,[56] S. Gkaitatzis,[83,82] J. Glanzer,[11] F. Glotin,[41] J. Godfrey,[79] R. V. Godley,[8,9] P. Godwin,[11] A. S. Goettel,[33] E. Goetz,[117] J. Golomb,[11] S. Gomez Lopez,[39,38] B. Goncharov,[44] G. González,[12] P. Goodarzi,[212] S. Goode,[6] M. Gosselin,[64] R. Gouaty,[31] D. W. Gould,[34] K. Govorkova,[35] A. Grado,[78,51] V. Graham,[88] A. E. Granados,[18] M. Granata,[177] V. Granata,[213,133] S. Gras,[35] P. Grassia,[11] J. Graves,[58] C. Gray,[2] R. Gray,[88] G. Greco,[51] A. C. Green,[37,110] L. Green,[214] S. M. Green,[75] S. R. Green,[215] C. Greenberg,[134] A. M. Gretarsson,[67] H. K. Griffin,[18] D. Griffith,[11] H. L. Griggs,[58] G. Grignani,[78,51] C. Grimaud,[31] H. Grote,[33] S. Grunewald,[1] D. Guerra,[139] D. Guetta,[216] G. M. Guidi,[62,63] A. R. Guimaraes,[12] H. K. Gulati,[95] F. Gulminelli,[174,175] H. Guo,[146] W. Guo,[74] Y. Guo,[37,36] Anuradha Gupta,[217] I. Gupta,[7] N. C. Gupta,[95] S. K. Gupta,[46] V. Gupta,[18] N. Gupte,[1] J. Gurs,[99] N. Gutierrez,[177] N. Guttman,[6] F. Guzman,[132] D. Haba,[218] M. Haberland,[1] S. Haino,[219] E. D. Hall,[35] E. Z. Hamilton,[100] G. Hammond,[88] M. Haney,[37] J. Hanks,[2] C. Hanna,[7] M. D. Hannam,[33] A. G. Hanselman,[131] H. Hansen,[2] J. Hanson,[65] S. Hanumasagar,[58] R. Harada,[42] A. R. Hardison,[182] S. Harikumar,[187] K. Haris,[37,73] I. Harley-Trochimczyk,[132] T. Harmark,[135] J. Harms,[44,45] G. M. Harry,[220] I. W. Harry,[75] J. Hart,[106] B. Haskell,[97,221,222] C. J. Haster,[214] K. Haughian,[88] H. Hayakawa,[50] K. Hayama,[223] M. C. Heintze,[65] J. Heinze,[109] J. Heinzel,[35] H. Heitmann,[116] F. Hellman,[208] A. F. Helmling-Cornell,[79] G. Hemming,[64] O. Henderson-Sapir,[118] M. Hendry,[88] I. S. Heng,[88] M. H. Hennig,[88] C. Henshaw,[58] M. Heurs,[8,9] A. L. Hewitt,[224,225] J. Heynen,[15] J. Heyns,[35] S. Higginbotham,[33] S. Hild,[36,37] S. Hill,[88] Y. Himemoto,[226] N. Hirata,[25] C. Hirose,[227] D. Hofman,[177] B. E. Hogan,[67] N. A. Holland,[37,110] I. J. Hollows,[176] D. E. Holz,[131] L. Honet,[114] D. J. Horton-Bailey,[208] J. Hough,[88] S. Hourihane,[11] N. T. Howard,[145] E. J. Howell,[74] C. G. Hoy,[75] C. A. Hrishikesh,[21] P. Hsi,[35] H.-F. Hsieh,[143] H.-Y. Hsieh,[143] C. Hsiung,[228] S.-H. Hsu,[147] W.-F. Hsu,[112] Q. Hu,[88] H. Y. Huang,[142] Y. Huang,[7] Y. T. Huang,[80] A. D. Huddart,[229] B. Hughey,[67] V. Hui,[31] S. Husa,[100] R. Huxford,[7] L. Iampieri,[39,38] G. A. Iandolo,[36] M. Ianni,[22,21] G. Iannone,[133] J. Iascau,[79] K. Ide,[230] R. Iden,[218] A. Ierardi,[44,45] S. Ikeda,[148] H. Imafuku,[42] Y. Inoue,[142] G. Iorio,[93] P. Iosif,[185,48] M. H. Iqbal,[34] J. Irwin,[88] R. Ishikawa,[230] M. Isi,[191,192] K. S. Isleif,[231] Y. Itoh,[206,232] M. Iwaya,[205] B. R. Iyer,[24] C. Jacquet,[102] P.-E. Jacquet,[123] T. Jacquot,[41] S. J. Jadhav,[233] S. P. Jadhav,[156] M. Jain,[134] T. Jain,[224] A. L. James,[11] K. Jani,[145] N. N. Janthalur,[233] S. Jaraba,[234] P. Jaranowski,[235] R. Jaume,[100] W. Javed,[33] A. Jennings,[2] M. Jensen,[2] W. Jia,[35] J. Jiang,[151] H.-B. Jin,[236,237] G. R. Johns,[124] N. A. Johnson,[46] N. K. Johnson-McDaniel,[217] M. C. Johnston,[214] R. Johnston,[88] N. Johny,[8,9] D. H. Jones,[34] D. I. Jones,[211] R. Jones,[88] H. E. Jose,[79] P. Joshi,[7] S. K. Joshi,[81] G. Joubert,[57] J. Ju,[238] L. Ju,[74] K. Jung,[239] J. Junker,[34] V. Juste,[114] H. B. Kabagoz,[65,35] T. Kajita,[240] I. Kaku,[206] V. Kalogera,[98] M. Kalomenopoulos,[214] M. Kamiizumi,[50] N. Kanda,[232,206] S. Kandhasamy,[81] G. Kang,[241] N. C. Kannachel,[6] J. B. Kanner,[11] S. A. KantiMahanty,[18] S. J. Kapadia,[81] D. P. Kapasi,[55] M. Karthikeyan,[134] M. Kasprzack,[11] H. Kato,[153] T. Kato,[205] E. Katsavounidis,[35] W. Katzman,[65] R. Kaushik,[105] K. Kawabe,[2] R. Kawamoto,[206] D. Keitel,[100] L. J. Kemperman,[118] J. Kennington,[7] F. A. Kerkow,[18] R. Kesharwani,[81] J. S. Key,[242] R. Khadela,[8,9] S. Khadka,[91] S. S. Khadkikar,[7] F. Y. Khalili,[111] F. Khan,[8,9] T. Khanam,[164] M. Khursheed,[105] N. M. Khusid,[191,192] W. Kiendrebeogo,[116,243] N. Kijbunchoo,[118] C. Kim,[244] J. C. Kim,[245] K. Kim,[246] M. H. Kim,[238] S. Kim,[247] Y.-M. Kim,[246] C. Kimball,[98] K. Kimes,[55] M. Kinnear,[33] J. S. Kissel,[2] S. Klimenko,[46] A. M. Knee,[117] E. J. Knox,[79] N. Knust,[8,9] K. Kobayashi,[205] S. M. Koehlenbeck,[91] G. Koekoek,[37,36] K. Kohri,[248,249] K. Kokeyama,[33,250] S. Koley,[44,167] P. Kolitsidou,[109] A. E. Koloniari,[251]

K. Komori,[42] A. K. H. Kong,[143] A. Kontos,[252] L. M. Koponen,[109] M. Korobko,[99] X. Kou,[18] A. Koushik,[23] N. Kouvatsos,[69] M. Kovalam,[74] T. Koyama,[153] D. B. Kozak,[11] S. L. Kranzhoff,[36,37] V. Kringel,[8,9] N. V. Krishnendu,[109] S. Kroker,[253] A. Królak,[254,187] K. Kruska,[8,9] J. Kubisz,[255] G. Kuehn,[8,9] S. Kulkarni,[217] A. Kulur Ramamohan,[34] Achal Kumar,[46] Anil Kumar,[233] Praveen Kumar,[54] Prayush Kumar,[24] Rahul Kumar,[2] Rakesh Kumar,[95] J. Kume,[256,257,42] K. Kuns,[35] N. Kuntimaddi,[33] S. Kuroyanagi,[209,258] S. Kuwahara,[42] K. Kwak,[239] K. Kwan,[34] S. Kwon,[42] G. Lacaille,[88] D. Laghi,[189,102] A. H. Laity,[165] E. Lalande,[259] M. Lalleman,[23] P. C. Lalremruati,[260] M. Landry,[2] B. B. Lane,[35] R. N. Lang,[35] J. Lange,[149] R. Langgin,[214] B. Lantz,[91] I. La Rosa,[100] J. Larsen,[200] A. Lartaux-Vollard,[41] P. D. Lasky,[6] J. Lawrence,[166] M. Laxen,[65] C. Lazarte,[139] A. Lazzarini,[11] C. Lazzaro,[158,157] P. Leaci,[39,38] L. Leali,[18] Y. K. Lecoeuche,[117] H. M. Lee,[261] H. W. Lee,[262] J. Lee,[80] K. Lee,[238] R.-K. Lee,[143] R. Lee,[35] Sungho Lee,[246] Sunjae Lee,[238] Y. Lee,[142] I. N. Legred,[11] J. Lehmann,[8,9] L. Lehner,[183] M. Le Jean,[177,119] A. Lemaître,[263] M. Lenti,[63,178] M. Leonardi,[76,77,264] M. Lequime,[40] N. Leroy,[41] M. Lesovsky,[11] N. Letendre,[31] M. Lethuillier,[57] Y. Levin,[6] K. Leyde,[75] A. K. Y. Li,[11] K. L. Li,[265] X. Li,[150] Y. Li,[98] Z. Li,[88] A. Lihos,[124] E. T. Lin,[143] F. Lin,[142] L. C.-C. Lin,[265] Y.-C. Lin,[143] C. Lindsay,[201] S. D. Linker,[181] A. Liu,[266] G. C. Liu,[228] Jian Liu,[74] F. Llamas Villarreal,[166] J. Llobera-Querol,[100] R. K. L. Lo,[141] J.-P. Locquet,[112] S. C. G. Loggins,[267] M. R. Loizou,[134] L. T. London,[69] A. Longo,[62,63] D. Lopez,[167] M. Lopez Portilla,[73] M. Lorenzini,[21,22] A. Lorenzo-Medina,[54] V. Loriette,[41] M. Lormand,[65] G. Losurdo,[268,82] E. Lotti,[134] T. P. Lott IV,[58] J. D. Lough,[8,9] H. A. Loughlin,[35] C. O. Lousto,[113] N. Low,[125] N. Lu,[34] L. Lucchesi,[82] H. Lück,[9,8,9] D. Lumaca,[22] A. P. Lundgren,[269,270] A. W. Lussier,[259] R. Macas,[75] M. MacInnis,[35] D. M. Macleod,[33] I. A. O. MacMillan,[11] A. Macquet,[41] K. Maeda,[153] S. Maenaut,[112] S. S. Magare,[81] R. M. Magee,[11] E. Maggio,[1] R. Maggiore,[37,110] M. Magnozzi,[29,30] M. Mahesh,[99] M. Maini,[165] S. Majhi,[81] E. Majorana,[39,38] C. N. Makarem,[11] D. Malakar,[107] J. A. Malaquias-Reis,[19] U. Mali,[190] S. Maliakal,[11] A. Malik,[105] L. Mallick,[170,190] A.-K. Malz,[60] N. Man,[116] M. Mancarella,[101] V. Mandic,[18] V. Mangano,[172,157] B. Mannix,[79] G. L. Mansell,[80] M. Manske,[10] M. Mantovani,[64] M. Mapelli,[93,94,271] C. Marinelli,[103] F. Marion,[31] A. S. Markosyan,[91] A. Markowitz,[11] E. Maros,[11] S. Marsat,[102] F. Martelli,[62,63] I. W. Martin,[88] R. M. Martin,[193] B. B. Martinez,[132] D. A. Martinez,[55] M. Martinez,[43,272] V. Martinez,[130] A. Martini,[76,77] J. C. Martins,[19] D. V. Martynov,[109] E. J. Marx,[35] L. Massaro,[36,37] A. Masserot,[31] M. Masso-Reid,[88] S. Mastrogiovanni,[38] T. Matcovich,[51] M. Matiushechkina,[8,9] L. Maurin,[210] N. Mavalvala,[35] N. Maxwell,[2] G. McCarrol,[65] R. McCarthy,[2] D. E. McClelland,[34] S. McCormick,[65] L. McCuller,[11] S. McEachin,[124] C. McElhenny,[124] G. I. McGhee,[88] J. McGinn,[88] K. B. M. McGowan,[145] J. McIver,[117] A. McLeod,[74] I. McMahon,[189] T. McRae,[34] R. McTeague,[88] D. Meacher,[10] B. N. Meagher,[80] R. Mechum,[113] Q. Meijer,[73] A. Melatos,[125] C. S. Menoni,[138] F. Mera,[2] R. A. Mercer,[10] L. Mereni,[177] K. Merfeld,[164] E. L. Merilh,[65] J. R. Mérou,[100] J. D. Merritt,[79] M. Merzougui,[116] C. Messick,[10] B. Mestichelli,[44] M. Meyer-Conde,[273] F. Meylahn,[8,9] A. Mhaske,[81] A. Miani,[76,77] H. Miao,[274] C. Michel,[177] Y. Michimura,[42] H. Middleton,[109] D. P. Mihaylov,[106] S. J. Miller,[11] M. Millhouse,[58] E. Milotti,[185,48] V. Milotti,[93] Y. Minenkov,[22] E. M. Minihan,[67] Ll. M. Mir,[43] L. Mirasola,[157,158] M. Miravet-Tenés,[139] C.-A. Miritescu,[43] A. Mishra,[24] C. Mishra,[108] T. Mishra,[46] A. L. Mitchell,[37,110] J. G. Mitchell,[67] S. Mitra,[81] V. P. Mitrofanov,[111] K. Mitsuhashi,[25] R. Mittleman,[35] O. Miyakawa,[50] S. Miyoki,[50] A. Miyoko,[67] G. Mo,[35] L. Mobilia,[62,63] S. R. P. Mohapatra,[11] S. R. Mohite,[7] M. Molina-Ruiz,[208] M. Mondin,[181] M. Montani,[62,63] C. J. Moore,[224] D. Moraru,[2] A. More,[81] S. More,[81] C. Moreno,[136] E. A. Moreno,[35] G. Moreno,[2] A. Moreso Serra,[84] S. Morisaki,[42,205] Y. Moriwaki,[153] G. Morras,[209] A. Moscatello,[93] M. Mould,[35] B. Mours,[66] C. M. Mow-Lowry,[37,110] L. Muccillo,[178,63] F. Muciaccia,[39,38] D. Mukherjee,[109] Samanwaya Mukherjee,[24] Soma Mukherjee,[166] Subroto Mukherjee,[95] Suvodip Mukherjee,[13] N. Mukund,[35] A. Mullavey,[65] H. Mullock,[117] J. Mundi,[220] C. L. Mungioli,[74] M. Murakoshi,[230] P. G. Murray,[88] D. Nabari,[76,77] S. L. Nadji,[8,9] A. Nagar,[28,275] N. Nagarajan,[88] K. Nakagaki,[50] K. Nakamura,[25] H. Nakano,[276] M. Nakano,[11] D. Nanadoumgar-Lacroze,[43] D. Nandi,[12] V. Napolano,[64] P. Narayan,[217] I. Nardecchia,[22] T. Narikawa,[205] H. Narola,[73] L. Naticchioni,[38] R. K. Nayak,[260] L. Negri,[73] A. Nela,[88] C. Nelle,[79] A. Nelson,[132] T. J. N. Nelson,[65] M. Nery,[8,9] A. Neunzert,[2] S. Ng,[55] L. Nguyen Quynh,[277] S. A. Nichols,[12] A. B. Nielsen,[278] Y. Nishino,[25,42] A. Nishizawa,[279] S. Nissanke,[280,37] W. Niu,[7] F. Nocera,[64] J. Noller,[281] M. Norman,[33] C. North,[33] J. Novak,[119,234,282] R. Nowicki,[145] J. F. Nuño Siles,[209] L. K. Nuttall,[75] K. Obayashi,[230] J. Oberling,[2] J. O'Dell,[229] E. Oelker,[35] M. Oertel,[234,119,283,282] G. Oganesyan,[44,45] T. O'Hanlon,[65] M. Ohashi,[50] F. Ohme,[8,9] R. Oliveri,[119,283,282] R. Omer,[18] B. O'Neal,[124] M. Onishi,[153] K. Oohara,[284] B. O'Reilly,[65] M. Orselli,[51,78] R. O'Shaughnessy,[113] S. O'Shea,[88] S. Oshino,[50] C. Osthelder,[11] I. Ota,[12] D. J. Ottaway,[118] A. Ouzriat,[57] H. Overmier,[65] B. J. Owen,[285] R. Ozaki,[230] A. E. Pace,[7] R. Pagano,[12] M. A. Page,[25] A. Pai,[195] L. Paiella,[44] A. Pal,[286] S. Pal,[260] M. A. Palaia,[82,83] M. Pálfi,[204] P. P. Palma,[39,21,22] C. Palomba,[38] P. Palud,[20] H. Pan,[143] J. Pan,[74] K. C. Pan,[143] P. K. Panda,[233] Shiksha Pandey,[7] Swadha Pandey,[35] P. T. H. Pang,[37,73] F. Pannarale,[39,38] K. A. Pannone,[55] B. C. Pant,[105] F. H. Panther,[74] M. Panzeri,[62,63] F. Paoletti,[82] A. Paolone,[38,287] A. Papadopoulos,[88] E. E. Papalexakis,[212] L. Papalini,[82,83] G. Papigkiotis,[251] A. Paquis,[41] A. Parisi,[78,51] B.-J. Park,[246] J. Park,[288] W. Parker,[65] G. Pascale,[8,9] D. Pascucci,[96] A. Pasqualetti,[64] R. Passaquieti,[83,82] L. Passenger,[6] D. Passuello,[82] O. Patane,[2] A. V. Patel,[142] D. Pathak,[81] A. Patra,[33] B. Patricelli,[83,82] B. G. Patterson,[33] K. Paul,[108] S. Paul,[79] E. Payne,[11] T. Pearce,[33] M. Pedraza,[11] A. Pele,[11] F. E. Peña Arellano,[289] X. Peng,[109] Y. Peng,[58] S. Penn,[290] M. D. Penuliar,[55] A. Perego,[76,77] Z. Pereira,[134] C. Périgois,[291,94,93] G. Perna,[93] A. Perreca,[76,77,44] J. Perret,[20] S. Perriès,[65] J. W. Perry,[37,110] D. Pesios,[251] S. Peters,[167] S. Petracca,[207] C. Petrillo,[78] H. P. Pfeiffer,[1] H. Pham,[65] K. A. Pham,[18] K. S. Phukon,[109] H. Phurailatpam,[266] M. Piarulli,[102] L. Piccari,[39,38] O. J. Piccinni,[34] M. Pichot,[116]

M. Piendibene,[83,82] F. Piergiovanni,[62,63] L. Pierini,[38] G. Pierra,[38] V. Pierro,[292,133] M. Pietrzak,[97] M. Pillas,[167] F. Pilo,[82] L. Pinard,[177] I. M. Pinto,[292,133,293,32] M. Pinto,[64] B. J. Piotrzkowski,[10] M. Pirello,[2] M. D. Pitkin,[224,88] A. Placidi,[51] E. Placidi,[39,38] M. L. Planas,[100] W. Plastino,[213,22] C. Plunkett,[35] R. Poggiani,[83,82] E. Polini,[35] J. Pomper,[82,83] L. Pompili,[1] J. Poon,[266] E. Porcelli,[37] E. K. Porter,[20] C. Posnansky,[7] R. Poulton,[64] J. Powell,[156] G. S. Prabhu,[81] M. Pracchia,[167] B. K. Pradhan,[81] T. Pradier,[66] A. K. Prajapati,[95] K. Prasai,[294] R. Prasanna,[233] P. Prasia,[81] G. Pratten,[109] G. Principe,[185,48] G. A. Prodi,[76,77] P. Prosperi,[82] P. Prosposito,[21,22] A. C. Providence,[67] A. Puecher,[1] J. Pullin,[12] P. Puppo,[38] M. Pürrer,[165] H. Qi,[16] J. Qin,[34] G. Quéméner,[175,119] V. Quetschke,[166] P. J. Quinonez,[67] N. Qutob,[58] R. Rading,[231] I. Rainho,[139] S. Raja,[105] C. Rajan,[105] B. Rajbhandari,[113] K. E. Ramirez,[65] F. A. Ramis Vidal,[100] M. Ramos Arevalo,[166] A. Ramos-Buades,[100,37] S. Ranjan,[58] K. Ransom,[65] P. Rapagnani,[39,38] B. Ratto,[67] A. Ravichandran,[134] A. Ray,[98] V. Raymond,[33] M. Razzano,[83,82] J. Read,[55] T. Regimbau,[31] S. Reid,[56] C. Reissel,[35] D. H. Reitze,[11] A. I. Renzini,[11,128] B. Revenu,[295,41] A. Revilla Peña,[84] R. Reyes,[181] L. Ricca,[15] F. Ricci,[39,38] M. Ricci,[38,39] A. Ricciardone,[83,82] J. Rice,[80] J. W. Richardson,[212] M. L. Richardson,[118] A. Rijal,[67] K. Riles,[92] H. K. Riley,[33] S. Rinaldi,[271] J. Rittmeyer,[99] C. Robertson,[229] F. Robinet,[41] M. Robinson,[2] A. Rocchi,[22] L. Rolland,[31] J. G. Rollins,[11] A. E. Romano,[296] R. Romano,[3,4] A. Romero,[31] I. M. Romero-Shaw,[224] J. H. Romie,[65] S. Ronchini,[7] T. J. Roocke,[118] L. Rosa,[4,32] T. J. Rosauer,[212] C. A. Rose,[58] D. Rosińska,[126] M. P. Ross,[53] M. Rossello-Sastre,[100] S. Rowan,[88] S. K. Roy,[191,192] S. Roy,[15] D. Rozza,[128,129] P. Ruggi,[64] N. Ruhama,[239] E. Ruiz Morales,[297,209] K. Ruiz-Rocha,[145] S. Sachdev,[58] T. Sadecki,[2] P. Saffarieh,[37,110] S. Safi-Harb,[170] M. R. Sah,[13] S. Saha,[143] T. Sainrat,[66] S. Sajith Menon,[216,39,38] K. Sakai,[298] Y. Sakai,[273] M. Sakellariadou,[69] S. Sakon,[7] O. S. Salafia,[160,129,128] F. Salces-Carcoba,[11] L. Salconi,[64] M. Saleem,[149] F. Salemi,[39,38] M. Sallé,[37] S. U. Salunkhe,[81] S. Salvador,[175,174] A. Salvarese,[149] A. Samajdar,[73,37] A. Sanchez,[2] E. J. Sanchez,[11] L. E. Sanchez,[11] N. Sanchis-Gual,[139] J. R. Sanders,[182] E. M. Sänger,[1] F. Santoliquido,[44,45] F. Sarandrea,[28] T. R. Saravanan,[81] N. Sarin,[6] P. Sarkar,[8,9] A. Sasli,[251] P. Sassi,[51,78] B. Sassolas,[177] B. S. Sathyaprakash,[7,33] R. Sato,[227] S. Sato,[153] Yukino Sato,[153] Yu Sato,[153] O. Sauter,[46] R. L. Savage,[2] T. Sawada,[50] H. L. Sawant,[81] S. Sayah,[177] V. Scacco,[21,22] D. Schaetzl,[11] M. Scheel,[150] A. Schiebelbein,[190] M. G. Schiworski,[80] P. Schmidt,[109] S. Schmidt,[73] R. Schnabel,[99] M. Schneewind,[8,9] R. M. S. Schofield,[79] K. Schouteden,[112] B. W. Schulte,[8,9] B. F. Schutz,[33,8,9] E. Schwartz,[299] M. Scialpi,[300] J. Scott,[88] S. M. Scott,[34] R. M. Sedas,[65] T. C. Seetharamu,[88] M. Seglar-Arroyo,[43] Y. Sekiguchi,[301] D. Sellers,[65] N. Sembo,[206] A. S. Sengupta,[302] E. G. Seo,[88] J. W. Seo,[112] V. Sequino,[32,4] M. Serra,[38] A. Sevrin,[188] T. Shaffer,[2] U. S. Shah,[58] M. A. Shaikh,[261] L. Shao,[303] A. K. Sharma,[100] Preeti Sharma,[12] Prianka Sharma,[105] Ritwik Sharma,[18] S. Sharma Chaudhary,[107] P. Shawhan,[127] N. S. Shcheblanov,[304,263] E. Sheridan,[145] Z.-H. Shi,[143] M. Shikauchi,[42] R. Shimomura,[305] H. Shinkai,[305] S. Shirke,[81] D. H. Shoemaker,[35] D. M. Shoemaker,[149] R. W. Short,[2] S. ShyamSundar,[105] A. Sider,[159] H. Siegel,[191,192] D. Sigg,[2] L. Silenzi,[36,37] L. Silvestri,[39,171] M. Simmonds,[118] L. P. Singer,[306] Amitesh Singh,[217] Anika Singh,[11] D. Singh,[208] N. Singh,[100] S. Singh,[218,61] A. M. Sintes,[100] V. Sipala,[172,157] V. Skliris,[33] B. J. J. Slagmolen,[34] D. A. Slater,[200] T. J. Slaven-Blair,[74] J. Smetana,[109] J. R. Smith,[55] L. Smith,[88,185,48] R. J. E. Smith,[6] W. J. Smith,[145] S. Soares de Albuquerque Filho,[62] M. Soares-Santos,[189] K. Somiya,[218] I. Song,[143] S. Soni,[35] V. Sordini,[57] F. Sorrentino,[29] H. Sotani,[307] F. Spada,[82] V. Spagnuolo,[37] A. P. Spencer,[88] P. Spinicelli,[64] A. K. Srivastava,[95] F. Stachurski,[88] C. J. Stark,[124] D. A. Steer,[308] N. Steinle,[170] J. Steinlechner,[36,37] S. Steinlechner,[36,37] N. Stergioulas,[251] P. Stevens,[41] S. P. Stevenson,[156] M. StPierre,[165] M. D. Strong,[12] A. Strunk,[2] A. L. Stuver,[104,*] M. Suchenek,[97] S. Sudhagar,[97] Y. Sudo,[230] N. Sueltmann,[99] L. Suleiman,[55] K. D. Sullivan,[12] J. Sun,[241] L. Sun,[34] S. Sunil,[95] J. Suresh,[116] B. J. Sutton,[69] P. J. Sutton,[33] K. Suzuki,[218] M. Suzuki,[205] S. Swain,[109] B. L. Swinkels,[37] A. Syx,[119] M. J. Szczepańczyk,[309] P. Szewczyk,[126] M. Tacca,[37] H. Tagoshi,[205] K. Takada,[205] H. Takahashi,[273] R. Takahashi,[25] A. Takamori,[42] S. Takano,[310] H. Takeda,[311,312] K. Takeshita,[218] I. Takimoto Schmiegelow,[44,45] M. Takou-Ayaoh,[80] C. Talbot,[131] M. Tamaki,[205] N. Tamanini,[102] D. Tanabe,[142] K. Tanaka,[50] S. J. Tanaka,[230] S. Tanioka,[33] D. B. Tanner,[46] W. Tanner,[8,9] L. Tao,[212] R. D. Tapia,[7] E. N. Tapia San Martín,[37] C. Taranto,[21,22] A. Taruya,[313] J. D. Tasson,[154] J. G. Tau,[113] D. Tellez,[55] R. Tenorio,[100] H. Themann,[181] A. Theodoropoulos,[139] M. P. Thirugnanasambandam,[81] L. M. Thomas,[11] M. Thomas,[65] P. Thomas,[2] J. E. Thompson,[211] S. R. Thondapu,[105] K. A. Thorne,[65] E. Thrane,[6] J. Tissino,[44,45] A. Tiwari,[81] Pawan Tiwari,[44] Praveer Tiwari,[195] S. Tiwari,[189] V. Tiwari,[109] M. R. Todd,[80] M. Toffano,[93] A. M. Toivonen,[18] K. Toland,[88] A. E. Tolley,[75] T. Tomaru,[25] V. Tommasini,[11] T. Tomura,[50] H. Tong,[6] C. Tong-Yu,[142] A. Torres-Forné,[139,140] C. I. Torrie,[11] I. Tosta e Melo,[314] E. Tournefier,[31] M. Trad Nery,[116] K. Tran,[124] A. Trapananti,[52,51] R. Travaglini,[169] F. Travasso,[52,51] G. Traylor,[65] M. Trevor,[127] M. C. Tringali,[64] A. Tripathee,[92] G. Troian,[185,48] A. Trovato,[185,48] L. Trozzo,[4] R. J. Trudeau,[11] T. Tsang,[33] S. Tsuchida,[315] L. Tsukada,[214] K. Turbang,[188,23] M. Turconi,[116] C. Turski,[96] H. Ubach,[84,85] N. Uchikata,[205] T. Uchiyama,[50] R. P. Udall,[11] T. Uehara,[316] K. Ueno,[42] V. Undheim,[278] L. E. Uronen,[266] T. Ushiba,[50] M. Vacatello,[82,83] H. Vahlbruch,[8,9] N. Vaidya,[11] G. Vajente,[11] A. Vajpeyi,[6] J. Valencia,[100] M. Valentini,[110,37] S. A. Vallejo-Peña,[296] S. Vallero,[28] V. Valsan,[10] M. van Dael,[37,317] E. Van den Bossche,[188] J. F. J. van den Brand,[36,110,37] C. Van Den Broeck,[73,37] M. van der Sluys,[37,73] A. Van de Walle,[41] J. van Dongen,[37,110] K. Vandra,[104] M. VanDyke,[121] H. van Haevermaet,[23] J. V. van Heijningen,[37,110] P. Van Hove,[66] J. Vanier,[259] M. VanKeuren,[106] J. Vanosky,[2] N. van Remortel,[23] M. Vardaro,[36,37] A. F. Vargas,[125] V. Varma,[134] A. N. Vazquez,[91] A. Vecchio,[109] G. Vedovato,[94] J. Veitch,[88] P. J. Veitch,[118] S. Venikoudis,[15] R. C. Venterea,[18] P. Verdier,[57] M. Vereecken,[15] D. Verkindt,[31] B. Verma,[134] Y. Verma,[105] S. M. Vermeulen,[11] F. Vetrano,[62] A. Veutro,[38,39] A. Viceré,[62,63]

S. Vidyant,[80] A. D. Viets,[90] A. Vijaykumar,[190] A. Vilkha,[113] N. Villanueva Espinosa,[139] V. Villa-Ortega,[54] E. T. Vincent,[58] J.-Y. Vinet,[116] S. Viret,[57] S. Vitale,[35] H. Vocca,[78,51] D. Voigt,[99] E. R. G. von Reis,[2] J. S. A. von Wrangel,[8,9] W. E. Vossius,[231] L. Vujeva,[141] S. P. Vyatchanin,[111] J. Wack,[11] L. E. Wade,[106] M. Wade,[106] K. J. Wagner,[113] L. Wallace,[11] E. J. Wang,[91] H. Wang,[218] J. Z. Wang,[92] W. H. Wang,[166] Y. F. Wang,[1] G. Waratkar,[195] J. Warner,[2] M. Was,[31] T. Washimi,[25] N. Y. Washington,[11] D. Watarai,[42] B. Weaver,[2] S. A. Webster,[88] N. L. Weickhardt,[99] M. Weinert,[8,9] A. J. Weinstein,[11] R. Weiss,[35] L. Wen,[74] K. Wette,[34] J. T. Whelan,[113] B. F. Whiting,[46] C. Whittle,[11] E. G. Wickens,[75] D. Wilken,[8,9,9] A. T. Wilkin,[212] B. M. Williams,[121] D. Williams,[88] M. J. Williams,[75] N. S. Williams,[1] J. L. Willis,[11] B. Willke,[9,8,9] M. Wils,[112] L. Wilson,[106] C. W. Winborn,[107] J. Winterflood,[74] C. C. Wipf,[11] G. Woan,[88] J. Woehler,[36,37] N. E. Wolfe,[35] H. T. Wong,[142] H. W. Y. Wong,[266] I. C. F. Wong,[266,112] K. Wong,[190] T. Wouters,[73,37] J. L. Wright,[2] B. Wu,[80] C. Wu,[143] D. S. Wu,[8,9] H. Wu,[143] K. Wu,[121] Q. Wu,[53] Y. Wu,[98] Z. Wu,[102] E. Wuchner,[55] D. M. Wysocki,[10] V. A. Xu,[208] Y. Xu,[100] N. Yadav,[28] H. Yamamoto,[11] K. Yamamoto,[153] T. S. Yamamoto,[42] T. Yamamoto,[50] R. Yamazaki,[230] T. Yan,[109] K. Z. Yang,[18] Y. Yang,[147] Z. Yarbrough,[12] J. Yebana,[100] S.-W. Yeh,[143] A. B. Yelikar,[145] X. Yin,[35] J. Yokoyama,[318,42] T. Yokozawa,[50] S. Yuan,[74] H. Yuzurihara,[50] M. Zanolin,[67] M. Zeeshan,[113] T. Zelenova,[64] J.-P. Zendri,[94] M. Zeoli,[15] M. Zerrad,[40] M. Zevin,[98] L. Zhang,[11] N. Zhang,[58] R. Zhang,[151] T. Zhang,[109] C. Zhao,[74] Yue Zhao,[163] Yuhang Zhao,[20] Z.-C. Zhao,[319] Y. Zheng,[107] H. Zhong,[18] H. Zhou,[80] H. O. Zhu,[74] Z.-H. Zhu,[319,320] A. B. Zimmerman,[149] L. Zimmermann,[57] M. E. Zucker,[35,11] and J. Zweizig[11]

[1] *Max Planck Institute for Gravitational Physics (Albert Einstein Institute), D-14476 Potsdam, Germany*

[2] *LIGO Hanford Observatory, Richland, WA 99352, USA*

[3] *Dipartimento di Farmacia, Università di Salerno, I-84084 Fisciano, Salerno, Italy*

[4] *INFN, Sezione di Napoli, I-80126 Napoli, Italy*

[5] *University of Warwick, Coventry CV4 7AL, United Kingdom*

[6] *OzGrav, School of Physics & Astronomy, Monash University, Clayton 3800, Victoria, Australia*

[7] *The Pennsylvania State University, University Park, PA 16802, USA*

[8] *Max Planck Institute for Gravitational Physics (Albert Einstein Institute), D-30167 Hannover, Germany*

[9] *Leibniz Universität Hannover, D-30167 Hannover, Germany*

[10] *University of Wisconsin-Milwaukee, Milwaukee, WI 53201, USA*

[11] *LIGO Laboratory, California Institute of Technology, Pasadena, CA 91125, USA*

[12] *Louisiana State University, Baton Rouge, LA 70803, USA*

[13] *Tata Institute of Fundamental Research, Mumbai 400005, India*

[14] *Centre de Physique Théorique, Aix-Marseille Université, Campus de Luminy, 163 Av. de Luminy, 13009 Marseille, France*

[15] *Université catholique de Louvain, B-1348 Louvain-la-Neuve, Belgium*

[16] *Queen Mary University of London, London E1 4NS, United Kingdom*

[17] *University of California, Davis, Davis, CA 95616, USA*

[18] *University of Minnesota, Minneapolis, MN 55455, USA*

[19] *Instituto Nacional de Pesquisas Espaciais, 12227-010 São José dos Campos, São Paulo, Brazil*

[20] *Université Paris Cité, CNRS, Astroparticule et Cosmologie, F-75013 Paris, France*

[21] *Università di Roma Tor Vergata, I-00133 Roma, Italy*

[22] *INFN, Sezione di Roma Tor Vergata, I-00133 Roma, Italy*

[23] *Universiteit Antwerpen, 2000 Antwerpen, Belgium*

[24] *International Centre for Theoretical Sciences, Tata Institute of Fundamental Research, Bengaluru 560089, India*

[25] *Gravitational Wave Science Project, National Astronomical Observatory of Japan, 2-21-1 Osawa, Mitaka City, Tokyo 181-8588, Japan*

[26] *Advanced Technology Center, National Astronomical Observatory of Japan, 2-21-1 Osawa, Mitaka City, Tokyo 181-8588, Japan*

[27] *Theoretisch-Physikalisches Institut, Friedrich-Schiller-Universität Jena, D-07743 Jena, Germany*

[28] *INFN Sezione di Torino, I-10125 Torino, Italy*

[29] *INFN, Sezione di Genova, I-16146 Genova, Italy*

[30] *Dipartimento di Fisica, Università degli Studi di Genova, I-16146 Genova, Italy*

[31] *Univ. Savoie Mont Blanc, CNRS, Laboratoire d'Annecy de Physique des Particules - IN2P3, F-74000 Annecy, France*

[32] *Università di Napoli "Federico II", I-80126 Napoli, Italy*

[33] *Cardiff University, Cardiff CF24 3AA, United Kingdom*

[34] *OzGrav, Australian National University, Canberra, Australian Capital Territory 0200, Australia*

[35] *LIGO Laboratory, Massachusetts Institute of Technology, Cambridge, MA 02139, USA*

[36] *Maastricht University, 6200 MD Maastricht, Netherlands*

[37] *Nikhef, 1098 XG Amsterdam, Netherlands*

[38] *INFN, Sezione di Roma, I-00185 Roma, Italy*

[39] *Università di Roma "La Sapienza", I-00185 Roma, Italy*

[40] *Aix Marseille Univ, CNRS, Centrale Med, Institut Fresnel, F-13013 Marseille, France*

[41] *Université Paris-Saclay, CNRS/IN2P3, IJCLab, 91405 Orsay, France*

[42] *University of Tokyo, Tokyo, 113-0033, Japan*
[43] *Institut de Física d'Altes Energies (IFAE), The Barcelona Institute of Science and Technology, Campus UAB, E-08193 Bellaterra (Barcelona), Spain*
[44] *Gran Sasso Science Institute (GSSI), I-67100 L'Aquila, Italy*
[45] *INFN, Laboratori Nazionali del Gran Sasso, I-67100 Assergi, Italy*
[46] *University of Florida, Gainesville, FL 32611, USA*
[47] *Dipartimento di Scienze Matematiche, Informatiche e Fisiche, Università di Udine, I-33100 Udine, Italy*
[48] *INFN, Sezione di Trieste, I-34127 Trieste, Italy*
[49] *Tecnologico de Monterrey, Escuela de Ingeniería y Ciencias, 64849 Monterrey, Nuevo León, Mexico*
[50] *Institute for Cosmic Ray Research, KAGRA Observatory, The University of Tokyo, 238 Higashi-Mozumi, Kamioka-cho, Hida City, Gifu 506-1205, Japan*
[51] *INFN, Sezione di Perugia, I-06123 Perugia, Italy*
[52] *Università di Camerino, I-62032 Camerino, Italy*
[53] *University of Washington, Seattle, WA 98195, USA*
[54] *IGFAE, Universidade de Santiago de Compostela, E-15782 Santiago de Compostela, Spain*
[55] *California State University Fullerton, Fullerton, CA 92831, USA*
[56] *SUPA, University of Strathclyde, Glasgow G1 1XQ, United Kingdom*
[57] *Université Claude Bernard Lyon 1, CNRS, IP2I Lyon / IN2P3, UMR 5822, F-69622 Villeurbanne, France*
[58] *Georgia Institute of Technology, Atlanta, GA 30332, USA*
[59] *Chennai Mathematical Institute, Chennai 603103, India*
[60] *Royal Holloway, University of London, London TW20 0EX, United Kingdom*
[61] *Astronomical course, The Graduate University for Advanced Studies (SOKENDAI), 2-21-1 Osawa, Mitaka City, Tokyo 181-8588, Japan*
[62] *Università degli Studi di Urbino "Carlo Bo", I-61029 Urbino, Italy*
[63] *INFN, Sezione di Firenze, I-50019 Sesto Fiorentino, Firenze, Italy*
[64] *European Gravitational Observatory (EGO), I-56021 Cascina, Pisa, Italy*
[65] *LIGO Livingston Observatory, Livingston, LA 70754, USA*
[66] *Université de Strasbourg, CNRS, IPHC UMR 7178, F-67000 Strasbourg, France*
[67] *Embry-Riddle Aeronautical University, Prescott, AZ 86301, USA*
[68] *Dipartimento di Fisica "E.R. Caianiello", Università di Salerno, I-84084 Fisciano, Salerno, Italy*
[69] *King's College London, University of London, London WC2R 2LS, United Kingdom*
[70] *Korea Institute of Science and Technology Information, Daejeon 34141, Republic of Korea*
[71] *International College, Osaka University, 1-1 Machikaneyama-cho, Toyonaka City, Osaka 560-0043, Japan*
[72] *Accelerator Laboratory, High Energy Accelerator Research Organization (KEK), 1-1 Oho, Tsukuba City, Ibaraki 305-0801, Japan*
[73] *Institute for Gravitational and Subatomic Physics (GRASP), Utrecht University, 3584 CC Utrecht, Netherlands*
[74] *OzGrav, University of Western Australia, Crawley, Western Australia 6009, Australia*
[75] *University of Portsmouth, Portsmouth, PO1 3FX, United Kingdom*
[76] *Università di Trento, Dipartimento di Fisica, I-38123 Povo, Trento, Italy*
[77] *INFN, Trento Institute for Fundamental Physics and Applications, I-38123 Povo, Trento, Italy*
[78] *Università di Perugia, I-06123 Perugia, Italy*
[79] *University of Oregon, Eugene, OR 97403, USA*
[80] *Syracuse University, Syracuse, NY 13244, USA*
[81] *Inter-University Centre for Astronomy and Astrophysics, Pune 411007, India*
[82] *INFN, Sezione di Pisa, I-56127 Pisa, Italy*
[83] *Università di Pisa, I-56127 Pisa, Italy*
[84] *Institut de Ciències del Cosmos (ICCUB), Universitat de Barcelona (UB), c. Martí i Franquès, 1, 08028 Barcelona, Spain*
[85] *Departament de Física Quàntica i Astrofísica (FQA), Universitat de Barcelona (UB), c. Martí i Franqués, 1, 08028 Barcelona, Spain*
[86] *Institut d'Estudis Espacials de Catalunya, c. Gran Capità, 2-4, 08034 Barcelona, Spain*
[87] *Dipartimento di Medicina, Chirurgia e Odontoiatria "Scuola Medica Salernitana", Università di Salerno, I-84081 Baronissi, Salerno, Italy*
[88] *IGR, University of Glasgow, Glasgow G12 8QQ, United Kingdom*
[89] *HUN-REN Wigner Research Centre for Physics, H-1121 Budapest, Hungary*
[90] *Concordia University Wisconsin, Mequon, WI 53097, USA*
[91] *Stanford University, Stanford, CA 94305, USA*
[92] *University of Michigan, Ann Arbor, MI 48109, USA*
[93] *Università di Padova, Dipartimento di Fisica e Astronomia, I-35131 Padova, Italy*
[94] *INFN, Sezione di Padova, I-35131 Padova, Italy*
[95] *Institute for Plasma Research, Bhat, Gandhinagar 382428, India*

[96] *Universiteit Gent, B-9000 Gent, Belgium*
[97] *Nicolaus Copernicus Astronomical Center, Polish Academy of Sciences, 00-716, Warsaw, Poland*
[98] *Northwestern University, Evanston, IL 60208, USA*
[99] *Universität Hamburg, D-22761 Hamburg, Germany*
[100] *IAC3–IEEC, Universitat de les Illes Balears, E-07122 Palma de Mallorca, Spain*
[101] *Aix-Marseille Université, Université de Toulon, CNRS, CPT, Marseille, France*
[102] *Laboratoire des 2 Infinis - Toulouse (L2IT-IN2P3), F-31062 Toulouse Cedex 9, France*
[103] *Università di Siena, Dipartimento di Scienze Fisiche, della Terra e dell'Ambiente, I-53100 Siena, Italy*
[104] *Villanova University, Villanova, PA 19085, USA*
[105] *RRCAT, Indore, Madhya Pradesh 452013, India*
[106] *Kenyon College, Gambier, OH 43022, USA*
[107] *Missouri University of Science and Technology, Rolla, MO 65409, USA*
[108] *Indian Institute of Technology Madras, Chennai 600036, India*
[109] *University of Birmingham, Birmingham B15 2TT, United Kingdom*
[110] *Department of Physics and Astronomy, Vrije Universiteit Amsterdam, 1081 HV Amsterdam, Netherlands*
[111] *Lomonosov Moscow State University, Moscow 119991, Russia*
[112] *Katholieke Universiteit Leuven, Oude Markt 13, 3000 Leuven, Belgium*
[113] *Rochester Institute of Technology, Rochester, NY 14623, USA*
[114] *Université libre de Bruxelles, 1050 Bruxelles, Belgium*
[115] *Bar-Ilan University, Ramat Gan, 5290002, Israel*
[116] *Université Côte d'Azur, Observatoire de la Côte d'Azur, CNRS, Artemis, F-06304 Nice, France*
[117] *University of British Columbia, Vancouver, BC V6T 1Z4, Canada*
[118] *OzGrav, University of Adelaide, Adelaide, South Australia 5005, Australia*
[119] *Centre national de la recherche scientifique, 75016 Paris, France*
[120] *Univ Rennes, CNRS, Institut FOTON - UMR 6082, F-35000 Rennes, France*
[121] *Washington State University, Pullman, WA 99164, USA*
[122] *Cornell University, Ithaca, NY 14850, USA*
[123] *Laboratoire Kastler Brossel, Sorbonne Université, CNRS, ENS-Université PSL, Collège de France, F-75005 Paris, France*
[124] *Christopher Newport University, Newport News, VA 23606, USA*
[125] *OzGrav, University of Melbourne, Parkville, Victoria 3010, Australia*
[126] *Astronomical Observatory Warsaw University, 00-478 Warsaw, Poland*
[127] *University of Maryland, College Park, MD 20742, USA*
[128] *Università degli Studi di Milano-Bicocca, I-20126 Milano, Italy*
[129] *INFN, Sezione di Milano-Bicocca, I-20126 Milano, Italy*
[130] *Université de Lyon, Université Claude Bernard Lyon 1, CNRS, Institut Lumière Matière, F-69622 Villeurbanne, France*
[131] *University of Chicago, Chicago, IL 60637, USA*
[132] *University of Arizona, Tucson, AZ 85721, USA*
[133] *INFN, Sezione di Napoli, Gruppo Collegato di Salerno, I-80126 Napoli, Italy*
[134] *University of Massachusetts Dartmouth, North Dartmouth, MA 02747, USA*
[135] *Niels Bohr Institute, Copenhagen University, 2100 København, Denmark*
[136] *Universidad de Guadalajara, 44430 Guadalajara, Jalisco, Mexico*
[137] *Istituto di Astrofisica e Planetologia Spaziali di Roma, 00133 Roma, Italy*
[138] *Colorado State University, Fort Collins, CO 80523, USA*
[139] *Departamento de Astronomía y Astrofísica, Universitat de València, E-46100 Burjassot, València, Spain*
[140] *Observatori Astronòmic, Universitat de València, E-46980 Paterna, València, Spain*
[141] *Niels Bohr Institute, University of Copenhagen, 2100 Kóbenhavn, Denmark*
[142] *National Central University, Taoyuan City 320317, Taiwan*
[143] *National Tsing Hua University, Hsinchu City 30013, Taiwan*
[144] *OzGrav, Charles Sturt University, Wagga Wagga, New South Wales 2678, Australia*
[145] *Vanderbilt University, Nashville, TN 37235, USA*
[146] *University of the Chinese Academy of Sciences / International Centre for Theoretical Physics Asia-Pacific, Bejing 100049, China*
[147] *Department of Electrophysics, National Yang Ming Chiao Tung University, 101 Univ. Street, Hsinchu, Taiwan*
[148] *Kamioka Branch, National Astronomical Observatory of Japan, 238 Higashi-Mozumi, Kamioka-cho, Hida City, Gifu 506-1205, Japan*
[149] *University of Texas, Austin, TX 78712, USA*
[150] *CaRT, California Institute of Technology, Pasadena, CA 91125, USA*
[151] *Northeastern University, Boston, MA 02115, USA*
[152] *Dipartimento di Ingegneria Industriale (DIIN), Università di Salerno, I-84084 Fisciano, Salerno, Italy*

[153] *Faculty of Science, University of Toyama, 3190 Gofuku, Toyama City, Toyama 930-8555, Japan*
[154] *Carleton College, Northfield, MN 55057, USA*
[155] *University of Szeged, Dóm tér 9, Szeged 6720, Hungary*
[156] *OzGrav, Swinburne University of Technology, Hawthorn VIC 3122, Australia*
[157] *INFN Cagliari, Physics Department, Università degli Studi di Cagliari, Cagliari 09042, Italy*
[158] *Università degli Studi di Cagliari, Via Università 40, 09124 Cagliari, Italy*
[159] *Université Libre de Bruxelles, Brussels 1050, Belgium*
[160] *INAF, Osservatorio Astronomico di Brera sede di Merate, I-23807 Merate, Lecco, Italy*
[161] *Departamento de Matemáticas, Universitat de València, E-46100 Burjassot, València, Spain*
[162] *Montana State University, Bozeman, MT 59717, USA*
[163] *The University of Utah, Salt Lake City, UT 84112, USA*
[164] *Johns Hopkins University, Baltimore, MD 21218, USA*
[165] *University of Rhode Island, Kingston, RI 02881, USA*
[166] *The University of Texas Rio Grande Valley, Brownsville, TX 78520, USA*
[167] *Université de Liège, B-4000 Liège, Belgium*
[168] *DIFA- Alma Mater Studiorum Università di Bologna, Via Zamboni, 33 - 40126 Bologna, Italy*
[169] *Istituto Nazionale Di Fisica Nucleare - Sezione di Bologna, viale Carlo Berti Pichat 6/2 - 40127 Bologna, Italy*
[170] *University of Manitoba, Winnipeg, MB R3T 2N2, Canada*
[171] *INFN-CNAF - Bologna, Viale Carlo Berti Pichat, 6/2, 40127 Bologna BO, Italy*
[172] *Università degli Studi di Sassari, I-07100 Sassari, Italy*
[173] *INFN, Laboratori Nazionali del Sud, I-95125 Catania, Italy*
[174] *Université de Normandie, ENSICAEN, UNICAEN, CNRS/IN2P3, LPC Caen, F-14000 Caen, France*
[175] *Laboratoire de Physique Corpusculaire Caen, 6 boulevard du maréchal Juin, F-14050 Caen, France*
[176] *The University of Sheffield, Sheffield S10 2TN, United Kingdom*
[177] *Université Claude Bernard Lyon 1, CNRS, Laboratoire des Matériaux Avancés (LMA), IP2I Lyon / IN2P3, UMR 5822, F-69622 Villeurbanne, France*
[178] *Università di Firenze, Sesto Fiorentino I-50019, Italy*
[179] *Dipartimento di Scienze Matematiche, Fisiche e Informatiche, Università di Parma, I-43124 Parma, Italy*
[180] *INFN, Sezione di Milano Bicocca, Gruppo Collegato di Parma, I-43124 Parma, Italy*
[181] *California State University, Los Angeles, Los Angeles, CA 90032, USA*
[182] *Marquette University, Milwaukee, WI 53233, USA*
[183] *Perimeter Institute, Waterloo, ON N2L 2Y5, Canada*
[184] *Corps des Mines, Mines Paris, Université PSL, 60 Bd Saint-Michel, 75272 Paris, France*
[185] *Dipartimento di Fisica, Università di Trieste, I-34127 Trieste, Italy*
[186] *Université Côte d'Azur, Observatoire de la Côte d'Azur, CNRS, Lagrange, F-06304 Nice, France*
[187] *National Center for Nuclear Research, 05-400 Świerk-Otwock, Poland*
[188] *Vrije Universiteit Brussel, 1050 Brussel, Belgium*
[189] *University of Zurich, Winterthurerstrasse 190, 8057 Zurich, Switzerland*
[190] *Canadian Institute for Theoretical Astrophysics, University of Toronto, Toronto, ON M5S 3H8, Canada*
[191] *Stony Brook University, Stony Brook, NY 11794, USA*
[192] *Center for Computational Astrophysics, Flatiron Institute, New York, NY 10010, USA*
[193] *Montclair State University, Montclair, NJ 07043, USA*
[194] *HUN-REN Institute for Nuclear Research, H-4026 Debrecen, Hungary*
[195] *Indian Institute of Technology Bombay, Powai, Mumbai 400 076, India*
[196] *Centro de Física das Universidades do Minho e do Porto, Universidade do Minho, PT-4710-057 Braga, Portugal*
[197] *Aix Marseille Univ, CNRS/IN2P3, CPPM, Marseille, France*
[198] *CNR-SPIN, I-84084 Fisciano, Salerno, Italy*
[199] *Scuola di Ingegneria, Università della Basilicata, I-85100 Potenza, Italy*
[200] *Western Washington University, Bellingham, WA 98225, USA*
[201] *SUPA, University of the West of Scotland, Paisley PA1 2BE, United Kingdom*
[202] *Barry University, Miami Shores, FL 33168, USA*
[203] *CENTRA, Departamento de Física, Instituto Superior Técnico – IST, Universidade de Lisboa – UL, Avenida Rovisco Pais 1, 1049-001 Lisboa, Portugal*
[204] *Eötvös University, Budapest 1117, Hungary*
[205] *Institute for Cosmic Ray Research, KAGRA Observatory, The University of Tokyo, 5-1-5 Kashiwa-no-Ha, Kashiwa City, Chiba 277-8582, Japan*

[206] *Department of Physics, Graduate School of Science, Osaka Metropolitan University, 3-3-138 Sugimoto-cho, Sumiyoshi-ku, Osaka City, Osaka 558-8585, Japan*
[207] *University of Sannio at Benevento, I-82100 Benevento, Italy and INFN, Sezione di Napoli, I-80100 Napoli, Italy*
[208] *University of California, Berkeley, CA 94720, USA*
[209] *Instituto de Fisica Teorica UAM-CSIC, Universidad Autonoma de Madrid, 28049 Madrid, Spain*
[210] *Laboratoire d'Acoustique de l'Université du Mans, UMR CNRS 6613, F-72085 Le Mans, France*
[211] *University of Southampton, Southampton SO17 1BJ, United Kingdom*
[212] *University of California, Riverside, Riverside, CA 92521, USA*
[213] *Dipartimento di Ingegneria Industriale, Elettronica e Meccanica, Università degli Studi Roma Tre, I-00146 Roma, Italy*
[214] *University of Nevada, Las Vegas, Las Vegas, NV 89154, USA*
[215] *University of Nottingham NG7 2RD, UK*
[216] *Ariel University, Ramat HaGolan St 65, Ari'el, Israel*
[217] *The University of Mississippi, University, MS 38677, USA*
[218] *Graduate School of Science, Institute of Science Tokyo, 2-12-1 Ookayama, Meguro-ku, Tokyo 152-8551, Japan*
[219] *Institute of Physics, Academia Sinica, 128 Sec. 2, Academia Rd., Nankang, Taipei 11529, Taiwan*
[220] *American University, Washington, DC 20016, USA*
[221] *Dipartimento di Fisica, Università degli studi di Milano, Via Celoria 16, I-20133, Milano, Italy*
[222] *INFN, sezione di Milano, Via Celoria 16, I-20133, Milano, Italy*
[223] *Department of Applied Physics, Fukuoka University, 8-19-1 Nanakuma, Jonan, Fukuoka City, Fukuoka 814-0180, Japan*
[224] *University of Cambridge, Cambridge CB2 1TN, United Kingdom*
[225] *University of Lancaster, Lancaster LA1 4YW, United Kingdom*
[226] *College of Industrial Technology, Nihon University, 1-2-1 Izumi, Narashino City, Chiba 275-8575, Japan*
[227] *Faculty of Engineering, Niigata University, 8050 Ikarashi-2-no-cho, Nishi-ku, Niigata City, Niigata 950-2181, Japan*
[228] *Department of Physics, Tamkang University, No. 151, Yingzhuan Rd., Danshui Dist., New Taipei City 25137, Taiwan*
[229] *Rutherford Appleton Laboratory, Didcot OX11 0DE, United Kingdom*
[230] *Department of Physical Sciences, Aoyama Gakuin University, 5-10-1 Fuchinobe, Sagamihara City, Kanagawa 252-5258, Japan*
[231] *Helmut Schmidt University, D-22043 Hamburg, Germany*
[232] *Nambu Yoichiro Institute of Theoretical and Experimental Physics (NITEP), Osaka Metropolitan University, 3-3-138 Sugimoto-cho, Sumiyoshi-ku, Osaka City, Osaka 558-8585, Japan*
[233] *Directorate of Construction, Services & Estate Management, Mumbai 400094, India*
[234] *Observatoire Astronomique de Strasbourg, 11 Rue de l'Université, 67000 Strasbourg, France*
[235] *Faculty of Physics, University of Białystok, 15-245 Białystok, Poland*
[236] *National Astronomical Observatories, Chinese Academic of Sciences, 20A Datun Road, Chaoyang District, Beijing, China*
[237] *School of Astronomy and Space Science, University of Chinese Academy of Sciences, 20A Datun Road, Chaoyang District, Beijing, China*
[238] *Sungkyunkwan University, Seoul 03063, Republic of Korea*
[239] *Department of Physics, Ulsan National Institute of Science and Technology (UNIST), 50 UNIST-gil, Ulju-gun, Ulsan 44919, Republic of Korea*
[240] *Institute for Cosmic Ray Research, The University of Tokyo, 5-1-5 Kashiwa-no-Ha, Kashiwa City, Chiba 277-8582, Japan*
[241] *Chung-Ang University, Seoul 06974, Republic of Korea*
[242] *University of Washington Bothell, Bothell, WA 98011, USA*
[243] *Laboratoire de Physique et de Chimie de l'Environnement, Université Joseph KI-ZERBO, 9GH2+3V5, Ouagadougou, Burkina Faso*
[244] *Ewha Womans University, Seoul 03760, Republic of Korea*
[245] *National Institute for Mathematical Sciences, Daejeon 34047, Republic of Korea*
[246] *Korea Astronomy and Space Science Institute, Daejeon 34055, Republic of Korea*
[247] *Department of Astronomy and Space Science, Chungnam National University, 9 Daehak-ro, Yuseong-gu, Daejeon 34134, Republic of Korea*
[248] *Institute of Particle and Nuclear Studies (IPNS), High Energy Accelerator Research Organization (KEK), 1-1 Oho, Tsukuba City, Ibaraki 305-0801, Japan*
[249] *Division of Science, National Astronomical Observatory of Japan, 2-21-1 Osawa, Mitaka City, Tokyo 181-8588, Japan*
[250] *Nagoya University, Nagoya, 464-8601, Japan*
[251] *Department of Physics, Aristotle University of Thessaloniki, 54124 Thessaloniki, Greece*
[252] *Bard College, Annandale-On-Hudson, NY 12504, USA*
[253] *Technical University of Braunschweig, D-38106 Braunschweig, Germany*
[254] *Institute of Mathematics, Polish Academy of Sciences, 00656 Warsaw, Poland*
[255] *Astronomical Observatory, Jagiellonian University, 31-007 Cracow, Poland*
[256] *Department of Physics and Astronomy, University of Padova, Via Marzolo, 8-35151 Padova, Italy*
[257] *Sezione di Padova, Istituto Nazionale di Fisica Nucleare (INFN), Via Marzolo, 8-35131 Padova, Italy*

[258] *Department of Physics, Nagoya University, ES building, Furocho, Chikusa-ku, Nagoya, Aichi 464-8602, Japan*
[259] *Université de Montréal/Polytechnique, Montreal, Quebec H3T 1J4, Canada*
[260] *Indian Institute of Science Education and Research, Kolkata, Mohanpur, West Bengal 741252, India*
[261] *Seoul National University, Seoul 08826, Republic of Korea*
[262] *Department of Computer Simulation, Inje University, 197 Inje-ro, Gimhae, Gyeongsangnam-do 50834, Republic of Korea*
[263] *NAVIER, École des Ponts, Univ Gustave Eiffel, CNRS, Marne-la-Vallée, France*
[264] *Gravitational Wave Science Project, National Astronomical Observatory of Japan (NAOJ), Mitaka City, Tokyo 181-8588, Japan*
[265] *Department of Physics, National Cheng Kung University, No.1, University Road, Tainan City 701, Taiwan*
[266] *The Chinese University of Hong Kong, Shatin, NT, Hong Kong*
[267] *St. Thomas University, Miami Gardens, FL 33054, USA*
[268] *Scuola Normale Superiore, I-56126 Pisa, Italy*
[269] *Institució Catalana de Recerca i Estudis Avançats, E-08010 Barcelona, Spain*
[270] *Institut de Física d'Altes Energies, E-08193 Barcelona, Spain*
[271] *Institut fuer Theoretische Astrophysik, Zentrum fuer Astronomie Heidelberg, Universitaet Heidelberg, Albert Ueberle Str. 2, 69120 Heidelberg, Germany*
[272] *Institucio Catalana de Recerca i Estudis Avançats (ICREA), Passeig de Lluís Companys, 23, 08010 Barcelona, Spain*
[273] *Research Center for Space Science, Advanced Research Laboratories, Tokyo City University, 3-3-1 Ushikubo-Nishi, Tsuzuki-Ku, Yokohama, Kanagawa 224-8551, Japan*
[274] *Tsinghua University, Beijing 100084, China*
[275] *Institut des Hautes Etudes Scientifiques, F-91440 Bures-sur-Yvette, France*
[276] *Faculty of Law, Ryukoku University, 67 Fukakusa Tsukamoto-cho, Fushimi-ku, Kyoto City, Kyoto 612-8577, Japan*
[277] *Phenikaa Institute for Advanced Study (PIAS), Phenikaa University, Yen Nghia, Ha Dong, Hanoi, Vietnam*
[278] *University of Stavanger, 4021 Stavanger, Norway*
[279] *Physics Program, Graduate School of Advanced Science and Engineering, Hiroshima University, 1-3-1 Kagamiyama, Higashihiroshima City, Hiroshima 739-8526, Japan*
[280] *GRAPPA, Anton Pannekoek Institute for Astronomy and Institute for High-Energy Physics, University of Amsterdam, 1098 XH Amsterdam, Netherlands*
[281] *University College London, London WC1E 6BT, United Kingdom*
[282] *Observatoire de Paris, 75014 Paris, France*
[283] *Laboratoire Univers et Théories, Observatoire de Paris, 92190 Meudon, France*
[284] *Graduate School of Science and Technology, Niigata University, 8050 Ikarashi-2-no-cho, Nishi-ku, Niigata City, Niigata 950-2181, Japan*
[285] *University of Maryland, Baltimore County, Baltimore, MD 21250, USA*
[286] *CSIR-Central Glass and Ceramic Research Institute, Kolkata, West Bengal 700032, India*
[287] *Consiglio Nazionale delle Ricerche - Istituto dei Sistemi Complessi, I-00185 Roma, Italy*
[288] *Department of Astronomy, Yonsei University, 50 Yonsei-Ro, Seodaemun-Gu, Seoul 03722, Republic of Korea*
[289] *Department of Physics, University of Guadalajara, Av. Revolucion 1500, Colonia Olimpica C.P. 44430, Guadalajara, Jalisco, Mexico*
[290] *Hobart and William Smith Colleges, Geneva, NY 14456, USA*
[291] *INAF, Osservatorio Astronomico di Padova, I-35122 Padova, Italy*
[292] *Dipartimento di Ingegneria, Università del Sannio, I-82100 Benevento, Italy*
[293] *Museo Storico della Fisica e Centro Studi e Ricerche "Enrico Fermi", I-00184 Roma, Italy*
[294] *Kennesaw State University, Kennesaw, GA 30144, USA*
[295] *Subatech, CNRS/IN2P3 - IMT Atlantique - Nantes Université, 4 rue Alfred Kastler BP 20722 44307 Nantes CÉDEX 03, France*
[296] *Universidad de Antioquia, Medellín, Colombia*
[297] *Departamento de Física - ETSIDI, Universidad Politécnica de Madrid, 28012 Madrid, Spain*
[298] *Department of Electronic Control Engineering, National Institute of Technology, Nagaoka College, 888 Nishikatakai, Nagaoka City, Niigata 940-8532, Japan*
[299] *Trinity College, Hartford, CT 06106, USA*
[300] *Dipartimento di Fisica e Scienze della Terra, Università Degli Studi di Ferrara, Via Saragat, 1, 44121 Ferrara FE, Italy*
[301] *Faculty of Science, Toho University, 2-2-1 Miyama, Funabashi City, Chiba 274-8510, Japan*
[302] *Indian Institute of Technology, Palaj, Gandhinagar, Gujarat 382355, India*
[303] *Kavli Institute for Astronomy and Astrophysics, Peking University, Yiheyuan Road 5, Haidian District, Beijing 100871, China*
[304] *Laboratoire MSME, Cité Descartes, 5 Boulevard Descartes, Champs-sur-Marne, 77454 Marne-la-Vallée Cedex 2, France*
[305] *Faculty of Information Science and Technology, Osaka Institute of Technology, 1-79-1 Kitayama, Hirakata City, Osaka 573-0196, Japan*
[306] *NASA Goddard Space Flight Center, Greenbelt, MD 20771, USA*
[307] *Faculty of Science and Technology, Kochi University, 2-5-1 Akebono-cho, Kochi-shi, Kochi 780-8520, Japan*

[308] Laboratoire de Physique de l'École Normale Supérieure, ENS, (CNRS, Université PSL, Sorbonne Université, Université Paris Cité), F-75005 Paris, France
[309] Faculty of Physics, University of Warsaw, Ludwika Pasteura 5, 02-093 Warszawa, Poland
[310] Laser Interferometry and Gravitational Wave Astronomy, Max Planck Institute for Gravitational Physics, Callinstrasse 38, 30167 Hannover, Germany
[311] The Hakubi Center for Advanced Research, Kyoto University, Yoshida-honmachi, Sakyou-ku, Kyoto City, Kyoto 606-8501, Japan
[312] Department of Physics, Kyoto University, Kita-Shirakawa Oiwake-cho, Sakyou-ku, Kyoto City, Kyoto 606-8502, Japan
[313] Yukawa Institute for Theoretical Physics (YITP), Kyoto University, Kita-Shirakawa Oiwake-cho, Sakyou-ku, Kyoto City, Kyoto 606-8502, Japan
[314] University of Catania, Department of Physics and Astronomy, Via S. Sofia, 64, 95123 Catania CT, Italy
[315] National Institute of Technology, Fukui College, Geshi-cho, Sabae-shi, Fukui 916-8507, Japan
[316] Department of Communications Engineering, National Defense Academy of Japan, 1-10-20 Hashirimizu, Yokosuka City, Kanagawa 239-8686, Japan
[317] Eindhoven University of Technology, 5600 MB Eindhoven, Netherlands
[318] Kavli Institute for the Physics and Mathematics of the Universe (Kavli IPMU), WPI, The University of Tokyo, 5-1-5 Kashiwa-no-Ha, Kashiwa City, Chiba 277-8583, Japan
[319] Department of Astronomy, Beijing Normal University, Xinjiekouwai Street 19, Haidian District, Beijing 100875, China
[320] School of Physics and Technology, Wuhan University, Bayi Road 299, Wuchang District, Wuhan, Hubei, 430072, China

(Compiled: 11 November 2025)

## ABSTRACT

On 2023 November 23 the two LIGO observatories both detected GW231123, a gravitational-wave signal consistent with the merger of two black holes with masses $137^{+23}_{-18}\,M_\odot$ and $101^{+22}_{-50}\,M_\odot$ (90% credible intervals), at luminosity distance 0.7–4.1 Gpc and redshift of $0.40^{+0.27}_{-0.25}$, and a network signal-to-noise ratio of ∼20.7. Both black holes exhibit high spins, $0.90^{+0.10}_{-0.19}$ and $0.80^{+0.20}_{-0.52}$ respectively. A massive black hole remnant is supported by an independent ringdown analysis. Some properties of GW231123 are subject to large systematic uncertainties, as indicated by differences in inferred parameters between signal models. The primary black hole lies within or above the theorized mass gap where black holes between 60–130 $M_\odot$ should be rare due to pair instability mechanisms, while the secondary spans the gap. The observation of GW231123 therefore suggests the formation of black holes from channels beyond standard stellar collapse, and that intermediate-mass black holes of mass ∼200 $M_\odot$ form through gravitational-wave driven mergers.

## 1. INTRODUCTION

From 2015 to 2020 the LIGO-Virgo-KAGRA Collaboration identified 69 gravitational-wave signals from binary black hole mergers with false alarm rates below one per year (Aasi et al. 2015; Acernese et al. 2015; Abbott et al. 2020c; Akutsu et al. 2020; Abbott et al. 2023a). Of these, the most massive was the source of GW190521, with a merger remnant of ∼140 $M_\odot$ (Abbott et al. 2020d,e). The small number of observable cycles of GW190521 limits our ability to accurately infer the source's properties, and subsequent studies have proposed a wide range of alternative interpretations, including highly eccentric orbits, dynamical capture scenarios, exotic object mergers, and cosmic string collapse (Gayathri et al. 2022; Romero-Shaw et al. 2020a; Gamba et al. 2023; Calderón Bustillo et al. 2021b; Aurrekoetxea et al. 2024). Here we present a yet more challenging signal: GW231123_135430 (hereafter referred to as GW231123), confidently observed through a coincident detection in both the LIGO Hanford and Livingston detectors during the first part of their fourth observing run, O4a (2023 May 24 to 2024 January 16). The combination of data from the two observatories was essential in making a confident detection.

GW231123 consists of ∼5 cycles over a frequency range of 30–80 Hz, similar to GW190521. We interpret GW231123 as a binary-black-hole merger and infer a total mass between 190 $M_\odot$ and 265 $M_\odot$ and high component black-hole spins (∼0.9 and ∼0.8). While a few gravitational-wave candidates have been observed with similarly high total masses (Abbott et al. 2023a; Wadekar et al. 2023), none have false alarm rates less than 1 per year; in addition, GW231123 has both a large signal-to-noise ratio and high statistical significance. Such high masses and spins pose a challenge to our most accurate waveform models, leading to larger uncertainties in the black-hole masses, and the binary

* Deceased, September 2024.

orientation and distance, than any previous signal of comparable strength.

Pair-instability supernova (PISN) and pulsational PISNe are expected to preclude stellar collapse to black holes with masses $\approx$ 60–130$M_\odot$ (Farmer et al. 2019; Farmer et al. 2020; Woosley & Heger 2021; Hendriks et al. 2023), and the majority of the astrophysical population of black holes inferred from gravitational-wave catalogs lies below this gap (Abbott et al. 2023b). The large measurement uncertainties in the source of GW231123 mean that the primary black hole may be within or *beyond* the mass gap, while the secondary mass spans the entire gap within the 90% credible intervals of our analysis. It is also possible that the two black-hole masses lie on either side of the gap. The scenarios with the highest probability require a formation channel that populates the mass gap, such as prior stellar mergers (e.g., Di Carlo et al. 2020; Renzo et al. 2020a; Kremer et al. 2020), black-hole mergers (for a review, see Gerosa & Fishbach 2021 and references therein), or accretion in a gaseous environment (e.g., McKernan et al. 2012). Though these channels can produce highly spinning black holes (e.g., a characteristic value of $\sim 0.7$ for black-hole mergers), the inferred spins may be higher than typical of remnant black holes and those of remnants from mergers previously observed with gravitational waves.

In this paper we present the LIGO-Virgo-KAGRA analysis of GW231123. In Section 2, we establish GW231123 as a confident gravitational wave (GW) detection. In Section 3, we discuss the data quality at the time of the observation. In Section 4, we first discuss our treatment of waveform uncertainties, then present the source properties and additional waveform consistency checks. In Section 5, we analyse the ringdown portion to test the consistency of a black hole (BH) remnant interpretation. In Section 6 we present a range of potential astrophysical implications. Although the binary black hole (BBH) merger scenario presented throughout this paper is the most plausible astrophysical explanation for the source of GW231123, alternative scenarios cannot be ruled out and we discuss a selection of these in Section 7. We conclude in Section 8, and provide additional material in support of our results in a series of appendices.

## 2. DETECTION SIGNIFICANCE

On 2023 November 23, at 13:54:30 UTC, the Advanced LIGO Hanford and Livingston detectors observed the GW transient GW231123. The Advanced Virgo and KAGRA detectors were not online at this time. Despite its short duration ($\sim$0.1 s) and limited bandwidth (Figure 1), coherent detection in both detectors allowed the signal to be identified in our analyses with high statistical significance, reported in terms of inverse false-alarm rate (IFAR); see Table 1. Without coincidence in two or more detectors, a high-mass BBH signal like GW231123 would likely have been dismissed as a noise artefact (glitch). It was first detected by PyCBC Live, a matched-filter search for compact binaries (Allen 2005; Usman et al. 2016; Nitz et al. 2017; Dal Canton et al. 2021). It was also reported by coherent WaveBurst (cWB)-BBH, a minimally modelled coherent excess power search (Mishra et al. 2025). The cWB-BBH search uses the *WaveScan* time–frequency (TF) transformation (Klimenko 2022) and ranks identified triggers using a machine-learning classifier trained specifically on BBH signals (Mishra et al. 2021, 2022, 2025). In addition, the event was also detected by two model-independent low-latency cWB searches, or burst searches, designed to identify generic GW transients: cWB-2G and cWB-XP. The former is based on the *Wilson–Debauchies–Meyer* TF transformation (Klimenko et al. 2008, 2016a; Drago et al. 2020), while the latter uses the *WaveScan* TF transformation. Both apply a machine-learning classifier (XGBoost), trained on generic white-noise-bursts to rank identified triggers (Szczepańczyk et al. 2023). For further details on model-independent searches, see Abac et al. (2025a).

Subsequent offline or archival reanalyses using improved background estimation and data quality information further increased the event's statistical significance in both the PyCBC and cWB pipelines (Table 1). Furthermore, two additional matched-filter searches, GstLAL (Messick et al. 2017; Sachdev et al. 2019; Hanna et al. 2020; Cannon et al. 2021; Sakon et al. 2024; Ewing et al. 2024; Tsukada et al. 2023; Joshi et al. 2025) and MBTA (Adams et al. 2016; Aubin et al. 2021; Alléné et al. 2025), which did not detect this event with significant confidence in low-latency (IFAR higher than 1 year), recovered it in their offline analyses. These searches differ from PyCBC (Davies et al. 2020; Chandra et al. 2021b; Davis et al. 2022; Kumar & Dent 2024) in their implementation and use of signal–noise discriminators. GstLAL's enhanced significance (the higher IFAR in Table. 1) is primarily driven by a higher mass extension of the search with specific settings to compute the background for such higher mass mergers accurately. More details of the settings are provided in (**?**Joshi et al. 2025). These changes improved the signal and noise models in this part of the parameter space in general, leading to a better recovery of this high mass signal. Additionally, cWB-GMM, an entirely offline model-independent search, uses Gaussian Mixture

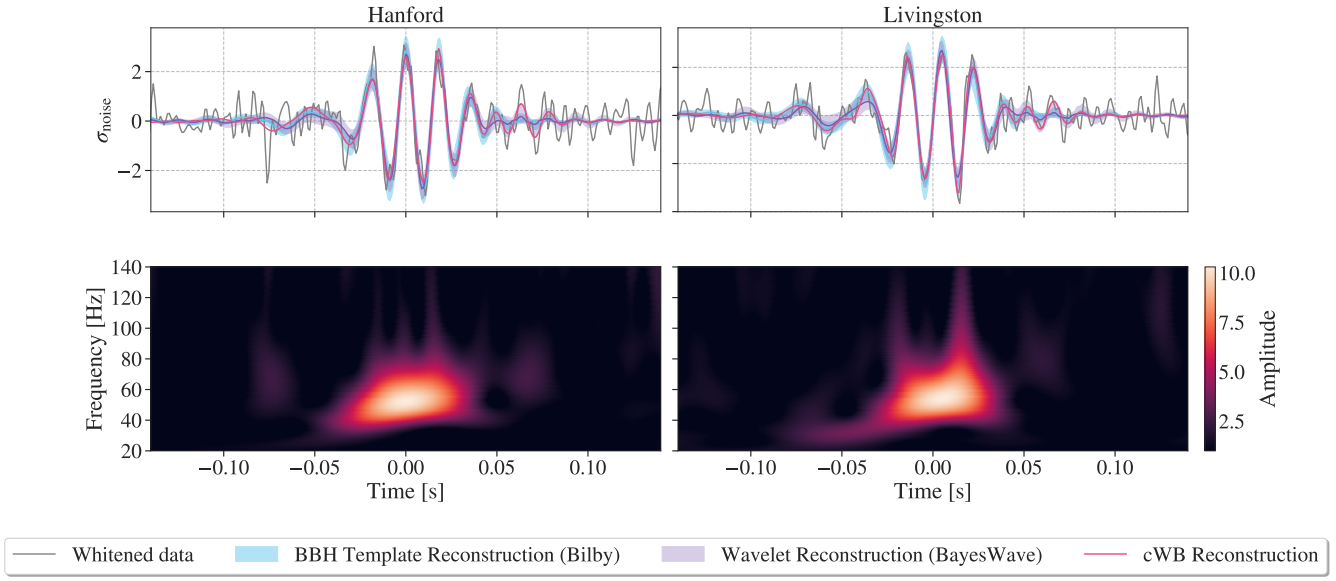


**Figure 1.** The GW event GW231123 as observed by the LIGO Hanford (left panels) and LIGO Livingston (right panels) detectors. Time is measured relative to 2023 November 23 at 13:54:30.619 UTC. The top panels show the time-domain strain data (black), sampled at 1024 Hz, whitened and then bandpass-filtered with a passband from 20 Hz to 256 Hz (Abbott et al. 2020a). Also shown are the point-estimate whitened waveform from the cWB-BBH search (red), the 90% credible interval of whitened waveforms inferred from a coherent Bayesian analysis using the combined samples from five BBH waveform models (blue bands), and the 90% credible interval inferred from BayesWave using a generic wavelet-based model (shaded purple). The vertical axis is in units of the noise standard deviation, $\sigma_{\rm noise}$. The bottom panels display the corresponding whitened time-frequency representations of the strain data, obtained using a continuous wavelet transform (CWT) with a Morlet–Gabor wavelet. The color scale is in units of the amplitude of the CWT coefficients.

**Table 1.** Properties of the detection of GW231123 by various search pipelines.

| **CBC pipelines** | Offline SNR | Online IFAR (yr) | Offline IFAR (yr) |
|---|---|---|---|
| PyCBC | 19.9 | $> 100$ | 160 |
| GstLAL | 20.1 | $2 \times 10^{-4}$ | $> 10000$ |
| MBTA | 19.0 | – | 60 |
| cWB-BBH | 21.8 | $> 490$ | 9700 |
| **Burst pipelines** | | | |
| cWB-2G | 21.4 | $> 250$ | $> 490$ |
| cWB-XP | 21.1 | $> 240$ | $> 480$ |
| cWB-GMM | 21.4 | – | 100 |

NOTE—The significance is reported in terms of the inverse false-alarm rate (FAR) (IFAR) = 1/FAR as measured by each search.

Models (Gayathri et al. 2020; Lopez et al. 2022; Smith et al. 2024) to rerank the triggers identified by cWB-2G.

The differences in the IFARs reported by the offline search pipelines—despite broadly consistent signal-to-noise ratios (SNRs)—primarily reflect differences in their ability to separate GW231123-like signals from background noise in a comparable parameter range. Similar discrepancies have been observed previously, particularly between matched-filter and minimally-modelled searches, when searching for non-eccentric intermediate-mass black hole (IMBH) binaries (Calderón Bustillo et al. 2018; Chandra et al. 2020; Abbott et al. 2020d; Chandra et al. 2021a; Szczepańczyk et al. 2021). These differences arise not only from how effectively each search separates signals from glitches, but also from the differing approaches used to estimate the noise background.

To assess whether the observed variation in statistical significance across pipelines is consistent with expectations, we conducted a dedicated injection campaign. Using the NRSur7dq4 (NRSur) waveform model (Varma et al. 2019), we simulated ∼8000 non-eccentric BBH signals with intrinsic parameters consistent with those inferred for GW231123 (Section 4). We sampled the sky positions and binary orientations isotropically and drew redshifts uniformly in comoving volume up to $z_{\rm max} = 1.5$, assuming a flat ΛCDM cosmology (Ade et al. 2016). We added these simulated signals uniformly over several days around the event and re-ran our offline search pipelines using the same configuration as applied to the real data.

We found that for simulated signals observed in both Advanced LIGO detectors, the CBC searches recovered

the following fractions with a IFAR above 100 years, cWB-BBH 32%, PyCBC 27%, GstLAL 41%, and MBTA 16%. For the Burst searches, cWB-2G and cWB-XP each recovered 22%, while cWB-GMM recovered 10%. Since Burst searches identify coherent power across the detector network without relying on BBH waveform models, their efficiencies are not directly comparable to CBC searches. However, within each search category, detection pipelines reporting a higher IFAR for GW231123 consistently demonstrated higher recovery fractions for simulated signals with masses and spins representative of those inferred for GW231123.

Given that all pipelines detected GW231123 with an IFAR above the typical threshold of 1 year used for population analyses, and a detailed background study for one pipeline (cWB-BBH) identified GW231123 with an IFAR of 9700 years, we consider GW231123 to be a confident detection.

## 3. DATA QUALITY

The event GW231123 was detected during the first part of the fourth observing run (O4a), a time when the LIGO Hanford and LIGO Livingston detectors were observing with a typical binary neutron star inspiral range of 152 Mpc and 160 Mpc (Capote et al. 2025). The detectors' data were calibrated in near real-time to produce the online dataset used for low-latency searches (Abbott et al. 2020b; Klimenko et al. 2016b; Tsukada et al. 2023; Ewing et al. 2024; Dal Canton et al. 2021; Chu et al. 2022; Aubin et al. 2021) and parameter estimation (Singer & Price 2016; Ashton et al. 2019; Pankow et al. 2015). The calibration process subtracts linear spectral features from known instrumental sources, identified through auxiliary witness sensors, and intentionally injected calibration lines used to measure the instruments' response at various frequencies (Viets et al. 2018a; Sun et al. 2020, 2021).

Following the data-quality procedures established for O4a (Soni et al. 2025), including broadband noise subtraction (Vajente et al. 2020) and data-quality report analysis routines (Davis et al. 2021), detector data surrounding the event were evaluated for signs of non-Gaussian excess power (glitches) within the target time-frequency analysis window using a spectrogram-based glitch-identification tool (Vazsonyi & Davis 2023). It was determined that glitches were present in each detector around, but not coincident with the event.

From spectrograms, we determined that a glitch was present in the LIGO Hanford data 1.7–1.1 s before the event, in a frequency range between 15–30 Hz. The glitch is possibly related to the LIGO Hanford differential arm control loop (Aasi et al. 2015). This control loop leads to nonstationary noise from the high root-mean-square drive applied to the electrostatic drive actuator. This issue has been fixed in the second part of the fourth observing run (Vajente 2024). This glitch was close to the event and within the time–frequency window used to infer the source properties, so BayesWave (Cornish & Littenberg 2015; Cornish et al. 2021; Chatziioannou et al. 2021) was used to model simultaneously the compact binary signal and the glitch (Soni et al. 2025). We removed this non-Gaussianity from the data by subtracting a phenomenological, wavelet-based model of the excess power noise (Hourihane et al. 2022; Ghonge et al. 2024). The glitch-subtracted data successfully passed the validation process, which compares the residual noise to Gaussian noise (Soni et al. 2025; Vazsonyi & Davis 2023). Additional broadband non-stationary noise was present in the Hanford detector in the hours of data surrounding GW231123, but we found no evidence that this impacted the analysis of GW231123.

In LIGO Livingston data, a glitch was identified 3.0–2.0 s before the event, in a frequency range between 10–20 Hz. Given that LIGO Livingston had recurring low-frequency scattered light glitches (Soni et al. 2025), this glitch was likely caused by scattered light. We determined the time–frequency profile of the glitch to have no measurable effect on the GW231123 analysis, so the analyses from here on use the LIGO Livingston original data and the LIGO Hanford glitch-subtracted data.

## 4. SOURCE PROPERTIES

In the following, we describe the methods used to estimate the source properties (Section 4.1), and how we deal with the systematic differences in results from multiple signal models (Section 4.2). Having discussed our methods and sources of error, we present and discuss our estimates of the source properties in Section 4.3, and finally our waveform consistency checks (Section 4.4).

### 4.1. *Methods*

We report the properties of GW231123 using signal models for non-eccentric BBH mergers in a coherent Bayesian analysis (Abbott et al. 2016a) of the LIGO Hanford and LIGO Livingston data around the time of GW231123. (We discuss potential eccentricity further in Section 6.) We calculate the likelihood using 8 s of data (6 s before and 2 s after the reported merger time of GW231123), and consider frequencies within the range 20–448 Hz. This range was chosen to contain the signal based on preliminary analyses at the time of the event, and to avoid loss of power at high frequencies due to low-pass filtering of the data (Abac et al. 2025b). All analyses employ standard priors used in previous analyses (Abbott et al. 2021a, 2024a, 2023a), and we use a

Planck 2015 ΛCDM cosmology (Ade et al. 2016). The NRSur analysis employs a reduced prior mass range due to model constraints, mass ratios below 6:1. The other models employ a wider mass prior, mass ratios below ∼10:1, and no posterior support is found beyond the NRSur analysis. We characterise the detector noise via the median estimate of different power spectral density (PSD) realizations calculated with BayesWave (Cornish & Littenberg 2015; Littenberg & Cornish 2015). As done previously (Chatziioannou et al. 2019; Abbott et al. 2023a), we calculate the median PSD for data containing the trigger. To sample the posterior distribution, we interface with the dynesty nested sampling package (Speagle 2020) via the bilby library (Ashton et al. 2019; Romero-Shaw et al. 2020b). We present results with 1000 live points, and verify that the results remain consistent when the number of live points is increased to 3000, as well as when we lower the frequency range to include data between 16–20 Hz.

### 4.2. *Waveform Systematics*

The source properties of GW231123 lie in a challenging region of parameter space for current waveform models, to such an extent that measurements using different models show significant disagreement, with multiple parameters failing to agree within 90% credible intervals. (See Appendix A for examples.) For typical signals, our models are well within our observations' accuracy requirements, and the level of model disagreement for GW231123 has not been seen in any previous LVK GW observation with moderate SNRs (>12). All models show strong support for spins >0.8, and since no theoretical signal model is calibrated to numerical-relativity (NR) waveforms from precessing binaries with spins above 0.8, waveform uncertainties are one possible cause of the measurement differences. Hence, before presenting the source properties, we describe how we quantify waveform-model uncertainties. We do not study in detail the impact of Gaussian noise fluctuations or low-SNR glitches that are difficult to identify and mitigate using the methods presented in Section 3.

We consider five state-of-the-art inspiral–merger–ringdown (IMR) signal models, NRSur7dq4 (NRSur; Varma et al. 2019), SEOBNRv5PHM (v5PHM; Ramos-Buades et al. 2023a), IMRPhenomTPHM (TPHM; Estellés et al. 2022a), IMRPhenomXPHM (XPHM; Colleoni et al. 2025) and IMRPhenomXO4a (XO4a; Thompson et al. 2024). The first three model the signal in the time domain while the latter two natively employ the frequency domain. All models use information from numerical relativity to inform the merger-ringdown in the aligned-spin sector. However only NRSur; fully interpolates two-spin precessing systems in the precessing sector, while XO4a is calibrated to single-spin precessing systems; all other models employ results from post-Newtonian and perturbation theory through merger and ringdown. (More details are given in Appendix A.) The model papers referenced here include studies to assess the accuracy of these models across the BBH parameter space, but here we focus on the likely region of parameter space for this observation; high total mass, $q = m_2/m_1 \geq 1/3$, and moderate to high spins.

We quantify the models' accuracy against NR results, including a set of simulations that extend up to spins of 0.95 (Boyle et al. 2019; Hamilton et al. 2024; Scheel et al. 2025). A standard waveform accuracy measure is the mismatch between two waveforms (Cutler & Flanagan 1994), where waveform uncertainties will not bias a parameter measurement if the model's mismatch uncertainty is less than $\chi^2_k(1-p)/(2\rho^2)$ (McWilliams et al. 2010; Baird et al. 2013), where $\rho$ is the SNR and $\chi^2_k(1-p)$ is the chi-square value for $k$ degrees of freedom at probability $p$. For single-parameter measurements $k = 1$ provides a lower bound (Thompson et al. 2025), so the mismatch criterion for the 90% credible interval at $\rho = 22$ is $1.35/\rho^2 = 0.0028$. Figure 2 reports the distribution of mismatches of each model against 1123 NR waveforms with $q \geq 1/3$, all scaled to the redshifted (detector-frame) total mass $(1+z)M = 300\,M_\odot$, at six equally spaced inclinations in $\cos\iota$ from $\iota = 0$ to $\pi/2$ inclusive. The mismatches are calculated for precessing systems (Schmidt et al. 2015; Harry et al. 2016) following the procedure described in Hamilton et al. (2021), maximising over time shifts, a global phase and template polarisation and optimising over in-plane spin rotations. A subset of the simulations come from the third release of the SXS catalog (Scheel et al. 2025) and contain GW memory, which introduces a constant late-time offset that we handle for the mismatch calculations with a highpass filtering technique (Xu et al. 2024; Valencia et al. 2024; Chen et al. 2024) to mitigate possible artefacts in the Fourier domain. We employ the same PSD for the LIGO Livingston detector as utilised in the coherent Bayesian analysis. NRSur performs better than the other models (by roughly an order of magnitude for low-spin cases), and all other models have comparable accuracy. However, NRSur does not meet the conservative accuracy criterion for all cases, and for spins greater than 0.8 the mismatches are higher in 10% of 98 cases. Even if we apply a less conservative mismatch criterion from the literature (e.g., with $k = 7$ for non-eccentric binaries and $p = 0.67$ (Chatziioannou et al. 2017; Scheel et al. 2025) we have 0.0072) there are configurations

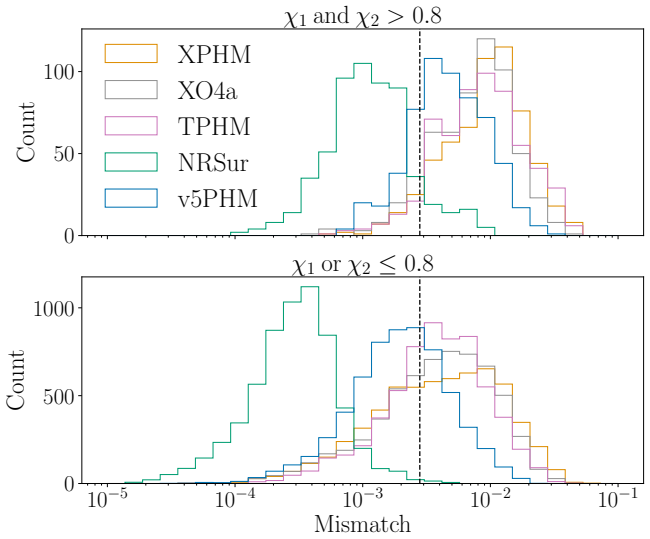


**Figure 2.** Mismatch accuracy of the waveform models considered in this paper against 1123 NR simulations at a total mass of $300M_\odot$ and a range of inclinations between $\iota = 0$ and $\pi/2$. The vertical dashed line at a mismatch of 0.0028 shows the conservative criterion discussed in the text.

where NRSur exceeds the criterion (2%). The relative accuracy of models is also not uniform across all cases, e.g., we find cases in which other models show comparable or improved performance relative to NRSur.

To test whether these waveform uncertainties will result in biases, we performed our standard Bayesian parameter estimation analysis on a series of NR injections, as detailed in Appendix A. We observe that, while the five models considered here perform well for most signals, there are configurations where *all models* may incur biases for massive high-spin signals. We also find that the relative performance of each model can change in the presence of Gaussian noise, although this requires more detailed study in future work. To properly correct for this, we would ideally marginalise over waveform uncertainties or incorporate model accuracy into Bayesian analyses (Read 2023; Khan 2024; Hoy et al. 2024; Pompili et al. 2024; Kumar et al. 2025; Mezzasoma et al. 2025). Without access to a model of the waveform-model uncertainties, we follow what has been done previously (Abbott et al. 2016a) and combine the results from multiple models to marginalise over the model uncertainties. In choosing models in addition to NRSur, we note that all other models exhibit a comparable range of mismatches, and no model is clearly preferred in our injection studies, and so we include all five state-of-the-art models. We combine posterior results inferred from NRSur, v5PHM, TPHM, XPHM, XO4a with equal weight and report the combined samples throughout this paper. To illustrate the variation between the combined results and single models, in some figures we also show the NRSur results. In some analyses we expect the choice of model to have little impact, e.g., the detection significance study in Section 2, and in these cases, we use only the NRSur samples.

**Table 2.** Source properties of GW231123.

| | |
|---|---|
| Primary mass $m_1/\mathrm{M}_\odot$ | $137^{+23}_{-18}$ |
| Secondary mass $m_2/\mathrm{M}_\odot$ | $101^{+22}_{-50}$ |
| Mass ratio $q = m_2/m_1$ | $0.74^{+0.23}_{-0.37}$ |
| Total mass $M/\mathrm{M}_\odot$ | $236^{+30}_{-47}$ |
| Final mass $M_\mathrm{f}/\mathrm{M}_\odot$ | $222^{+28}_{-42}$ |
| Primary spin magnitude $\chi_1$ | $0.90^{+0.10}_{-0.19}$ |
| Secondary spin magnitude $\chi_2$ | $0.80^{+0.20}_{-0.52}$ |
| Effective inspiral spin $\chi_\mathrm{eff}$ | $0.32^{+0.25}_{-0.41}$ |
| Effective precessing spin $\chi_\mathrm{p}$ | $0.77^{+0.18}_{-0.19}$ |
| Final spin $\chi_\mathrm{f}$ | $0.84^{+0.08}_{-0.16}$ |
| Luminosity distance $D_\mathrm{L}/\mathrm{Gpc}$ | $2.2^{+1.9}_{-1.5}$ |
| Inclination angle $\theta_\mathrm{JN}/\mathrm{rad}$ | $1.3^{+0.9}_{-0.9}$ |
| Source redshift $z$ | $0.40^{+0.27}_{-0.25}$ |
| Network matched filter SNR $\rho$ | $20.7^{+0.2}_{-0.3}$ |

Note—We report combined results from five models that have been mixed with equal weight. In most cases we present the median value of the 1D marginalized posterior distribution and the 90% symmetric credible intervals. For properties that have physical bounds, including the primary spin magnitude, secondary spin magnitude, mass ratio, effective precessing-spin, inclination angle and the final spin of the remnant, we report the median value as well as the 90% highest posterior density (HPD) credible interval. The inclination of the binary is defined as the angle between the total angular momentum and the line of sight, $\theta_\mathrm{JN}$. All mass measurements are reported in the source frame. Our results are reported at a reference frequency of 10 Hz. Results obtained with individual models can be found in Appendix B.

### 4.3. *Inference*

Our Bayesian analysis indicates that GW231123 was produced from a high-mass compact binary merger with highly spinning components. We infer individual source component masses $m_1 = 137^{+23}_{-18}\,M_\odot$ and $m_2 = 101^{+22}_{-50}\,M_\odot$ with spin magnitudes $\chi_1 = 0.90^{+0.10}_{-0.19}$ and $\chi_2 = 0.80^{+0.20}_{-0.52}$. We present a summary of the key source properties of GW231123 in Table 2. Unless otherwise stated, we report all mass measurements in the source frame, and all measurements correspond to the median and 90% symmetric credible level.

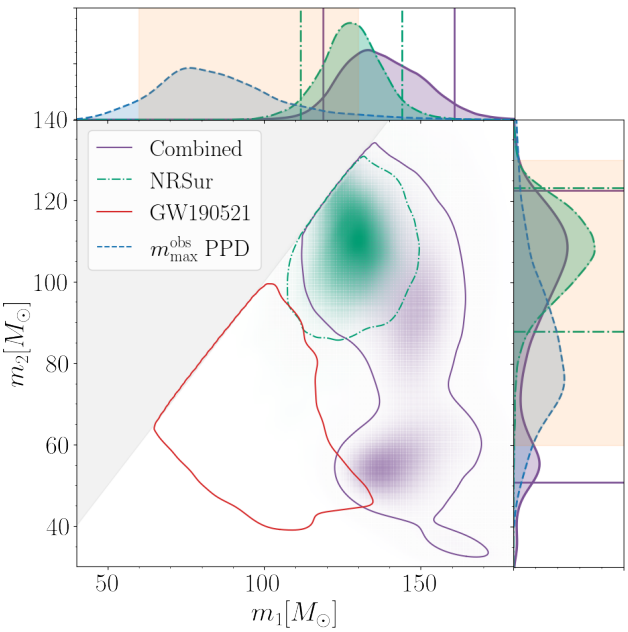


**Figure 3.** The posterior distribution of the primary and secondary source masses. We show the posterior distribution resulting from equally combining samples from five waveform models that include precession and higher-order multipoles (purple). We separately show the posterior distribution obtained with NRSur (green dash dot). We compare against estimates for the source frame masses of GW190521 (red solid, Abbott et al. 2020d,e, 2023a). Each contour, as well as the colored horizontal and vertical lines, shows the 90% credible intervals. In blue dashed we show the posterior predictive distribution for the largest BH mass $m_{\rm max}^{\rm obs}$ in mock catalogs similar to GWTC-3 (Abbott et al. 2023a,b); see Section 6. The solid orange bands show the putative mass gap from (pulsational) pair instability from 60–130 $M_\odot$.

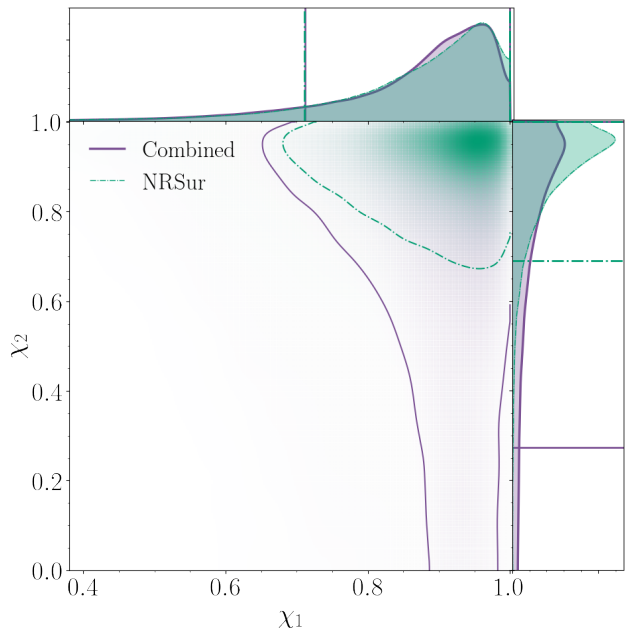


**Figure 4.** The posterior distribution of the primary and secondary spin magnitudes. We show the posterior distribution based on the combined samples (purple) and from the NRSur7dq4 waveform model (NRSur, green dash dot). Each contour, as well as the colored horizontal and vertical lines, shows the 90% credible intervals.

Although we observe differences depending on the model, the primary and secondary component masses nevertheless have a significant probability of lying within the mass gap from (pulsational) PISN processes, as shown in Figure 3, where we assume a nominal gap ranging from ∼60–130 $M_\odot$ (see Section 6 for a detailed discussion). The binary's total mass is constrained to be within 189–266 $M_\odot$. This measurement exceeds the 95th percentile of the inferred total mass from GW190521 (Abbott et al. 2023a). Assuming a FAR threshold of one per year, similar to Abbott et al. (2023b), the source of GW231123 is the highest mass BBH observed by the LVK to date; other lower significance high-mass observations have been discussed in Abbott et al. (2024a); Wadekar et al. (2023); Williams (2025); Ruiz-Rocha et al. (2025).

We consistently infer that both BHs are highly spinning independent of the model we use. As shown in Figure 4, we infer that the primary spin magnitude $\chi_1 \geq 0.7$ at 91% probability and the secondary spin magnitude $\chi_2 \geq 0.7$ at 63% probability, see Sec. 6.5 for details. The primary component of GW231123 has one of the highest confidently measured BH spins observed through GWs (evidence for highly spinning BHs has also been presented in Hannam et al. 2022; Nitz et al. 2020; Abbott et al. 2024a, 2023a; Wadekar et al. 2023; Williams 2025).

We are unable to reliably infer the spin orientation of the binary; we infer polar angles between each spin vector and the orbital angular momentum that vary not only between models, but also when independently analysing data obtained by LIGO Livingston compared to LIGO Hanford, see Appendix B. In an attempt to understand these differences we carried out a series of analyses with different frequency ranges. We found that all models consistently infer greater support for spin components aligned with the orbital angular momentum, and no sign of systematics, when independently analysing LIGO Hanford data, and when excluding data from LIGO Livingston below 50 Hz. However, as with the systematics issues discussed in Section 4.2 and Appendix A, we were not able to conclusively reproduce this behaviour with injections of mock signals, and did not find any significant noise features below 50 Hz that could be the cause, although we did not perform a de-

tailed study of Gaussian noise fluctuations or low-SNR glitches. When spin misalignment is inferred, we are unable to conclusively constrain the spin orientation away from aligned.

The uncertainty in the spin misalignment affects the inferred effective inspiral spin $\chi_{\rm eff}$, which parameterizes the spin aligned with the orbital angular momentum (Santamaria et al. 2010; Ajith et al. 2011). Negative $\chi_{\rm eff}$ would imply that at least one spin is misaligned with the orbital angular momentum by more than ninety degrees. We cannot rule out $\chi_{\rm eff} < 0$, but there is an 89% probability that $\chi_{\rm eff}$ is positive. The inferred effective precessing spin (Schmidt et al. 2015) is consistently measured between models and deviates from the prior, $\chi_{\rm p} = 0.77^{+0.18}_{-0.19}$. Although we infer variation between models, we consistently obtain large Bayes factors ($10^3 : 1 - 10^8 : 1$) in favor of the precessing hypothesis compared to the spin-aligned hypothesis (spins aligned with the orbital angular momentum). Since the distribution of Bayes factors from noise alone is unknown, we additionally quantify the evidence for precession in GW231123 by computing the precession SNR, $\rho_{\rm p}$ (Fairhurst et al. 2020a,b). In the absence of any precession in the signal, we expect $\rho_{\rm p} < 2.1$ in 90% of cases. We infer an SNR of $\rho_{\rm p} = 2.0^{+5.2}_{-1.2}$. Although the high SNR tail is consistent with the large Bayes factors (Green et al. 2021; Pratten et al. 2020b), we infer non-negligible support below $\rho_{\rm p} = 2.1$. We are therefore unable to confidently claim precession in GW231123. GW190521 was also found to exhibit mild evidence for spin-precession (Abbott et al. 2020d,e).

We observe significant differences in the inferred luminosity distance and inclination angle of GW231123's source, depending on the model, although we repeatedly infer nearly symmetric distributions for the inclination angle around $\pi/2$ rad for all models except XO4a. We also infer substantial variation in the detector-frame quantities, despite seeing agreement between several models in the source-frame parameters. See Appendix A for a detailed discussion. Owing to disagreements in the inferred inclination angle of the binary, we similarly observe differences in the inferred SNRs in each higher-order multipole obtained by each model. Following the methodology in Abbott et al. (2020f,g), where for each multipole the IMRPhenomXHM signal model (García-Quirós et al. 2020) is used to remove any contribution parallel to the dominant multipole and to calculate the orthogonal optimal SNR (Mills & Fairhurst 2021), we nevertheless find that all models provide support for the $(\ell, m) = (3, 3)$ multipole in GW231123. We infer an average orthogonal optimal SNR of 3.3 when combining the results from all models with equal weight.

The properties of the remnant BH are estimated in different ways depending on the model. We apply the NRSur7dq4Remnant model (Varma et al. 2019) to the samples obtained by NRSur, and we average several fits calibrated to numerical relativity simulations (Hofmann et al. 2016; Healy & Lousto 2017; Jiménez-Forteza et al. 2017) for samples obtained by v5PHM, TPHM, XPHM, XO4a. When combining the results with equal weight, we infer the final mass and spin of the remnant BH to be $M_{\rm f} = 222^{+28}_{-42}\,M_\odot$ and $\chi_{\rm f} = 0.84^{+0.08}_{-0.16}$ respectively. For certain binary configurations, the remnant BH may receive a recoil velocity that is enough to eject the remnant from its host galaxy (Merritt et al. 2004). We infer a measurement of the remnant BH's recoil velocity that differs from the effective prior distribution: $v_{\rm f} = 884^{+973}_{-814}\,{\rm km\,s^{-1}}$. This measurement is based on the NRSur analysis and the NRSur7dq4Remnant remnant model, the only fit providing recoil velocities estimates (Varma et al. 2019, 2020).

### 4.4. *Waveform Consistency Checks*

To further assess whether a CBC signal with the inferred parameters in Section 4.3 adequately represents the data, we perform several consistency checks using a signal-agnostic approach that reconstructs coherent transient power, and through a model incorporating a modified wave dispersion relationship. First, we compare the waveform of the maximum-likelihood sample from parameter estimation in Section 4.1 to one obtained through minimally modelled analyses that make no assumptions about the source or morphology of the signal (Szczepańczyk et al. 2021; Salemi et al. 2019; Ghonge et al. 2020). Second, we conduct a residuals analysis, subtracting the best-fit waveform from the detector data and searching for coherent residual power (Abbott et al. 2021b). Discrepancies between the modelled and minimally modelled waveforms, or the presence of significant excess residual power, could indicate physical effects in addition to or alternative to those in our BBH signal models or unaccounted-for noise features (Johnson-McDaniel et al. 2022).

For the waveform reconstruction comparisons, we use BayesWave (Cornish & Littenberg 2015; Cornish et al. 2021; Chatziioannou et al. 2021), cWB-2G (Klimenko et al. 2008, 2016a; Drago et al. 2020), and cWB-BBH (Mishra et al. 2025) for the minimally modelled analysis. To evaluate the agreement between the signal as found by the modelled analysis and minimally modelled approach, we calculate the overlap between the maximum-likelihood sample from parameter estimation using the NRSur model and the median BayesWave or cWB maximum-likelihood waveform. An overlap of

1 indicates perfect agreement, while an overlap of 0 indicates no similarity between waveforms. To assess whether the overlaps are consistent with signals of comparable parameters and noise realizations, we perform a dedicated set of injections wherein we inject waveforms generated by draws from the posterior distribution of the source parameters into detector data surrounding the event. The BayesWave analysis performed 400 injections into approximately 8 hours of data surrounding the event, and the cWB analysis injected about 2800 draws from the posterior distribution in an interval of two weeks around the event. We find good agreement between the minimally modelled and CBC waveform reconstructions. The overlaps between the CBC maximum-likelihood waveform and BayesWave, cWB-2G, and cWB-BBH are 0.97, 0.96, and 0.98, respectively. Compared to the distributions of overlaps from the injections, the $p$-values (defined as the fraction of injections with overlaps below that of the real event) are 0.74, 0.57, and 0.92 for BayesWave, cWB-2G, and cWB-BBH, respectively. Under the hypothesis that the overlaps between the BayesWave and cWB reconstructions with the maximum-likelihood waveform are drawn from the same distribution as the injection overlaps, the $p$-values should be distributed uniformly from 0 to 1, so these results indicate that the overlaps are consistent with expectations from systems similar to GW231123.

For the residuals test, we produce residual data by subtracting from the original data the maximum-likelihood waveform from the NRSur parameter estimation samples. If the signal has been modelled sufficiently, the residual data should be consistent with Gaussian noise. We analyze the residual data with BayesWave, and calculate the 90% credible upper limit on the recovered network SNR ($\mathrm{SNR}_{90}$). To compare to expected values of $\mathrm{SNR}_{90}$, we also analyze segments of data (with no injected signal) selected randomly from 16384 s of data surrounding the event, and calculate the probability of obtaining an $\mathrm{SNR}_{90}$ higher than that of residual data. Details of this procedure can be found in (Abbott et al. 2021b). We find no significant excess SNR in the residual data beyond what is expected from only Gaussian noise. Compared to the distribution of $\mathrm{SNR}_{90}$ from the noise-only runs, the $p$-value is 0.35. This further confirms that minimally modelled tests do not flag any features in the data missed by the analyses described in Section 4.1.

We additionally search for post-ringdown echo signals (Tsang et al. 2018, 2020) with a BayesWave-based search, finding negative evidence for their presence (as quantified by the Bayes factor $\log_{10}\mathcal{B}^{\mathrm{signal}}_{\mathrm{noise}} < 0$), consistent with the above findings. As a final consistency check, an analysis incorporating a modified wave dispersion relation due to non-zero graviton mass (Abbott et al. 2021b) yields agreement with massless wave propagation when based on the NRSur or TPHM models. Instead, when assuming the XPHM or XO4a templates, a statistically significant violation is found, suggesting missing signal components not captured by these models, which is consistent with the discussion of systematics in Section 4.2.

## 5. BLACK-HOLE RINGDOWN

Massive systems dominated by merger-ringdown, such as GW231123, are ideal to test the BH signal interpretation by applying BH spectroscopy techniques (Detweiler 1980; Dreyer et al. 2004; Berti et al. 2006, 2009, 2025), yielding remnant properties under minimal assumptions on the remnant formation process. We fit superpositions of damped sinusoids, aiming to associate them with characteristic quasi-normal modes (QNMs) of a BH, which drive its relaxation to equilibrium. In principle, the resulting parameter estimates make it possible to robustly validate IMR measurements, since a QNM description is generic to any BH remnant (e.g., a BH formed from an eccentric binary).

We truncate portions of data in the time domain at different analysis start times $t_{\mathrm{start}}$, and fit two sets of models. The first (`DS-`$N$) is a superposition of $N$ damped-sinusoids $\sum_{j=1}^{N} A_j e^{i[2\pi f_j (t-t_{\mathrm{start}})+\phi_j]} e^{-(t-t_{\mathrm{start}})/\tau_j}$, with constants $A_j, \phi_j, f_j, \tau_j$ as free parameters, assuming $f_j > 0$ (circularly polarized wave). In the second (`Kerr`), complex frequencies are identified with QNMs of a Kerr BH, $f_i = f_{\ell mn}(M_{\mathrm{f}}^{\mathrm{det}}, \chi_{\mathrm{f}})$ and $\tau_i = \tau_{\ell mn}(M_{\mathrm{f}}^{\mathrm{det}}, \chi_{\mathrm{f}})$, with detector frame (redshifted) mass $M_{\mathrm{f}}^{\mathrm{det}}$, spin $\chi_{\mathrm{f}}$, and $\ell mn$ the QNM angular $(\ell, m)$ and overtone $(n)$ indices. In addition to the longest-lived $\ell mn = 220$, we consider $\ell mn = \{221, 210, 200, 330, 320, 440\}$, the linear QNMs with the largest predicted amplitudes for binary mergers (Kamaretsos et al. 2012; London et al. 2014; Cheung et al. 2024; Zhu et al. 2025; Nobili et al. 2025; Carullo 2024). Here, we include both $\pm f_{\ell mn}$ contributions, accommodating generic signal polarizations, and $M_{\mathrm{f}}^{\mathrm{det}}$ enters the expression as mode amplitudes $A_{\ell mn}$ are degenerate with the source distance.

We use the `pyRing` pipeline (Carullo et al. 2019) with standard analysis settings (Isi & Farr 2021; Abbott et al. 2021b; Gennari et al. 2024). We pre-condition the data by subtracting the 60 Hz power line, which reduces the required analysis duration to $T = 0.2\,\mathrm{s}$ (Siegel et al. 2025). We sample the posterior distribution using the `CPNest` nested sampling algorithm (Veitch et al. 2020). Times are relative to $t^{\mathrm{pol}}_{\mathrm{peak}} := \max_t[h_+^2(t) + h_\times^2(t)] =$

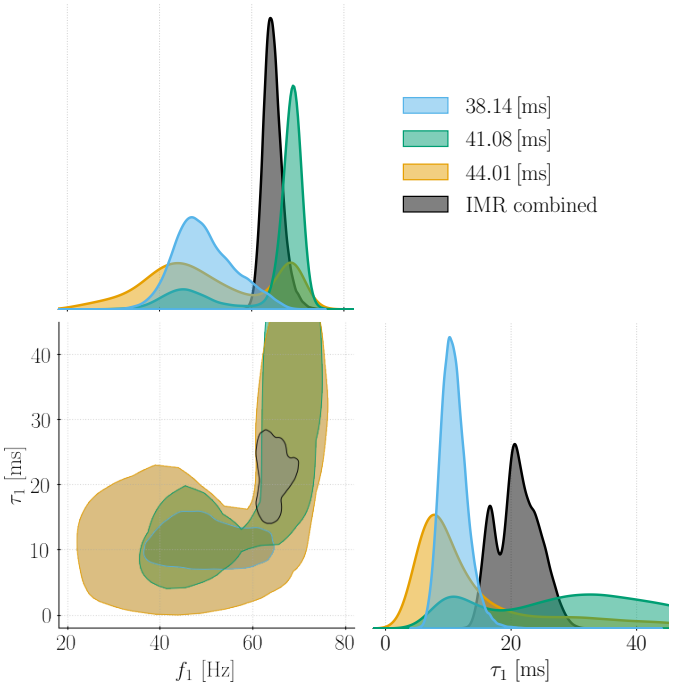


**Figure 5.** Two-dimensional frequency and damping time posterior distribution (90% credible levels), when starting the analysis at late times and assuming a single damped sinusoid with positive frequency; the combined IMR estimates for the longest-lived $\ell mn = 220$ QNM are shown for comparison. For visualisation purposes, we display up to $\tau_1 = 45$ms, while the posterior tail extends up to $\tau_1 = 80$ms.

1384782888.5998s in the LIGO Hanford data, compatible with the median of the polarizations peak time from the NRSur reconstructed waveform, subject to an uncertainty $\mathcal{O}(0.01)$s. The sky location is fixed to a value compatible with the NRSur maximum likelihood value, fixing the analysis start time in LIGO Livingston, as required by the truncated time-domain formulation of the analysis (Isi & Farr 2021). We have verified that repeating the analysis at different sky location values drawn from the NRSur posterior does not affect our conclusions.

Damped sinusoids are expected to be valid in the stationary regime of BH relaxation, typically $[10, 20]GM_{\rm f}^{\rm det}/c^3$ (namely $[14.7, 29.4]$ ms assuming $M_{\rm f}^{\rm det} \simeq 298 M_\odot$) past the signal peak; fitting earlier may provide spurious support for additional modes (Berti et al. 2025). However, a time-domain waveform reconstruction of GW231123 indicates a highly complex morphology, displaying a monotonic decay only after $t_{\rm peak}^{\rm strain} \simeq t_{\rm peak}^{\rm pol} + 19$ ms. This is significantly later than the nominal $t_{\rm peak}^{\rm pol}$, after which monotonic decay is expected for vanilla signal morphologies; see Appendix C. Given this uncertainty, we explore a wide range of times $t_{\rm start} = t_{\rm peak}^{\rm pol} + [-7.4, 58.7]$ ms in steps of $\approx 3$ ms.

Fits that start at late times $t^{\rm start} \simeq t_{\rm peak}^{\rm pol} + 41$ ms, when we are confident on the validity of an exponential decay description, find preference for a single mode with both models (as quantified by Bayes factors $\mathcal{B}$). A single damped sinusoid (`DS-1`) fit yields a multi-modal $f_1 - \tau_1$ distribution, shown in Figure 5, unlike what is observed in previous events at such late times. One peak with $f_1 \approx 68$ Hz and $A_1 \approx 2 \times 10^{-22}$ overlaps with the dominant Kerr $\ell mn = 220$ frequency $f_{220}$ as predicted by IMR models, supporting the BH hypothesis. The damping time spans a broad range, overlapping with $\tau_{220}$. A second peak is centred around $f_1 \approx 45$ Hz, correlating with a larger amplitude value $A_1 \approx 6 \times 10^{-22}$. Among linear Kerr QNMs predicted by the IMR models, this frequency peak shows the largest overlap with $f_{200}$. The damping time is also bimodal: the peak associated to $f_1 \approx 45$ Hz is centred around $\tau_1 \approx 10$ ms, a smaller value compared to $\tau_{200} \approx 18$ ms, but overlapping the latter distribution. Under a `Kerr` 220 fit, the two-dimensional $M_{\rm f}^{\rm det} - \chi_{\rm f}$ distribution is also multi-modal: one peak overlaps with the IMR predictions, while a second prefers lower remnant spins.

Fitting at earlier times, Bayes factors indicate overwhelming preference ($\log_{10}\mathcal{B} > 6$) for two modes over one until $t_{\rm start} \simeq t_{\rm peak}^{\rm pol} + 32.3$ ms in both the `DS-`$N$ and `Kerr` models, but in this range we may be fitting a complex merger signal, and a QNM superposition may not be valid. At these early times, a `DS-2` fit yields two frequencies consistent with the two peaks observed at later times. Amplitudes and damping times are comparable in magnitude between the two damped sinusoids, and both damping times are larger than the $\approx 10$ ms peak observed at later times. In addition to the 220 mode, in the time range explored we find the `Kerr` $320, 210, 200$ modes to be on average the most favoured by Bayes factors, while 330 is preferred around $t_{\rm start} \simeq t_{\rm peak}^{\rm pol} + 23.5$ ms. The `Kerr` two-modes combinations robustly yield a massive remnant, $M_{\rm f}^{\rm det} \gtrsim 200 M_\odot$, also at these earlier times.

These multi-mode combinations are in tension with IMR analyses. The most favoured `Kerr` mode in addition to the 220 according to Bayes factors, the 320, implies a $M_{\rm f}^{\rm det} - \chi_{\rm f}$ distribution that does not overlap with IMR estimates. Adding 210 only results in partial overlap, while the 221 overlaps to a larger degree. However, the short-lived 221 mode alone is not expected to give rise to the features observed in the signal until late times. The 200 mode addition results in the most significant overlap, with a 200 amplitude comparable to the 220, consistently with later times results.

While $\ell mn = 210, 200$ QNMs can be strongly excited in highly precessing systems with large mass asymmetry (O'Shaughnessy et al. 2013; Zhu et al. 2025; Nobili et al. 2025), the IMR analyses of GW231123 predict minimal power in the 200 mode, as discussed in Appendix D. Highly eccentric configurations can excite $m = 0$ modes (Sperhake et al. 2008), but we lack sufficiently complete merger–ringdown models for eccentric-binary signals to reliably assess this possibility; see Section 7 for further discussion. `DS-`$N$ analyses with $N > 3$ did not prefer more than two modes, but future investigations will be required to determine whether the observed features can be induced by a superposition of many overlapping modes.

In summary, the `Kerr` fits recover the remnant spin with large uncertainty, and they robustly predict $M_{\rm f}^{\rm det} \gtrsim 200 M_\odot$ at all times, supporting the interpretation of a massive BH remnant. Further investigations will be required to characterize the nature of the bi-modal features persistently observed in the signal and consistently interpret the multi-mode fits at earlier times. Given these large uncertainties, we do not consider tests of the no-hair properties of BHs in general relativity that would be enabled by a confident two-mode identification (Detweiler 1980; Dreyer et al. 2004; Berti et al. 2006, 2009; Gossan et al. 2012; Brito et al. 2018; Carullo et al. 2018; Bhagwat et al. 2020; Isi & Farr 2021; Berti et al. 2025).

## 6. ASTROPHYSICAL IMPLICATIONS

Here, we discuss the astrophysical implications of the large masses and spins of GW231123's source and its possible origin given current understanding of (pulsational) PISNe and formation channels of merging BBHs.

### 6.1. *Single-event rate estimate*

First, we quantify the merger rate of GW231123-like events following (Kim et al. 2003; Abbott et al. 2016b). The sensitive volume–time of the detectors to signals whose source properties are consistent with the posterior distribution of GW231123 is estimated using the cWB-BBH results for the injection campaign in Section 2. Assuming a constant merger rate $\mathcal{R}$ over comoving volume and source-frame time with prior $\propto 1/\sqrt{\mathcal{R}}$ and a Poisson likelihood for the number of triggers, we find $\mathcal{R} = 0.08^{+0.19}_{-0.07}\,\mathrm{Gpc^{-3}\,yr^{-1}}$. This is consistent with the rate of mergers like GW190521 ($0.13^{+0.30}_{-0.11}\,\mathrm{Gpc^{-3}\,yr^{-1}}$; Abbott et al. 2020d,e) and upper limits of IMBH mergers (e.g., even the most stringent 90% upper limit $< 0.06\,\mathrm{Gpc^{-3}\,yr^{-1}}$ from Abbott et al. 2022 and see Table 3 therein for constraints across source properties), but lower than the overall rate of BBHs with component masses $< 100\,M_\odot$ inferred through GWTC-3 (16–$61\,\mathrm{Gpc^{-3}\,yr^{-1}}$; Abbott et al. 2023b).

### 6.2. *Relation to the previous inferred population*

To further assess GW231123 in the context of the 69 BBH mergers with FARs $< 1\,\mathrm{yr^{-1}}$ through GWTC-3 (Abbott et al. 2023a) and test if its masses and spins are surprising, we perform posterior predictive checks based on the *fiducial* BBH population fit from (Abbott et al. 2023b, Section III C; we extend the prior on the maximum BH mass up to $200\,M_\odot$ as there is support from GW190521 above the limit of $100\,M_\odot$ imposed in the original GWTC-3 analysis). From the inferred population, we construct mock catalogs containing 69 detected events and plot the distribution of their largest BH mass $\approx 83^{+43}_{-26}\,M_\odot$ in Figure 3. Using the combined parameter estimates in Section 4.3, the primary mass of GW231123 falls at the $98^{+2}_{-5}\,\%$ level of this distribution, indeed indicating that this event is an unlikely draw. However, due to large uncertainties in its masses, it is not conclusively an outlier as it may be less massive than the most massive mock events (equivalent comparisons for secondary and total mass are less significant). Similarly, the largest BH spin in these catalogs is $0.78^{+0.14}_{-0.14}$, against which the primary and secondary spins of GW231123 can fall at any percentile and thus are not outliers. Compared to its masses, the spins of GW231123's source are more consistent with the known population as it does not rule out large values.

### 6.3. *Possible formation channels*

From theoretical predictions for the late-stage evolution of massive stars (Fowler & Hoyle 1964; Barkat et al. 1967; Rakavy & Shaviv 1967; Fraley 1968; Bond et al. 1984; Woosley et al. 2002; Woosley 2017), contraction of the core leads to electron–positron pair production that reduces internal pressure support, causing further contraction that powers explosive nuclear burning and a rebounding shock. For helium-core masses $\approx 32$–$64\,M_\odot$, multiple pulsational episodes can eject sufficient material to reduce the mass below the pair-instability regime, ending with a BH remnant. A single pulse can entirely disrupt stars with larger helium cores, leaving behind no remnant in a PISN. At even larger helium-core masses $\gtrsim 135\,M_\odot$, this is avoided as the high core temperature results in photodisintegration that accelerates gravitational collapse to a massive BH. This leads to the robust prediction from single-star evolution of the existence of a gap in the BH mass distribution. Though this gap is broadly consistent with the range $\approx 60$–$130\,M_\odot$, there are several theoretical uncertainties that affect both the lower edge and total extent of the gap (Belczynski et al.

2016; Stevenson et al. 2019; Farmer et al. 2019; Mapelli et al. 2020; Renzo et al. 2020b; Marchant & Moriya 2020; Woosley & Heger 2021; Hendriks et al. 2023). Uncertainties in nuclear reaction rates alone can shift the lower edge of the pair-instability mass gap from $\approx 50\,M_\odot$ to $\approx 100\,M_\odot$ (Farmer et al. 2020).

Some stellar and binary evolution processes are predicted to be able to populate the pair-instability mass gap. Weaker stellar winds (Mapelli et al. 2020) or core dredge-up episodes (Costa et al. 2021) may allow a star to retain a hydrogen envelope and collapse to a BH with mass inside the gap (Spera et al. 2019). Short-period stellar binaries might avoid merging and produce binary BHs with large, equal masses $\sim 100\,M_\odot$ from rapidly rotating metal-poor stars due to chemically homogeneous evolution (de Mink & Mandel 2016; Mandel & de Mink 2016; Marchant et al. 2016). However, most models of isolated-binary formation predict small natal spins and at most one of the BHs spinning, due to tidal synchronization or accretion-induced spin up, and so binaries with masses and spins like those inferred from GW231123 are difficult to form (Belczynski et al. 2020; Qin et al. 2018; Fuller & Ma 2019; Bavera et al. 2020; Belczynski et al. 2020; van Son et al. 2020). In fact, the components BHs and especially the primary are so massive that they may have formed through core collapse above the pair-instability mass gap (Ezquiaga & Holz 2021; Franciolini et al. 2024).

Alternatively, in hierarchical mergers, one or both of the binary components is the product of a previous BBH merger, with characteristically large masses and spins (Gerosa & Fishbach 2021). As seen in Figure 4, the spins inferred from GW231123 may be even larger than typically predicted from hierarchical BH mergers (Gerosa & Berti 2017; Fishbach et al. 2017), although the expected distribution for sources retained in their host environments may accommodate a wider range of spins (Borchers et al. 2025). Previous analyses have suggested evidence for hierarchical mergers in GW catalogs (Kimball et al. 2021; Mould et al. 2022; Wang et al. 2022; Li et al. 2024; Pierra et al. 2024; Hussain et al. 2024; Antonini et al. 2025), but the population of BH remnants receive gravitational recoils as high as $10^2$–$10^4\,\mathrm{km\,s^{-1}}$ (Doctor et al. 2021; Mahapatra et al. 2021), requiring environments with high escape speeds (Antonini & Rasio 2016) such as dense stellar clusters (Miller & Hamilton 2002; Antonini et al. 2019; Rodriguez et al. 2019; Fragione & Silk 2020; Mapelli et al. 2021; Arca Sedda et al. 2021; Kritos et al. 2023; Mahapatra et al. 2025) or active galactic nucleus (AGN) disks (Bartos et al. 2017; Stone et al. 2017; Mckernan et al. 2018; Yang et al. 2019; Tagawa et al. 2020; McKernan et al. 2020; Vaccaro et al. 2024; Arca Sedda et al. 2023b) to be retained.

This is in contrast to stellar mergers, which receive smaller recoils from asymmetric mass loss (Gaburov et al. 2010; Glebbeek et al. 2013) and therefore may be more efficient at producing BHs with large masses in dynamical environments. The large masses inferred from GW231123 may be explained by multiple such mergers in dense clusters or multiple systems (Mapelli 2016; Di Carlo et al. 2020; Renzo et al. 2020a; Kremer et al. 2020; González et al. 2021; Rizzuto et al. 2022; Costa et al. 2022; Arca Sedda et al. 2023a), a scenario that could also describe the formation of massive central BHs (Portegies Zwart et al. 2004; Greene et al. 2020).

Besides mass transfer between the components of a stellar binary, BH mass growth may also occur via accretion in other gaseous environments. BHs embedded in the disk of an AGN may accrete material directly from the disk or from collisions with disk stars (McKernan et al. 2012). Similarly, in dense clusters, BHs may accrete from stars after undoing dynamical interactions (Giersz et al. 2015; Lopez et al. 2019; Kıroğlu et al. 2025). Furthermore, these accretion processes may also increase BH spins.

A different possibility is that of primordial BHs being the binary components, which may exist across a range of mass scales, including within the pair-instability mass gap (Bird et al. 2016, 2023; Clesse & García-Bellido 2017, 2022). However, there are remaining theoretical uncertainties, e.g., on whether primordial BHs could accrete sufficiently to spin up as rapidly as the BHs inferred from GW231123 (Green & Kavanagh 2021).

Altogether, these theoretical predictions and their uncertainties make it difficult to determine whether or not the BHs in the source of GW231123 have an astrophysical origin directly from stellar collapse. We quantify this in more detail below.

### 6.4. *Stellar collapse*

To account for a range of possible locations for the pair-instability mass gap, in Figure 6 we compute the probability that one or both component masses fall within the gap as a function of its lower edge from 40–$100\,M_\odot$ and upper edge from 120–$180\,M_\odot$, using the combined parameter estimates. In the following, we quote these probabilities specifically for the putative gap 60–$130\,M_\odot$. The probabilities that the secondary (primary) BH lies in, above, and below this gap are 83 % (28 %), 1 % (72 %), and 16 % (0 %), respectively. Considering scenarios in which at least one of the components falls in this gap, the joint probability that: both BHs are in the gap (upper left panel of Figure 6) is 26 %;

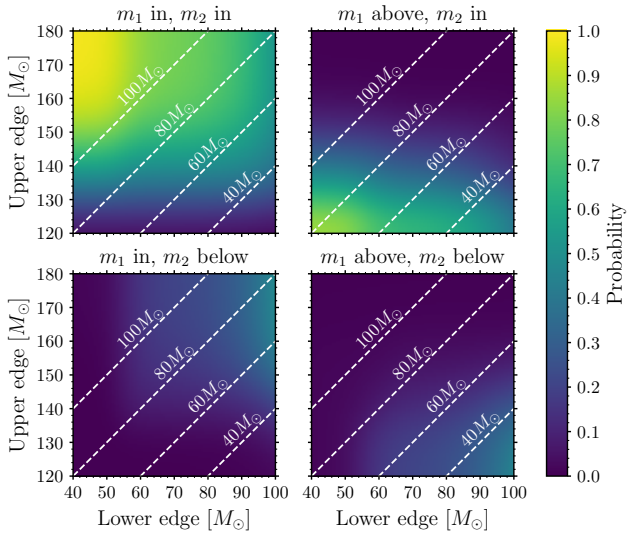


**Figure 6.** Probability using the combined parameter estimates for GW231123 that: both BHs are in the pair-instability mass gap (top left); the primary is above the gap and the secondary is within (top right); the primary is within and the secondary is below (bottom left); the primary is above and the secondary is below (bottom right). Probabilities are computed varying the lower and upper edges of the gap, while dashed lines mark constant gap widths.

the primary is above while the secondary is within (upper right) is 57 %; and that the primary is within while the secondary is below (lower left) is 2 %. Alternatively, a scenario with neither BH in the gap is possible in the case of a straddling binary (Fishbach & Holz 2020), with a primary BH above the upper edge and secondary below the lower edge (lower right) having a probability of 14 %.

Overall, this implies that within the uncertainties on the combined parameter estimates (assuming our default prior) and the location of the pair-instability mass gap, scenarios with both BHs outside the gap have lower probability than those with at least one BH in the gap.

### 6.5. *Hierarchical mergers*

Given the high probability of at least one of the BHs lying inside the pair-instability mass gap, we consider the possibility that this is due to repeated BBH mergers. Assuming hierarchical origins, several works have inferred the source properties of potential BBHs whose merger products are observed with GWs in a subsequent merger (Baibhav et al. 2021; Barrera & Bartos 2022; Álvarez et al. 2024; Mahapatra et al. 2024). We follow (Álvarez et al. 2024) and use the NRSur7dq4Remnant surrogate model (Varma et al. 2019) to find the distribution of BBH source properties such that the corresponding distribution of BH remnant properties reproduces the combined parameter estimates over mass and spin for the primary and secondary BH inferred from GW231123. As the primary-spin posterior favors large values $\gtrsim 0.7$, this constrains the parent binary of the primary BH to have unequal masses $105^{+24}_{-29}\,M_\odot$ and $38^{+33}_{-17}\,M_\odot$; for more equal masses, both BH spins can reduce the total angular momentum if misaligned, whereas unequal-mass binaries are dominated by the single heavier BH. The parent binary of the primary BH may have had a large effective inspiral spin, with $\chi_{\rm eff} = 0.55^{+0.25}_{-0.60}$, but $\chi_{\rm eff} \lesssim 0$ is not ruled out. A similar picture holds for the secondary BH, with parent masses $73^{+26}_{-37}\,M_\odot$ and $25^{+28}_{-15}\,M_\odot$, but more uncertain effective inspiral spin $\chi_{\rm eff} = 0.29^{+0.47}_{-0.88}$ due to the larger uncertainty on the secondary spin in the source of GW231123. These mergers would have imparted kicks of $749^{+1320}_{-630}\,{\rm km\,s^{-1}}$ and $494^{+1410}_{-363}\,{\rm km\,s^{-1}}$ in the case of the primary and secondary, respectively, resulting in ejection from environments with escape speeds $\lesssim 100\,{\rm km\,s^{-1}}$, such as young star clusters or globular clusters (Antonini & Rasio 2016).

The heavier of the two BHs in both parent binaries may also lie within the pair-instability mass gap, with probabilities 96 % and 71 % for the heavier parent of the primary and secondary, respectively, when taking a gap from 60–130 $M_\odot$, as above. Therefore, if either of the component BHs of GW231123's source is interpreted as the product of a previous BH merger, it may be the result of multiple previous mergers or require the components of the parent binary to have formed with larger masses via other astrophysical processes, such as stellar mergers or BH accretion, as discussed in Section 6.3.

## 7. ALTERNATIVE INTERPRETATIONS

All GW observations to date have been inferred to be from compact binaries consisting of BHs and/or neutron stars (Abbott et al. 2016c, 2021a, 2024a, 2023a; Venumadhav et al. 2020; Olsen et al. 2022; Mehta et al. 2025; Nitz et al. 2023; Wadekar et al. 2023), and we consider a BBH the most astrophysically plausible interpretation of GW231123, finding that a non-eccentric BBH model fits the signal with no significant residual. Nonetheless, the low number of observable GW cycles invites alternative interpretations. We discuss several here.

### 7.1. *Eccentricity*

Binaries formed in dense environments may retain residual eccentricity in the sensitive band of current GW detectors (Antonini et al. 2014; Samsing 2018; Rodriguez et al. 2018; Zevin et al. 2019; Chattopadhyay et al. 2023; Dall'Amico et al. 2024) or form with large eccentricities and merge promptly after due to a dynamical capture (Gold & Brügmann 2013; East et al. 2013; Gamba

et al. 2023; Andrade et al. 2024; Albanesi et al. 2025b), but for high masses their GW signals can be confused with those of non-eccentric mergers (Romero-Shaw et al. 2020a; Calderón Bustillo et al. 2021a; Romero-Shaw et al. 2023). Our signal models assume a non-eccentric inspiral, while state-of-the-art IMR models that include eccentricity (Liu et al. 2022; Gamboa et al. 2024; Paul et al. 2025; Albanesi et al. 2025a; Planas et al. 2025a) assume circularization in the merger–ringdown stages and would thus be unsuitable to infer the parameters of GW231123's source if it was eccentric when observed (Ramos-Buades et al. 2023b; Iglesias et al. 2024; Gupte et al. 2024; Planas et al. 2025b). Extensions of QNM amplitude models beyond eccentric non-spinning configurations (Carullo 2024) will be required to investigate the possible $m = 0$ ringdown mode excitation hinted at in Section 5. Many studies have found that the merger-ringdown signal is robust with respect to moderate inspiral eccentricity (Hinder et al. 2008; Huerta et al. 2019; Healy & Lousto 2022; Carullo et al. 2024; Nee et al. 2025). Relaxing the non-eccentric assumption is not expected to significantly change our results unless the eccentricity is larger than $\sim 0.6$ close to merger (Healy & Lousto 2022; Carullo et al. 2024), which would be rare in the dynamical-capture scenarios above. For example, Chattopadhyay et al. (2023) find an overall merger rate $< 1\,\mathrm{Gpc}^{-3}\,\mathrm{yr}^{-1}$ in dense stellar clusters, ∼10% with eccentricity $> 0.1$ at a GW frequency of 10 Hz and ∼10% involving BHs with masses $> 100\,M_\odot$, implying a rate of massive eccentric mergers $< 0.01\,\mathrm{Gpc}^{-3}\,\mathrm{yr}^{-1}$, already at the lower limit of our constraint for GW231123 without considering the decline in the number of sources at increasing mass and eccentricity. Although we do not explicitly rule out large eccentricity for the source of GW231123, we therefore consider it astrophysically unlikely.

### 7.2. *Gravitational lensing*

GW signals may be strongly lensed by galaxies or galaxy clusters, producing multiple copies of the original signal (Hannuksela et al. 2019; Abbott et al. 2021c, 2024b). However, no closely matching super-threshold counterpart candidates for GW231123 have been found from standard CBC searches. GWs can also undergo wave-optics lensing (Takahashi & Nakamura 2003) when they encounter smaller objects ($\sim 10^2$–$10^6\,M_\odot$ for signals in the LVK band). GW231123 shows the strongest support for distorted lensed signals seen so far for both a point-mass model (Wright & Hendry 2022) and phenomenological analyses (Liu et al. 2023), although preliminary background analyses suggest that some GW231123-like signals may be mis-identified as lensed. More in-depth investigations are needed to assess the significance of the lensing hypothesis, and these will be presented in future work.

### 7.3. *Other scenarios*

Several possible burst-like sources (Powell & Lasky 2025) of astrophysical and cosmological origin may produce signals of similar duration to GW231123, such as core-collapse supernovae, cosmic strings, and exotic compact objects. For most supernova waveforms, the peak signal is expected at frequencies higher than observed in GW231123 (Abdikamalov et al. 2020; Mezzacappa & Zanolin 2024). The ringdown-dominated signals of high-mass BBH mergers can be mimicked by waveforms from the collapse of cosmic strings (Abbott et al. 2020e; Aurrekoetxea et al. 2024) and collisions of exotic compact objects (e.g. boson stars) (Calderón Bustillo et al. 2021b; Siemonsen & East 2023; Evstafyeva et al. 2024). Though we do not explicitly rule out these scenarios, the detection of GW231123 is consistent with the rates and properties of the currently understood population under the interpretation of a high-mass BBH merger, which has higher astrophysical probability.

## 8. SUMMARY

GW231123 is a short-duration GW signal consisting of ∼5 observable cycles, most likely produced by a binary-black-hole merger. On that basis, we infer a total mass between $190\,M_\odot$ and $265\,M_\odot$, which is larger than any previously observed with high confidence in GWs, and strong support for large spins on both black holes. We report source property measurements with larger uncertainties than we would expect for a binary of this mass and a signal with SNR ∼21, most likely due to uncertainties in current signal models at high spins. A ringdown analysis also supports a massive remnant under minimal assumptions, consistent with full-signal estimates. The measured masses of GW231123's source lie at the edge of the currently understood population of binary black holes. The scenario with the highest probability is that at least one of the black hole sits in the pair-instability mass gap. If either is interpreted as the product of a previous black-hole merger, at least one of the black holes in its parent binary probably also lies in the mass gap. Such a sequence of black-hole mergers would require an environment with high escape speed, unless the black-hole masses are grown by other astrophysical processes, such as stellar mergers.

Given the small number of observable GW cycles, the large uncertainties in our measurements, and the limitations of current signal models, we expect that there

is much still to learn about GW231123 and its source. The feasibility of a wide range of other alternatives to black-hole mergers remains to be investigated. Even within the binary-black-hole merger interpretation, we expect to learn more from detailed studies of high-spin binaries, high-eccentricity mergers, hyperbolic encounters, and lensed signals. Forthcoming analyses of the combined catalog of GW events, alongside continued studies of pair-instability processes and the formation of intermediate-mass black holes, may help to reveal the origins of GW231123. All studies will have to contend with the limited information that can be extracted from short signals, but a clearer picture may emerge if a population of such signals is observed in future observing runs.

Strain data from the LIGO detectors associated with GW231123 are available from the Gravitational Wave Open Science Center [1]. Samples from posterior distributions of the source parameters, additional materials, and notebooks for reproducing the figures are available on Zenodo (LIGO Scientific, Virgo, and KAGRA Collaboration 2025). The software packages used in our analyses are open-source.

This material is based upon work supported by NSF's LIGO Laboratory, which is a major facility fully funded by the National Science Foundation. The authors also gratefully acknowledge the support of the Science and Technology Facilities Council (STFC) of the United Kingdom, the Max-Planck-Society (MPS), and the State of Niedersachsen/Germany for support of the construction of Advanced LIGO and construction and operation of the GEO 600 detector. Additional support for Advanced LIGO was provided by the Australian Research Council. The authors gratefully acknowledge the Italian Istituto Nazionale di Fisica Nucleare (INFN), the French Centre National de la Recherche Scientifique (CNRS) and the Netherlands Organization for Scientific Research (NWO) for the construction and operation of the Virgo detector and the creation and support of the EGO consortium. The authors also gratefully acknowledge research support from these agencies as well as by the Council of Scientific and Industrial Research of India, the Department of Science and Technology, India, the Science & Engineering Research Board (SERB), India, the Ministry of Human Resource Development, India, the Spanish Agencia Estatal de Investigación (AEI), the Spanish Ministerio de Ciencia, Innovación y Universidades, the European Union NextGenerationEU/PRTR (PRTR-C17.I1), the ICSC - CentroNazionale di Ricerca in High Performance Computing, Big Data and Quantum Computing, funded by the European Union NextGenerationEU, the Comunitat Autonòma de les Illes Balears through the Conselleria d'Educació i Universitats, the Conselleria d'Innovació, Universitats, Ciència i Societat Digital de la Generalitat Valenciana and the CERCA Programme Generalitat de Catalunya, Spain, the Polish National Agency for Academic Exchange, the National Science Centre of Poland and the European Union - European Regional Development Fund; the Foundation for Polish Science (FNP), the Polish Ministry of Science and Higher Education, the Swiss National Science Foundation (SNSF), the Russian Science Foundation, the European Commission, the European Social Funds (ESF), the European Regional Development Funds (ERDF), the Royal Society, the Scottish Funding Council, the Scottish Universities Physics Alliance, the Hungarian Scientific Research Fund (OTKA), the French Lyon Institute of Origins (LIO), the Belgian Fonds de la Recherche Scientifique (FRS-FNRS), Actions de Recherche Concertées (ARC) and Fonds Wetenschappelijk Onderzoek - Vlaanderen (FWO), Belgium, the Paris Île-de-France Region, the National Research, Development and Innovation Office of Hungary (NKFIH), the National Research Foundation of Korea, the Natural Sciences and Engineering Research Council of Canada (NSERC), the Canadian Foundation for Innovation (CFI), the Brazilian Ministry of Science, Technology, and Innovations, the International Center for Theoretical Physics South American Institute for Fundamental Research (ICTP-SAIFR), the Research Grants Council of Hong Kong, the National Natural Science Foundation of China (NSFC), the Israel Science Foundation (ISF), the US-Israel Binational Science Fund (BSF), the Leverhulme Trust, the Research Corporation, the National Science and Technology Council (NSTC), Taiwan, the United States Department of Energy, and the Kavli Foundation. The authors gratefully acknowledge the support of the NSF, STFC, INFN and CNRS for provision of computational resources.

This work was supported by MEXT, the JSPS Leading-edge Research Infrastructure Program, JSPS Grant-in-Aid for Specially Promoted Research 26000005, JSPS Grant-in-Aid for Scientific Research on Innovative Areas 2402: 24103006, 24103005, and 2905: JP17H06358, JP17H06361 and JP17H06364, JSPS Core-to-Core Program A. Advanced Research Networks, JSPS Grants-in-Aid for Scientific Research (S) 17H06133 and 20H05639, JSPS Grant-in-Aid for Transformative Research Areas (A) 20A203: JP20H05854, the joint research program of the Institute for Cos-

[1] https://doi.org/10.7935/anj7-6q40

mic Ray Research, University of Tokyo, the National Research Foundation (NRF), the Computing Infrastructure Project of the Global Science experimental Data hub Center (GSDC) at KISTI, the Korea Astronomy and Space Science Institute (KASI), the Ministry of Science and ICT (MSIT) in Korea, Academia Sinica (AS), the AS Grid Center (ASGC) and the National Science and Technology Council (NSTC) in Taiwan under grants including the Science Vanguard Research Program, the Advanced Technology Center (ATC) of NAOJ, and the Mechanical Engineering Center of KEK.

Additional acknowledgements for support of individual authors may be found in the following document: `https://dcc.ligo.org/LIGO-M2300033/public`. For the purpose of open access, the authors have applied a Creative Commons Attribution (CC BY) license to any Author Accepted Manuscript version arising. We request that citations to this article use 'A. G. Abac *et al.* (LIGO-Virgo-KAGRA Collaboration), ...' or similar phrasing, depending on journal convention.

*Software:* Calibration of the LIGO strain data was performed with a GstLAL-based calibration software pipeline (Viets et al. 2018b). Data-quality products and event-validation results were computed using the DMT (Zweizig, J. 2006), DQR (LIGO Scientific Collaboration and Virgo Collaboration 2018), DQSEGDB (Fisher et al. 2021), gwdetchar (Urban et al. 2021), hveto (Smith et al. 2011), iDQ (Essick et al. 2020), Omicron (Robinet et al. 2020), and PythonVirgoTools (Virgo Collaboration 2021) software packages and contributing software tools. Analyses in this catalog relied on software from the LVK Algorithm Library Suite (LIGO Scientific, Virgo, and KAGRA Collaboration 2018; Wette 2020). The detection of the signals and subsequent significance evaluations were performed with the GstLAL-based inspiral software pipeline (Messick et al. 2017; Sachdev et al. 2019; Hanna et al. 2020; Cannon et al. 2021), with the MBTA pipeline (Adams et al. 2016; Aubin et al. 2021), with the PyCBC (Usman et al. 2016; Nitz et al. 2017; Davies et al. 2020) packages, with cWB-BBH pipeline (Mishra et al. 2025), cWB-2G (Klimenko et al. 2008, 2016a; Drago et al. 2020) cWB-XP (Klimenko 2022), cWB-GMM (Gayathri et al. 2020; Lopez et al. 2022; Smith et al. 2024). Low-latency source localization was performed using BAYESTAR (Singer & Price 2016). Estimates of the noise spectra and glitch models were obtained using BayesWave (Cornish & Littenberg 2015; Littenberg & Cornish 2015; Cornish et al. 2021). Source-parameter estimation was primarily performed with the Bilby and BilbyPipe libraries (Ashton et al. 2019; Smith et al. 2020; Romero-Shaw et al. 2020b) using the Dynesty nested sampling package (Speagle 2020). SEOBNRv5PHM waveforms used in parameter estimation were generated using pySEOBNR (Mihaylov et al. 2025). PESummary was used to postprocess and collate parameter-estimation results (Hoy & Raymond 2021). Some of the parameter-estimation analyses were managed with the Asimov library (Williams et al. 2023). Ringdown analyses were performed using the `pyRing` (Carullo et al. 2025) library, relying on the `CPNest` nested sampling algorithm (Veitch et al. 2020). The manuscript content has been derived making use of additional publicly available software: matplotlib (Hunter 2007), numpy (Harris et al. 2020), scipy (Virtanen & others 2020), seaborn (Waskom et al. 2021), sxs (Scheel et al. 2025).

# APPENDIX

## A. SYSTEMATICS STUDIES

For this analysis we consider the models NRSur, v5PHM, TPHM, XPHM and XO4a. These models all describe precessing quasi-circular binaries and include higher multipole content. The three model families NRSur, SEOBNR and Phenom use different approaches to model the waveforms (Chatziioannou et al. 2024). In short, NRSur interpolates between NR data (Field et al. 2014; Blackman et al. 2015), making it typically the most accurate of the models for high-mass signals, such as GW231123. The SEOBNR and Phenom families instead use a combination of analytical and numerical information to create a complete inspiral-merger-ringdown model applicable to systems at any total mass (Buonanno & Damour 1999, 2000; Buonanno et al. 2007; Ajith et al. 2011). The models NRSur, v5PHM, and TPHM calculate the signal in the time domain, while XPHM and XO4a model directly in the frequency domain. These models comprise the five state-of-the-art models currently available for LVK analyses of observations in O4a.

NRSur is fully calibrated to numerical waveforms over the binary parameter space up to dimensionless spin magnitudes $\chi_1 = \chi_2 = 0.8$ and mass ratios $q = 1/4$, and can be extrapolated up to dimensionless spin magnitudes $\chi_1 = \chi_2 = 1.0$ and mass ratios $q = 1/6$. By construction, NRSur automatically includes all multipoles up to $\ell = 4$ and characteristics of precession such as mode asymmetry (Varma et al. 2019). By contrast, v5PHM, TPHM,

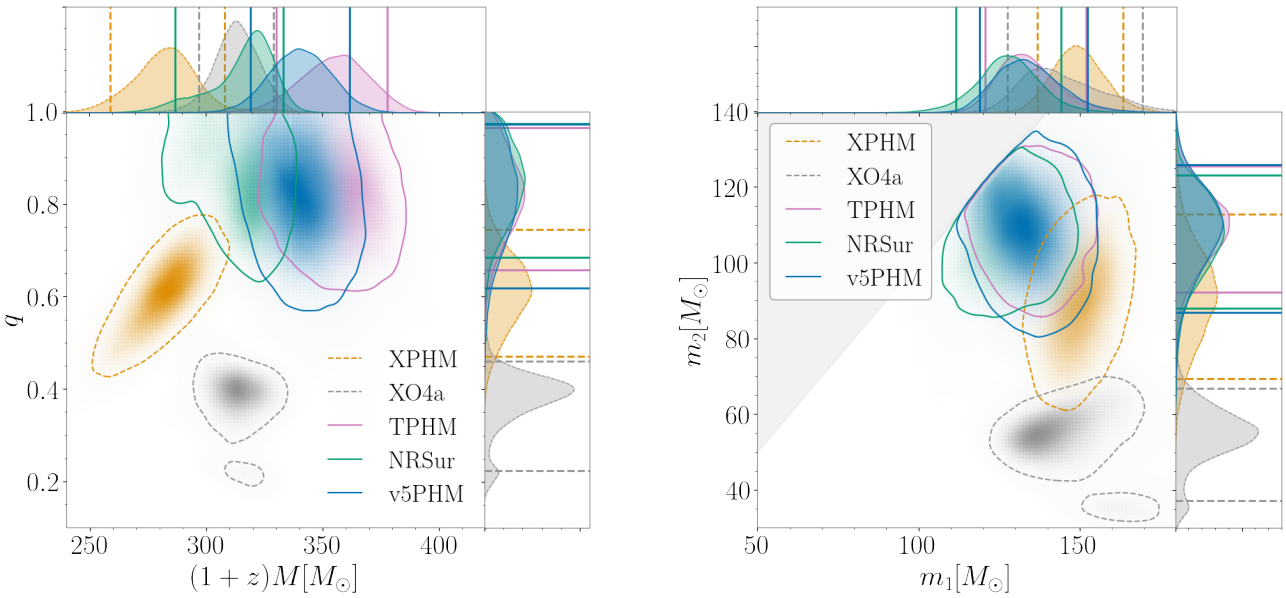


**Figure 7.** Marginalized posterior probability for the *Left*: redshifted (detector-frame) total binary mass and the mass ratio, and *Right*: primary and secondary source-frame masses inferred from GW231123 for each of the five models considered. Each contour, as well as the colored horizontal and vertical lines, shows the 90% credible intervals.

and XPHM are calibrated to NR only in the aligned-spin sector (Pompili et al. 2023; Estellés et al. 2022b; Pratten et al. 2020a; García-Quirós et al. 2020) and instead model precession either by extending post-Newtonian and effective-one-body results or by employing BH perturbation theory results through merger and ringdown. During the inspiral, v5PHM, TPHM, and XPHM implement precession dynamics by numerically evolving the spins (Khalil et al. 2023; Estellés et al. 2021; Colleoni et al. 2025). XO4a uses closed-form, orbit-averaged expressions during the inspiral (Chatziioannou et al. 2017; Pratten et al. 2021) and phenomenological expressions calibrated to single-spin precessing simulations with $\chi_1 < 0.8$ through merger and ringdown (Hamilton et al. 2021). Further, XO4a includes mode asymmetry of the dominant multipole (Ghosh et al. 2024).

The different modeling approaches and treatments of the precession dynamics make these models relatively independent. In the presence of features in the data beyond the physical effects incorporated in the models (e.g., mismodelling in the high-spin regime, eccentricity, GW memory, or noise artefacts) one might therefore expect the models to interact with these features differently and display model systematics, as are seen in the posteriors for this event. The accuracy of these models for typical signals has been comprehensively assessed through comparison to NR, both in the modelling papers themselves and elsewhere (Mac Uilliam et al. 2024, e.g., []).For GW231123 we have performed the accuracy analysis in Section 4.2, and a series of targeted NR injections, which we now describe. We hope that more can be learned in the future from improved models in the high-spin regime, and a detailed study of the behaviour of our models in Gaussian noise.

In order to investigate the likelihood of the presence of waveform systematics in the high total mass, comparable-mass ($q > 1/3$), highly precessing region of parameter space, we perform a simulation study where we simulate a set of signals consisting of highly precessing NR waveforms from the SXS catalog (Boyle et al. 2019; Scheel et al. 2025) and recover with the five waveform models under consideration. From several tens of simulations, we discuss here the results from two that span the range of observed results, from unbiased parameter estimation displaying no systematics to large systematic differences between models and clear biases in parameter recovery.

For both configurations, we show the total mass and mass ratio as measured in the data (the detector frame). For high-mass binaries, we expect the total mass to be one of the most reliably measured quantities. The detector-frame masses are not the true source masses, but the *redshifted* masses, and to calculate the true masses, we must also measure the redshift. The relative accuracy of the detector-frame and source-frame masses may therefore differ, depending on

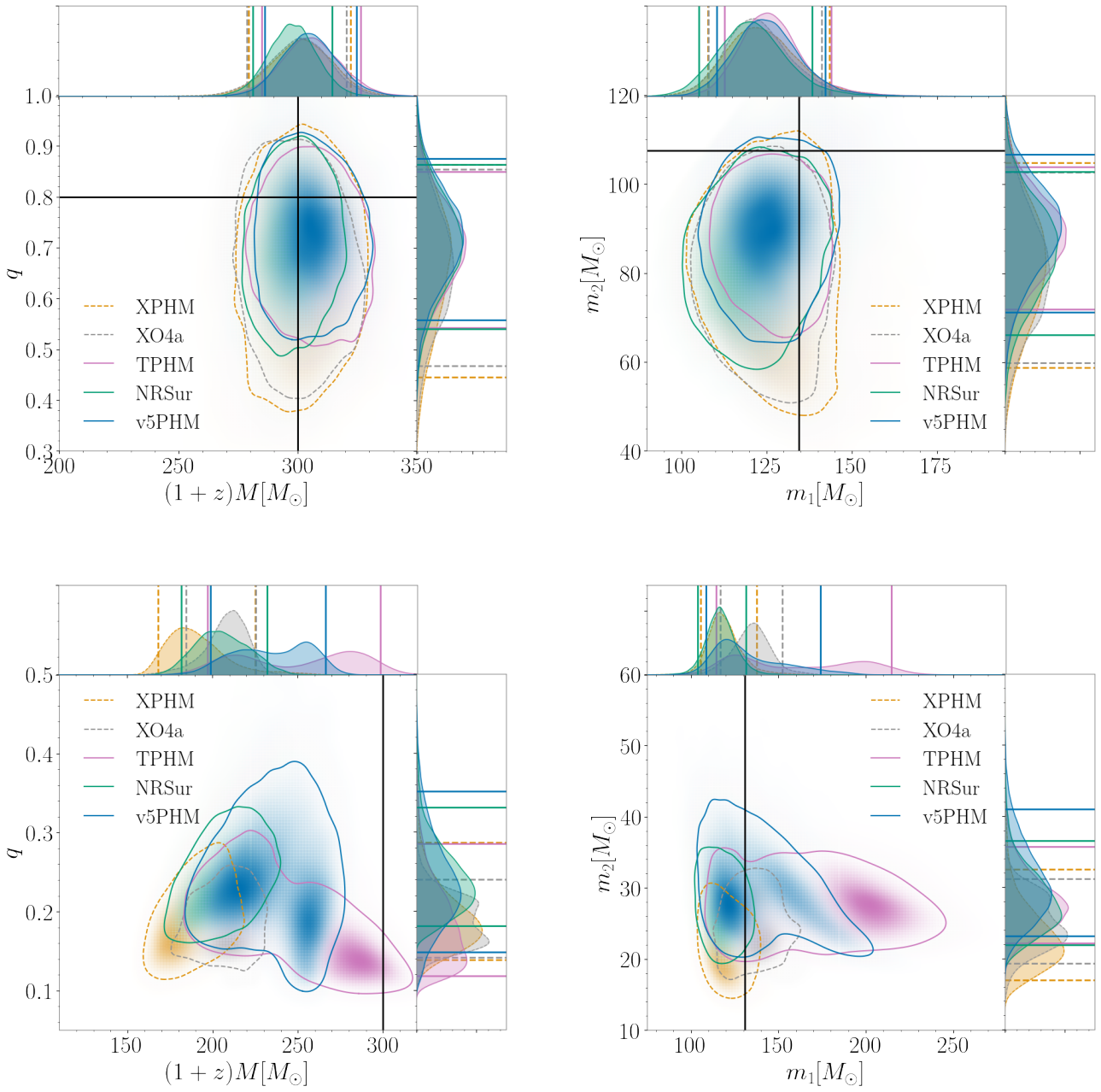


**Figure 8.** Marginalized posterior probability for (left column) redshifted (detector-frame) total binary mass and the mass ratio and (right column) primary and secondary source-frame masses inferred from two highly spinning precessing NR simulations with (detector-frame) total binary mass of $300\,M_\odot$ observed approximately edge on. The Top row shows the results for the SXS:BBH:0483 (Boyle et al. 2019) with masses $m_1 \sim 135\,M_\odot$, $m_2 \sim 110\,M_\odot$ and mass ratio $q = 0.8$. The Bottom row shows the results for the SXS:BBH:4030 (Scheel et al. 2025) with masses $m_1 = m_2 \sim 130\,M_\odot$. The 5 models used to analyse GW231123 were also used to analyse these simulations. Each contour, as well as the colored horizontal and vertical lines, shows the 90% credible intervals. The black vertical and horizontal lines indicate the true source properties. In some panels, the true value is beyond the axis range of the figure.

the accuracy of the redshift. For this reason, we also show the individual masses $m_1$ and $m_2$ after correcting for the redshift.

The results for GW231123 are shown in Figure 7. In the left panel, we see clear evidence of systematics in the measurement of both the total mass and the mass ratio, with no overlap of the 90% credible intervals for some models in both parameters. When we correct for the redshift, some of the differences appear to "cancel out", and we see agreement between several models in the source masses. This is likely coincidental; we expect any model biases in the detector-frame masses and redshift to be independent. This expectation is borne out in the examples below.

In the majority of cases simulated, we were unable to reproduce this degree of systematics. In both examples discussed here, we choose a large inclination angle as the mismatch performance is worst, and thus the associated expectations of evidence of systematics are greater, for systems with the greatest contribution from higher multipoles. It should be noted, however, that since the orbital plane precesses, the inclination is not constant over the binary's evolution. An example of a typical recovery is shown in the top row of Figure 8, where we consider the SXS:BBH:0483 precessing NR simulation with total mass $M = 300\,M_\odot$, mass ratio $q = 0.8$, and spin magnitudes $\chi_1 = \chi_2 = 0.80$ on both BHs. The simulation is added to zero-noise using the fiducial inclination angle $\iota = \pi/2\,\mathrm{rad}$ at 10 Hz. For this configuration, the mismatch for NRSur was unambiguously below the conservative distinguishability criterion, with a value of $3.92 \times 10^{-4}$, while for the other models we see values $\mathcal{O}\left(10^{-3}\right)$. In this case, the large differences in mismatch do not translate into noticeable differences in the accuracy of parameter recovery. The posteriors from all models overlap and we can be confident in our recovered source properties. Note, however, that the source-frame $m_2$ is too low. This is a known bias for edge-on configurations: signals from face-on and face-off binaries are louder, meaning that larger distances (redshifts) are consistent with a fixed GW amplitude. This leads to a significantly larger prior volume, and thus a prior preference for smaller inclination angles (Usman et al. 2019), larger distances, and thus lower (redshifted) source masses.

Clear evidence of systematics was nevertheless seen in a limited number of simulations, as is demonstrated in the bottom row of Figure 8. We consider the SXS:BBH:4030 precessing NR simulation with total mass $M = 300\,M_\odot$, equal mass components ($q = 1$), and spin magnitudes $\chi_1 = \chi_2 = 0.95$ on both BHs. The simulation is added to zero-noise using the fiducial inclination angle $\iota = \pi/2\,\mathrm{rad}$ at 15 Hz. This injection was chosen from the set of cases with very high spins, with a mismatch between $2.36 \times 10^{-3}$ (NRSur) and $9.45 \times 10^{-3}$ (TPHM), mostly above the conservative indistinguishability criterion. This numerical relativity (NR) waveform also includes GW memory, which can require additional data processing for injection (Xu et al. 2024; Valencia et al. 2024; Chen et al. 2024), but we find that our results are unchanged if we first subtract the memory features before injection. We see unequivocal evidence of waveform systematics and biases in all models. Only the posterior of TPHM includes the true value of the detector-frame total mass, and all models exclude it at 90% credibility. No model recovers the true mass ratio ($q = 1$). In the source-frame, the true value of $m_1$ lies in the 90% credible region for all models, but $m_2$ is significantly biased from its true value of $100\,M_\odot$.

## B. SOURCE PROPERTIES

In Table 3, we present the individual source properties of GW231123 for each of the five models considered in the analysis of this event for those interested in a more detailed picture of the systematics. As demonstrated in Appendix A, the source properties of this event lie in a challenging region of parameter space for all waveform models employed. From the analysis performed here, we cannot guarantee that the results from any given model will be free from bias in this region of parameter space. We also find that different models fit the data better than others. All models except XPHM obtain a larger Bayesian evidence than the NRSur analysis, as reflected in the differing SNRs in Table 3. For example, for some parameters XO4a yields significantly different results to many of the other models, yet it obtains a Bayes factor of at least 140:1 over NRSur. However, such differences are not necessarily indicative of one model being more accurate than another (Hoy 2022; Hoy et al. 2024). Consequently, we combine the posteriors from multiple models to achieve a conservative error estimate, which is reported throughout the main body of the paper.

We also illustrate in Figure 9 the differences in inferred spin orientation when considering the data from LIGO Hanford (left), LIGO Livingston (middle), and the full detector network (right). LIGO Hanford shows support for aligned-spin binaries, while LIGO Livingston has a clear preference for misalignment. The stronger signal in LIGO Livingston dominates the network results. The differences between the results in the two detectors could potentially be explained by lower signal power in LIGO Hanford (such that precession is not measurable), but we have not been able to reproduce this discrepancy between detectors with injections in zero-noise, for example, of the NRSur waveform at its maximum-likelihood parameters.

**Table 3.** Individual source properties of GW231123 from each of the five models considered.

| | XPHM | XO4a | TPHM | NRSur | v5PHM |
|---|---|---|---|---|---|
| Primary mass $m_1/\mathrm{M}_\odot$ | $149^{+14}_{-13}$ | $143^{+26}_{-16}$ | $133^{+19}_{-13}$ | $128^{+16}_{-16}$ | $133^{+19}_{-15}$ |
| Secondary mass $m_2/\mathrm{M}_\odot$ | $92^{+21}_{-22}$ | $55^{+12}_{-18}$ | $110^{+16}_{-17}$ | $108^{+16}_{-20}$ | $109^{+17}_{-22}$ |
| Mass ratio $q = m_2/m_1$ | $0.61^{+0.13}_{-0.14}$ | $0.39^{+0.07}_{-0.16}$ | $0.82^{+0.16}_{-0.14}$ | $0.85^{+0.15}_{-0.12}$ | $0.82^{+0.18}_{-0.15}$ |
| Total mass $M/\mathrm{M}_\odot$ | $241^{+30}_{-28}$ | $198^{+30}_{-18}$ | $242^{+28}_{-19}$ | $237^{+23}_{-32}$ | $241^{+28}_{-23}$ |
| Final mass $M_\mathrm{f}/\mathrm{M}_\odot$ | $231^{+27}_{-25}$ | $190^{+29}_{-17}$ | $227^{+26}_{-17}$ | $222^{+22}_{-32}$ | $226^{+25}_{-22}$ |
| Primary spin magnitude $\chi_1$ | $0.79^{+0.21}_{-0.20}$ | $0.92^{+0.07}_{-0.06}$ | $0.92^{+0.08}_{-0.14}$ | $0.90^{+0.10}_{-0.19}$ | $0.91^{+0.09}_{-0.16}$ |
| Secondary spin magnitude $\chi_2$ | $0.67^{+0.33}_{-0.47}$ | $0.47^{+0.41}_{-0.47}$ | $0.87^{+0.13}_{-0.25}$ | $0.91^{+0.09}_{-0.22}$ | $0.81^{+0.19}_{-0.35}$ |
| Effective inspiral spin $\chi_\mathrm{eff}$ | $0.03^{+0.17}_{-0.25}$ | $0.31^{+0.19}_{-0.19}$ | $0.43^{+0.16}_{-0.19}$ | $0.27^{+0.24}_{-0.35}$ | $0.43^{+0.20}_{-0.25}$ |
| Effective precessing spin $\chi_\mathrm{P}$ | $0.74^{+0.21}_{-0.21}$ | $0.82^{+0.10}_{-0.12}$ | $0.76^{+0.17}_{-0.17}$ | $0.76^{+0.19}_{-0.17}$ | $0.74^{+0.20}_{-0.19}$ |
| Final spin $\chi_\mathrm{f}$ | $0.70^{+0.08}_{-0.11}$ | $0.85^{+0.06}_{-0.07}$ | $0.88^{+0.04}_{-0.04}$ | $0.82^{+0.06}_{-0.11}$ | $0.88^{+0.05}_{-0.06}$ |
| Luminosity distance $D_\mathrm{L}/\mathrm{Gpc}$ | $0.9^{+0.4}_{-0.3}$ | $3.5^{+1.2}_{-1.4}$ | $2.7^{+1.2}_{-1.1}$ | $1.9^{+1.7}_{-1.0}$ | $2.3^{+1.4}_{-1.0}$ |
| Inclination angle $\theta_\mathrm{JN}/\mathrm{rad}$ | $1.6^{+0.4}_{-0.4}$ | $0.5^{+2.1}_{-0.3}$ | $1.9^{+0.3}_{-1.0}$ | $1.3^{+0.8}_{-0.4}$ | $1.2^{+1.0}_{-0.4}$ |
| Source redshift $z$ | $0.18^{+0.07}_{-0.06}$ | $0.58^{+0.17}_{-0.20}$ | $0.46^{+0.16}_{-0.16}$ | $0.34^{+0.24}_{-0.18}$ | $0.40^{+0.20}_{-0.16}$ |
| Network matched filter SNR $\rho$ | $20.5^{+0.2}_{-0.3}$ | $20.8^{+0.2}_{-0.2}$ | $20.8^{+0.2}_{-0.3}$ | $20.6^{+0.2}_{-0.3}$ | $20.7^{+0.2}_{-0.3}$ |

NOTE—As in Table 2 in most cases we present the median value of the 1D marginalized posterior distribution and the symmetric 90% credible interval. For properties that have physical bounds we report the median value as well as the 90% highest posterior density (HPD) credible interval. Our results are reported at a reference frequency of 10 Hz.

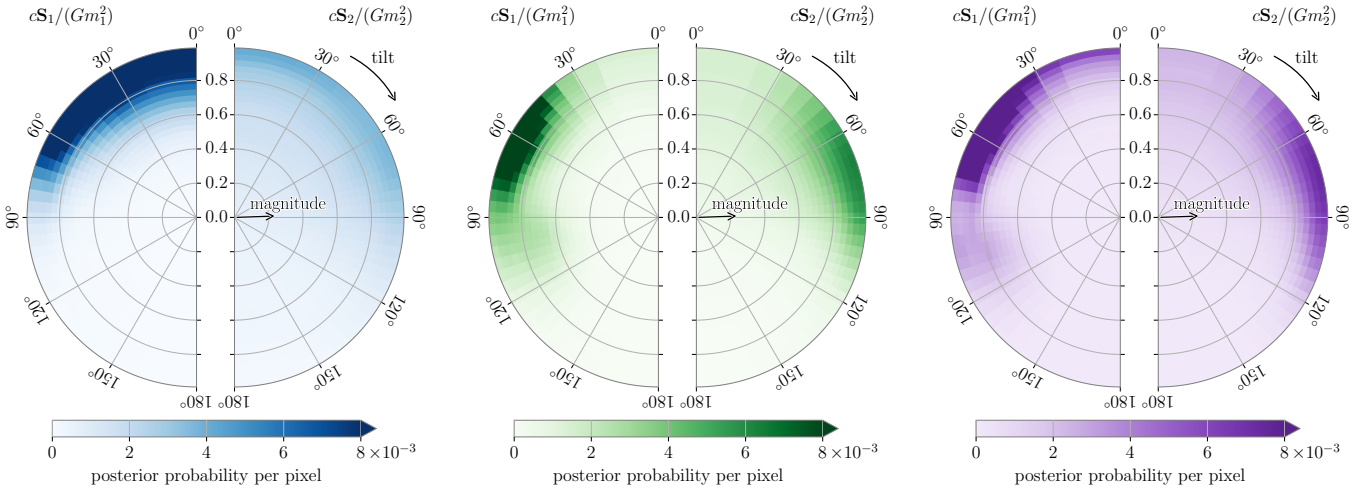


**Figure 9.** Posterior probabilities for the dimensionless component spins, $c\boldsymbol{S}_1/(Gm_1^2)$ and $c\boldsymbol{S}_2/(Gm_1^2)$, relative to the orbital angular momentum axis $\hat{\boldsymbol{L}}$. From left to right, we compare the posterior probabilities obtained when analysing LIGO Hanford data only (blue), LIGO Livingston data only (green), and a coherent analysis of LIGO Hanford and LIGO Livingston data (purple). In all cases, we show the posterior distribution resulting from equally combining samples from five waveform models. The tilt angles are 0° for spins aligned with the orbital angular momentum and 180° for spins anti-aligned. Probabilities are marginalized over the azimuthal angles. The pixels have equal prior probability, being equally spaced in the spin magnitudes and the cosines of tilt angles. The spin orientations are defined at a fiducial GW frequency of 10 Hz.

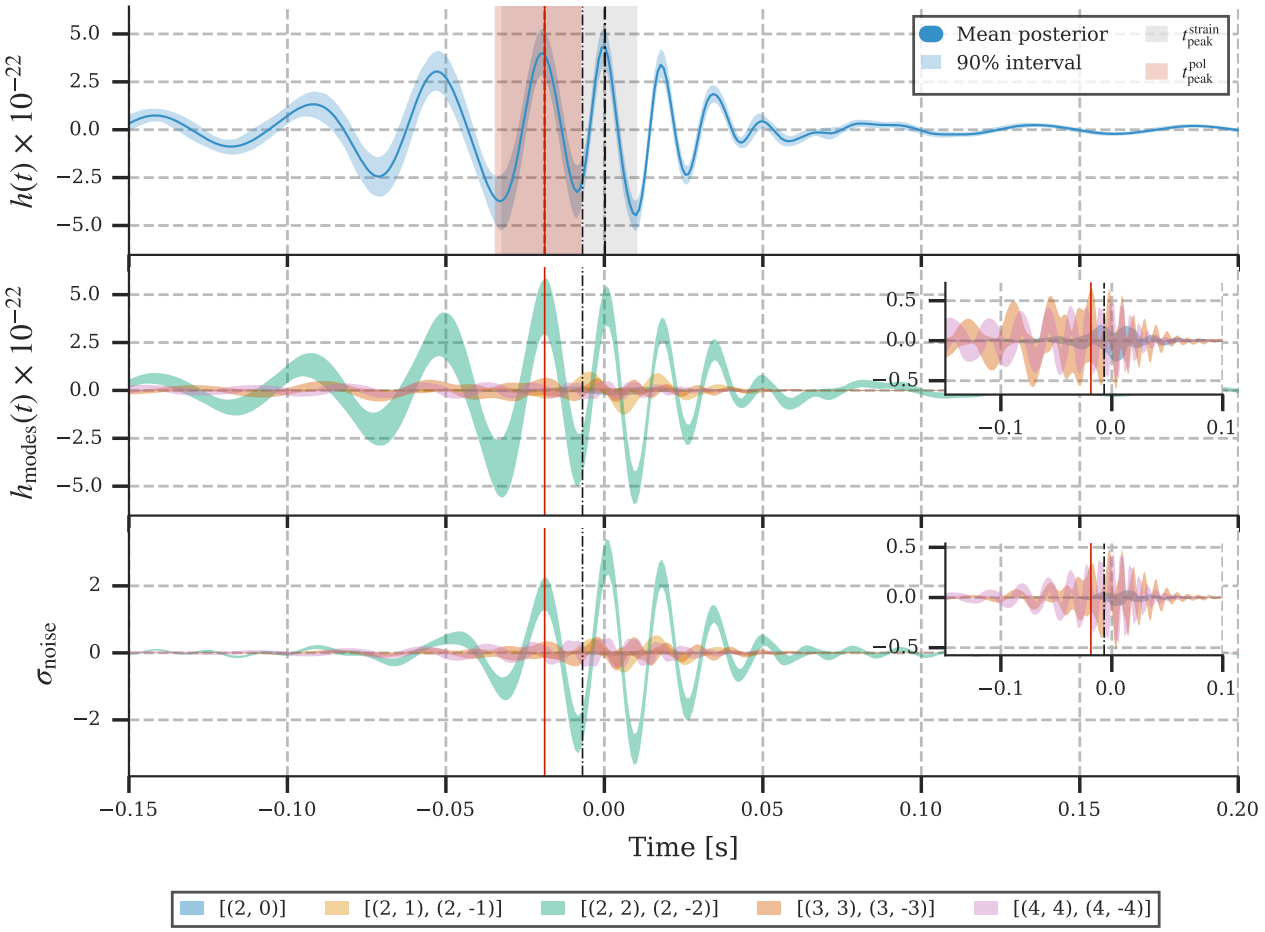


**Figure 10.** **Top panel:** Posterior probability density functions of the NRSur waveform timeseries, obtained via Bilby using the NRSur waveform model in the LIGO Hanford detector. The red band shows the uncertainty in the measurement of $t^{\rm pol}_{\rm peak}$, and the grey band shows the uncertainty in $t^{\rm strain}_{\rm peak}$. **Middle and bottom panel:** Posterior probability density functions of the mode strain, $F_+h_+ + F_\times h_\times$, with $h_+ - ih_\times = {}^{-2}Y_{\ell,m}h_{\ell,m} + {}^{-2}Y_{\ell,-m}h_{\ell,-m}$, shown for the LIGO Hanford detector. The top part reports the unwhitened waveform and the bottom part the whitened one, showcasing the impact of whitening in visualising the signal morphology. The inset focuses on the $(\ell, \pm m) = (2,0), (3,3), (4,4)$ modes. The red line indicates the median of $t^{\rm pol}_{\rm peak}$, and the dashed-dotted black lines show the median of $t^{\rm modes}_{\rm peak}$.

## C. SIGNAL PEAK TIME

We require the time of peak GW emission to determine a valid starting time for ringdown analyses. The peak GW power is emitted at time $t^{\rm modes}_{\rm peak} = \max_t \sqrt{\sum_{\ell,m} \left|\dot{h}_{\ell m}(t)\right|^2}$, where $h_{\ell m}(t)$ are the multipoles in a spin-weighted spherical-harmonic decomposition of the signal. Alternatively, we can estimate the peak time using the peak of the polarisation $t^{\rm pol}_{\rm peak} = \max_t |h_+ - ih_\times|^2$. This quantity depends on the binary's relative orientation to the detector and will be uncertain to within roughly one GW period, but it can be compared to an estimate computed through an unmodelled waveform reconstruction, allowing for a more agnostic analysis. One can also conservatively estimate the onset of ringdown directly from the maximum value of the strain $t^{\rm strain}_{\rm peak}$, after which the signal displays a clear decay. Figure 10 shows these times for GW231123, on top of the unwhitened NRSur strain reconstruction from which they were computed. From this reconstruction, we find $t^{\rm strain}_{\rm peak}$ is $1384782888.6191^{+0.0098}_{-0.0322}$ s and $1384782888.6142^{+0.0107}_{-0.0195}$ s in the LIGO Hanford and Livingston detectors respectively. Instead, in the LIGO Hanford detector (chosen as reference for the ringdown analysis), we find $t^{\rm modes}_{\rm peak} - t^{\rm pol}_{\rm peak} \approx 6\,$ms.

The differences among these estimates, together with the time-domain reconstruction shown in Figure 10, attest to the highly complex signal morphology and invite care when selecting a peak time definition to be used as reference in a ringdown analysis. Hence, in the main text we repeat the analysis over a wide range of times, and plot results around a conservative $t^{\rm start} \approx t^{\rm strain}_{\rm peak} + 15GM^{\rm det}_{\rm f}/c^3$ (assuming $M^{\rm det}_{\rm f} \simeq 298M_\odot$), when we are confident on the validity of a QNM description.

## D. HIGHER-ORDER RADIATION MULTIPOLES

Given the support for large binary inclination from most IMR models, subdominant multipole moments (referred to as "modes" below) beyond the dominant $(\ell, m) = (2, \pm 2)$ spherical-harmonic multipole moment are expected to contribute appreciably to the observed signal (Blanchet 2014). Here, we investigate in detail their contribution throughout the signal. Using NRSur posterior samples, we estimate optimal SNR values of $2.27^{+1.45}_{-1.05}$ for the $(3, \pm 3)$ mode, $2.92^{+0.70}_{-0.89}$ for the $(4, \pm 4)$ mode, $0.68^{+3.29}_{-0.48}$ for the $(2, \pm 1)$ mode and $0.25^{+0.65}_{-0.16}$ for the $(2, 0)$ mode. Unlike the $(3, 3)$ and $(4, 4)$ modes, the inferred distribution for the $(2, 1), (2, 0)$ modes are consistent with expectations from random Gaussian noise fluctuations, implying a lack of statistically significant support for their presence in the data. Relevant to the ringdown analysis, the strain contribution from the $(2, 0)$ mode remains significantly subdominant compared to the more prominent $(3, \pm 3)$ and $(4, \pm 4)$ modes throughout the signal duration, as illustrated in Figure 10 (showing LIGO Hanford, with similar conclusions obtained for LIGO Livingston). As seen in the bottom panel, the whitening process suppresses the lower-frequency content of the signal, causing the peak amplitude to appear quieter relative to the higher-frequency ringdown. This filtering effect also reduces the visibility of subdominant modes such as $(2, \pm 1)$ and $(2, 0)$, which fall largely outside the detector's sensitive band. In contrast, the $(3, \pm 3)$ and $(4, \pm 4)$ modes remain visible post-merger due to their higher frequency content, making them detectable. This result is consistent with the SNR estimates above. The IMR modes are defined with respect to the binary's total angular momentum at a given reference time during the inspiral, while the ringdown modes are defined with respect to the remnant spin at asymptotically late times. The direction between these two vectors may be offset by a few degrees (Hamilton et al. 2021), but we do not expect that would be sufficient to increase the power in $(2, 1)$ or $(2, 0)$ to a level measurable in Gaussian noise, i.e., above an SNR of $\sim$2.1.

In summary, we conclude that a significant excitation of the $(2, 0, 0)$ or $(2, 1, 0)$ ringdown modes, suggested by the overlap of damped sinusoids fitting parameters with the remnant properties inferred by NRSur, is in tension with NRSur multipole moments content.

REFERENCES


Aasi, J., et al. 2015, Class. Quant. Grav., 32, 074001

Abac, A. G., et al. 2025a, in preparation

—. 2025b, arXiv:2508.18081

Abbott, B. P., et al. 2016a, Phys. Rev. Lett., 116, 241102

—. 2016b, Astrophys. J. Lett., 833, L1

—. 2016c, Phys. Rev. X, 6, 041015, [Erratum: Phys.Rev.X 8, 039903 (2018)]

—. 2020a, Class. Quant. Grav., 37, 055002

Abbott, B. P., Abbott, R., Abbott, T. D., et al. 2020b, Classical and Quantum Gravity, 37, 055002

Abbott, R., Abbott, T., Ackley, K., et al. 2020c, Living reviews in relativity, 23, 1

Abbott, R., et al. 2020d, Phys. Rev. Lett., 125, 101102

—. 2020e, Astrophys. J. Lett., 900, L13

—. 2020f, Phys. Rev. D, 102, 043015

—. 2020g, Astrophys. J. Lett., 896, L44

—. 2021a, Phys. Rev. X, 11, 021053

—. 2021b, arXiv:2112.06861

—. 2021c, Astrophys. J., 923, 14

—. 2022, Astron. Astrophys., 659, A84

—. 2023a, Phys. Rev. X, 13, 041039

—. 2023b, Phys. Rev. X, 13, 011048

—. 2024a, Phys. Rev. D, 109, 022001

—. 2024b, Astrophys. J., 970, 191

Abdikamalov, E., Pagliaroli, G., & Radice, D. 2020, arXiv:2010.04356

Acernese, F., et al. 2015, Class. Quant. Grav., 32, 024001

Adams, T., Buskulic, D., Germain, V., et al. 2016, Class. Quant. Grav., 33, 175012

Ade, P. A. R., et al. 2016, Astron. Astrophys., 594, A13

Ajith, P., et al. 2011, Phys. Rev. Lett., 106, 241101

Akutsu, T., Ando, M., Arai, K., et al. 2020, Progress of Theoretical and Experimental Physics, 2021, 05A101. https://doi.org/10.1093/ptep/ptaa125

Albanesi, S., Gamba, R., Bernuzzi, S., et al. 2025a, arXiv:2503.14580

Albanesi, S., Rashti, A., Zappa, F., et al. 2025b, Phys. Rev. D, 111, 024069

Allen, B. 2005, Phys. Rev. D, 71, 062001

Alléné, C., et al. 2025, Class. Quant. Grav., 42, 105009

Álvarez, C. A., Wong, H. W. Y., Liu, A., & Calderón Bustillo, J. 2024, Astrophys. J., 977, 220

Andrade, T., et al. 2024, Phys. Rev. D, 109, 084025

Antonini, F., Gieles, M., & Gualandris, A. 2019, Mon. Not. Roy. Astron. Soc., 486, 5008

Antonini, F., Murray, N., & Mikkola, S. 2014, Astrophys. J., 781, 45

Antonini, F., & Rasio, F. A. 2016, Astrophys. J., 831, 187

Antonini, F., Romero-Shaw, I. M., & Callister, T. 2025, Phys. Rev. Lett., 134, 011401

Arca Sedda, M., Kamlah, A. W. H., Spurzem, R., et al. 2023a, Mon. Not. Roy. Astron. Soc., 526, 429

Arca Sedda, M., Naoz, S., & Kocsis, B. 2023b, Universe, 9, 138

Arca Sedda, M., Rizzuto, F. P., Naab, T., et al. 2021, Astrophys. J., 920, 128

Ashton, G., et al. 2019, Astrophys. J. Suppl., 241, 27

Aubin, F., et al. 2021, Class. Quant. Grav., 38, 095004

Aurrekoetxea, J. C., Hoy, C., & Hannam, M. 2024, Phys. Rev. Lett., 132, 181401

Baibhav, V., Berti, E., Gerosa, D., Mould, M., & Wong, K. W. K. 2021, Phys. Rev. D, 104, 084002

Baird, E., Fairhurst, S., Hannam, M., & Murphy, P. 2013, Phys. Rev. D, 87, 024035

Barkat, Z., Rakavy, G., & Sack, N. 1967, Phys. Rev. Lett., 18, 379

Barrera, O., & Bartos, I. 2022, Astrophys. J. Lett., 929, L1

Bartos, I., Kocsis, B., Haiman, Z., & Márka, S. 2017, Astrophys. J., 835, 165

Bavera, S. S., Fragos, T., Qin, Y., et al. 2020, Astron. Astrophys., 635, A97

Belczynski, K., et al. 2016, Astron. Astrophys., 594, A97

—. 2020, Astron. Astrophys., 636, A104

Berti, E., Cardoso, V., & Starinets, A. O. 2009, Class. Quant. Grav., 26, 163001

Berti, E., Cardoso, V., & Will, C. M. 2006, Phys. Rev. D, 73, 064030

Berti, E., et al. 2025, arXiv:2505.23895

Bhagwat, S., Cabero, M., Capano, C. D., Krishnan, B., & Brown, D. A. 2020, Phys. Rev. D, 102, 024023

Bird, S., Cholis, I., Muñoz, J. B., et al. 2016, Phys. Rev. Lett., 116, 201301

Bird, S., et al. 2023, Phys. Dark Univ., 41, 101231

Blackman, J., Field, S. E., Galley, C. R., et al. 2015, Phys. Rev. Lett., 115, 121102

Blanchet, L. 2014, Living Rev. Rel., 17, 2

Bond, J. R., Arnett, W. D., & Carr, B. J. 1984, Astrophys. J., 280, 825

Borchers, A., Ye, C. S., & Fishbach, M. 2025, arXiv:2503.21278

Boyle, M., et al. 2019, Class. Quant. Grav., 36, 195006

Brito, R., Buonanno, A., & Raymond, V. 2018, Phys. Rev. D, 98, 084038

Buonanno, A., & Damour, T. 1999, Phys. Rev. D, 59, 084006

—. 2000, Phys. Rev. D, 62, 064015

Buonanno, A., Pan, Y., Baker, J. G., et al. 2007, Phys. Rev. D, 76, 104049
Calderón Bustillo, J., Salemi, F., Dal Canton, T., & Jani, K. P. 2018, Phys. Rev. D, 97, 024016
Calderón Bustillo, J., Sanchis-Gual, N., Torres-Forné, A., & Font, J. A. 2021a, Phys. Rev. Lett., 126, 201101
Calderón Bustillo, J., Sanchis-Gual, N., Torres-Forné, A., et al. 2021b, Phys. Rev. Lett., 126, 081101
Cannon, K., Caudill, S., Chan, C., et al. 2021, SoftwareX, 14, 100680
Capote, E., et al. 2025, Phys. Rev. D, 111, 062002
Carullo, G. 2024, JCAP, 10, 061
Carullo, G., Albanesi, S., Nagar, A., et al. 2024, Phys. Rev. Lett., 132, 101401
Carullo, G., Del Pozzo, W., & Veitch, J. 2019, Phys. Rev. D, 99, 123029, [Erratum: Phys.Rev.D 100, 089903 (2019)]
—. 2025, pyRing, v2.7.0, Zenodo, doi:10.5281/zenodo.8165507. https://doi.org/10.5281/zenodo.8165507
Carullo, G., et al. 2018, Phys. Rev. D, 98, 104020
Chandra, K., Gayathri, V., Bustillo, J. C., & Pai, A. 2020, Phys. Rev. D, 102, 044035
Chandra, K., Pai, A., Villa-Ortega, V., et al. 2021a, in 16th Marcel Grossmann Meeting on Recent Developments in Theoretical and Experimental General Relativity, Astrophysics and Relativistic Field Theories
Chandra, K., Villa-Ortega, V., Dent, T., et al. 2021b, Phys. Rev. D, 104, 042004
Chattopadhyay, D., Stegmann, J., Antonini, F., Barber, J., & Romero-Shaw, I. M. 2023, Mon. Not. Roy. Astron. Soc., 526, 4908
Chatziioannou, K., Cornish, N., Wijngaarden, M., & Littenberg, T. B. 2021, Phys. Rev. D, 103, 044013
Chatziioannou, K., Dent, T., Fishbach, M., et al. 2024, arXiv:2409.02037
Chatziioannou, K., Haster, C.-J., Littenberg, T. B., et al. 2019, Phys. Rev. D, 100, 104004
Chatziioannou, K., Klein, A., Yunes, N., & Cornish, N. 2017, Phys. Rev. D, 95, 104004
Chen, Y., et al. 2024, Phys. Rev. D, 110, 064049
Cheung, M. H.-Y., Berti, E., Baibhav, V., & Cotesta, R. 2024, Phys. Rev. D, 109, 044069, [Erratum: Phys.Rev.D 110, 049902 (2024)]
Chu, Q., et al. 2022, Phys. Rev. D, 105, 024023
Clesse, S., & García-Bellido, J. 2017, Phys. Dark Univ., 15, 142
—. 2022, Phys. Dark Univ., 38, 101111
Colleoni, M., Vidal, F. A. R., García-Quirós, C., Akçay, S., & Bera, S. 2025, Phys. Rev. D, 111, 104019
Cornish, N. J., & Littenberg, T. B. 2015, Class. Quant. Grav., 32, 135012
Cornish, N. J., Littenberg, T. B., Bécsy, B., et al. 2021, Phys. Rev. D, 103, 044006
Costa, G., Ballone, A., Mapelli, M., & Bressan, A. 2022, Mon. Not. Roy. Astron. Soc., 516, 1072
Costa, G., Bressan, A., Mapelli, M., et al. 2021, Mon. Not. Roy. Astron. Soc., 501, 4514
Cutler, C., & Flanagan, E. E. 1994, Phys. Rev. D, 49, 2658
Dal Canton, T., Nitz, A. H., Gadre, B., et al. 2021, Astrophys. J., 923, 254
Dall'Amico, M., Mapelli, M., Torniamenti, S., & Arca Sedda, M. 2024, Astron. Astrophys., 683, A186
Davies, G. S., Dent, T., Tápai, M., et al. 2020, Phys. Rev. D, 102, 022004
Davis, D., Trevor, M., Mozzon, S., & Nuttall, L. K. 2022, Phys. Rev. D, 106, 102006
Davis, D., et al. 2021, Class. Quant. Grav., 38, 135014
de Mink, S. E., & Mandel, I. 2016, Mon. Not. Roy. Astron. Soc., 460, 3545
Detweiler, S. L. 1980, Astrophys. J., 239, 292
Di Carlo, U. N., Mapelli, M., Bouffanais, Y., et al. 2020, Mon. Not. Roy. Astron. Soc., 497, 1043
Doctor, Z., Farr, B., & Holz, D. E. 2021, Astrophys. J. Lett., 914, L18
Drago, M., et al. 2020, arXiv:2006.12604
Dreyer, O., Kelly, B. J., Krishnan, B., et al. 2004, Class. Quant. Grav., 21, 787
East, W. E., McWilliams, S. T., Levin, J., & Pretorius, F. 2013, Phys. Rev. D, 87, 043004
Essick, R., Godwin, P., Hanna, C., Blackburn, L., & Katsavounidis, E. 2020, Mach. Learn. Sci. Technol., 2, 015004
Estellés, H., Colleoni, M., García-Quirós, C., et al. 2022a, Phys. Rev. D, 105, 084040
Estellés, H., Husa, S., Colleoni, M., et al. 2022b, Phys. Rev. D, 105, 084039
Estellés, H., Ramos-Buades, A., Husa, S., et al. 2021, Phys. Rev. D, 103, 124060
Evstafyeva, T., Sperhake, U., Romero-Shaw, I. M., & Agathos, M. 2024, Phys. Rev. Lett., 133, 131401
Ewing, B., Huxford, R., Singh, D., et al. 2024, Phys. Rev. D, 109, 042008
Ewing, B., et al. 2024, Phys. Rev. D, 109, 042008
Ezquiaga, J. M., & Holz, D. E. 2021, Astrophys. J. Lett., 909, L23
Fairhurst, S., Green, R., Hannam, M., & Hoy, C. 2020a, Phys. Rev. D, 102, 041302
Fairhurst, S., Green, R., Hoy, C., Hannam, M., & Muir, A. 2020b, Phys. Rev. D, 102, 024055

Farmer, R., Renzo, M., de Mink, S., Fishbach, M., & Justham, S. 2020, Astrophys. J. Lett., 902, L36
Farmer, R., Renzo, M., de Mink, S. E., Marchant, P., & Justham, S. 2019, ApJ, 887, 53
Field, S. E., Galley, C. R., Hesthaven, J. S., Kaye, J., & Tiglio, M. 2014, Phys. Rev. X, 4, 031006
Fishbach, M., & Holz, D. E. 2020, Astrophys. J. Lett., 904, L26
Fishbach, M., Holz, D. E., & Farr, B. 2017, Astrophys. J. Lett., 840, L24
Fisher, R. P., Hemming, G., Bizouard, M.-A., et al. 2021, SoftwareX, 14, 100677
Fowler, W. A., & Hoyle, F. 1964, Astrophys. J. Suppl., 9, 201
Fragione, G., & Silk, J. 2020, Mon. Not. Roy. Astron. Soc., 498, 4591
Fraley, G. S. 1968, Ap&SS, 2, 96
Franciolini, G., Kritos, K., Reali, L., Broekgaarden, F., & Berti, E. 2024, Phys. Rev. D, 110, 023036
Fuller, J., & Ma, L. 2019, Astrophys. J. Lett., 881, L1
Gaburov, E., Lombardi, J., & Portegies Zwart, S. 2010, Mon. Not. Roy. Astron. Soc., 402, 105
Gamba, R., Breschi, M., Carullo, G., et al. 2023, Nature Astron., 7, 11
Gamboa, A., et al. 2024, arXiv:2412.12823
García-Quirós, C., Colleoni, M., Husa, S., et al. 2020, Phys. Rev. D, 102, 064002
Gayathri, V., Lopez, D., Pranjal, R. S., et al. 2020, Phys. Rev. D, 102, 104023
Gayathri, V., Healy, J., Lange, J., et al. 2022, Nature Astron., 6, 344
Gennari, V., Carullo, G., & Del Pozzo, W. 2024, Eur. Phys. J. C, 84, 233
Gerosa, D., & Berti, E. 2017, Phys. Rev. D, 95, 124046
Gerosa, D., & Fishbach, M. 2021, Nature Astron., 5, 749
Ghonge, S., Chatziioannou, K., Clark, J. A., et al. 2020, Phys. Rev. D, 102, 064056
Ghonge, S., Brandt, J., Sullivan, J. M., et al. 2024, Phys. Rev. D, 110, 122002
Ghosh, S., Kolitsidou, P., & Hannam, M. 2024, Phys. Rev. D, 109, 024061
Giersz, M., Leigh, N., Hypki, A., Lützgendorf, N., & Askar, A. 2015, Mon. Not. Roy. Astron. Soc., 454, 3150
Glebbeek, E., Gaburov, E., Portegies Zwart, S., & Pols, O. R. 2013, Mon. Not. Roy. Astron. Soc., 434, 3497
Gold, R., & Brügmann, B. 2013, Phys. Rev. D, 88, 064051
González, E., Kremer, K., Chatterjee, S., et al. 2021, Astrophys. J. Lett., 908, L29
Gossan, S., Veitch, J., & Sathyaprakash, B. S. 2012, Phys. Rev. D, 85, 124056
Green, A. M., & Kavanagh, B. J. 2021, J. Phys. G, 48, 043001
Green, R., Hoy, C., Fairhurst, S., et al. 2021, Phys. Rev. D, 103, 124023
Greene, J. E., Strader, J., & Ho, L. C. 2020, Ann. Rev. Astron. Astrophys., 58, 257
Gupte, N., et al. 2024, arXiv:2404.14286
Hamilton, E., London, L., Thompson, J. E., et al. 2021, Phys. Rev. D, 104, 124027
Hamilton, E., et al. 2024, Phys. Rev. D, 109, 044032
Hanna, C., et al. 2020, Phys. Rev. D, 101, 022003
Hannam, M., et al. 2022, Nature, 610, 652
Hannuksela, O. A., Haris, K., Ng, K. K. Y., et al. 2019, Astrophys. J. Lett., 874, L2
Harris, C. R., et al. 2020, Nature (London), 585, 357. https://doi.org/10.1038/s41586-020-2649-2
Harry, I., Privitera, S., Bohé, A., & Buonanno, A. 2016, Phys. Rev. D, 94, 024012
Healy, J., & Lousto, C. O. 2017, Phys. Rev. D, 95, 024037
—. 2022, Phys. Rev. D, 105, 124010
Hendriks, D. D., van Son, L. A. C., Renzo, M., Izzard, R. G., & Farmer, R. 2023, Mon. Not. Roy. Astron. Soc., 526, 4130
Hinder, I., Vaishnav, B., Herrmann, F., Shoemaker, D., & Laguna, P. 2008, Phys. Rev. D, 77, 081502
Hofmann, F., Barausse, E., & Rezzolla, L. 2016, Astrophys. J. Lett., 825, L19
Hourihane, S., Chatziioannou, K., Wijngaarden, M., et al. 2022, Phys. Rev. D, 106, 042006
Hoy, C. 2022, Phys. Rev. D, 106, 083003
Hoy, C., Akcay, S., Mac Uilliam, J., & Thompson, J. E. 2024, arXiv:2409.19404
Hoy, C., & Raymond, V. 2021, SoftwareX, 15, 100765
Huerta, E. A., et al. 2019, Phys. Rev. D, 100, 064003
Hunter, J. D. 2007, Comput. Sci. Eng., 9, 90
Hussain, A., Isi, M., & Zimmerman, A. 2024, arXiv:2411.02252
Iglesias, H. L., et al. 2024, Astrophys. J., 972, 65
Isi, M., & Farr, W. M. 2021, arXiv:2107.05609
Jiménez-Forteza, X., Keitel, D., Husa, S., et al. 2017, Phys. Rev. D, 95, 064024
Johnson-McDaniel, N. K., Ghosh, A., Ghonge, S., et al. 2022, Phys. Rev. D, 105, 044020
Joshi, P., et al. 2025, arXiv:2506.06497
Kamaretsos, I., Hannam, M., & Sathyaprakash, B. 2012, Phys. Rev. Lett., 109, 141102
Khalil, M., Buonanno, A., Estelles, H., et al. 2023, Phys. Rev. D, 108, 124036
Khan, S. 2024, Phys. Rev. D, 109, 104045

Kim, C., Kalogera, V., & Lorimer, D. R. 2003, Astrophys. J., 584, 985
Kimball, C., et al. 2021, Astrophys. J. Lett., 915, L35
Kıroğlu, F., Kremer, K., Biscoveanu, S., Prieto, E. G., & Rasio, F. A. 2025, Astrophys. J., 979, 237
Klimenko, S. 2022, arXiv:2201.01096
Klimenko, S., Yakushin, I., Mercer, A., & Mitselmakher, G. 2008, Class. Quant. Grav., 25, 114029
Klimenko, S., et al. 2016a, Phys. Rev. D, 93, 042004
Klimenko, S., Vedovato, G., Drago, M., et al. 2016b, Phys. Rev. D, 93, 042004
Kremer, K., Spera, M., Becker, D., et al. 2020, Astrophys. J., 903, 45
Kritos, K., Berti, E., & Silk, J. 2023, Phys. Rev. D, 108, 083012
Kumar, P., & Dent, T. 2024, Phys. Rev. D, 110, 043036
Kumar, S., Melching, M., & Ohme, F. 2025, arXiv:2502.17400
Li, Y.-J., Wang, Y.-Z., Tang, S.-P., & Fan, Y.-Z. 2024, Phys. Rev. Lett., 133, 051401
LIGO Scientific Collaboration and Virgo Collaboration. 2018, Data quality report user documentation, docs.ligo.org/detchar/data-quality-report/, ,
LIGO Scientific, Virgo, and KAGRA Collaboration. 2018, LVK Algorithm Library - LALSuite, Free software (GPL), , , doi:10.7935/GT1W-FZ16
—. 2025, GW231123: a Binary Black Hole Merger with Total Mass 190-265 $M_\odot$ — Data Release, Zenodo, doi:10.5281/zenodo.15832843. https://doi.org/10.5281/zenodo.15832843
Littenberg, T. B., & Cornish, N. J. 2015, Phys. Rev. D, 91, 084034
Liu, A., Wong, I. C. F., Leong, S. H. W., et al. 2023, Mon. Not. Roy. Astron. Soc., 525, 4149
Liu, X., Cao, Z., & Zhu, Z.-H. 2022, Class. Quant. Grav., 39, 035009
London, L., Shoemaker, D., & Healy, J. 2014, Phys. Rev. D, 90, 124032, [Erratum: Phys.Rev.D 94, 069902 (2016)]
Lopez, D., Gayathri, V., Pai, A., et al. 2022, Phys. Rev. D, 105, 063024
Lopez, M., Batta, A., Ramirez-Ruiz, E., Martinez, I., & Samsing, J. 2019, Astrophys. J., 877, 56
Mac Uilliam, J., Akcay, S., & Thompson, J. E. 2024, Phys. Rev. D, 109, 084077
Mahapatra, P., Chattopadhyay, D., Gupta, A., et al. 2024, Astrophys. J., 975, 117
—. 2025, Phys. Rev. D, 111, 023013
Mahapatra, P., Gupta, A., Favata, M., Arun, K. G., & Sathyaprakash, B. S. 2021, Astrophys. J. Lett., 918, L31
Mandel, I., & de Mink, S. E. 2016, Mon. Not. Roy. Astron. Soc., 458, 2634
Mapelli, M. 2016, Mon. Not. Roy. Astron. Soc., 459, 3432
Mapelli, M., Santoliquido, F., Bouffanais, Y., et al. 2021, Symmetry, 13, 1678
Mapelli, M., Spera, M., Montanari, E., et al. 2020, Astrophys. J., 888, 76
Marchant, P., Langer, N., Podsiadlowski, P., Tauris, T. M., & Moriya, T. J. 2016, Astron. Astrophys., 588, A50
Marchant, P., & Moriya, T. 2020, Astron. Astrophys., 640, L18
McKernan, B., Ford, K. E. S., Lyra, W., & Perets, H. B. 2012, Mon. Not. Roy. Astron. Soc., 425, 460
McKernan, B., Ford, K. E. S., O'Shaughnessy, R., & Wysocki, D. 2020, Mon. Not. Roy. Astron. Soc., 494, 1203
Mckernan, B., et al. 2018, Astrophys. J., 866, 66
McWilliams, S. T., Kelly, B. J., & Baker, J. G. 2010, Phys. Rev. D, 82, 024014
Mehta, A. K., Olsen, S., Wadekar, D., et al. 2025, Phys. Rev. D, 111, 024049
Merritt, D., Milosavljevic, M., Favata, M., Hughes, S. A., & Holz, D. E. 2004, Astrophys. J. Lett., 607, L9
Messick, C., et al. 2017, Phys. Rev. D, 95, 042001
Mezzacappa, A., & Zanolin, M. 2024, arXiv:2401.11635
Mezzasoma, S., Haster, C.-J., Owen, C. B., Cornish, N. J., & Yunes, N. 2025, arXiv:2503.23304
Mihaylov, D. P., Ossokine, S., Buonanno, A., et al. 2025, SoftwareX, 30, 102080
Miller, M. C., & Hamilton, D. P. 2002, Mon. Not. Roy. Astron. Soc., 330, 232
Mills, C., & Fairhurst, S. 2021, Phys. Rev. D, 103, 024042
Mishra, T., Bhaumik, S., Gayathri, V., et al. 2025, Phys. Rev. D, 111, 023054
Mishra, T., O'Brien, B., Gayathri, V., et al. 2021, Phys. Rev. D, 104, 023014
Mishra, T., et al. 2022, Phys. Rev. D, 105, 083018
Mould, M., Gerosa, D., & Taylor, S. R. 2022, Phys. Rev. D, 106, 103013
Nee, P. J., et al. 2025, arXiv:2503.05422
Nitz, A. H., Dent, T., Dal Canton, T., Fairhurst, S., & Brown, D. A. 2017, Astrophys. J., 849, 118
Nitz, A. H., Kumar, S., Wang, Y.-F., et al. 2023, Astrophys. J., 946, 59
Nitz, A. H., Dent, T., Davies, G. S., et al. 2020, Astrophys. J., 891, 123
Nobili, F., Bhagwat, S., Pacilio, C., & Gerosa, D. 2025, arXiv:2504.17021
Olsen, S., Venumadhav, T., Mushkin, J., et al. 2022, Phys. Rev. D, 106, 043009

O'Shaughnessy, R., London, L., Healy, J., & Shoemaker, D. 2013, Phys. Rev. D, 87, 044038
Pankow, C., Brady, P., Ochsner, E., & O'Shaughnessy, R. 2015, Phys. Rev. D, 92, 023002
Paul, K., Maurya, A., Henry, Q., et al. 2025, Phys. Rev. D, 111, 084074
Pierra, G., Mastrogiovanni, S., & Perrièss, S. 2024, Astron. Astrophys., 692, A80
Planas, M. d. L., Ramos-Buades, A., García-Quirós, C., et al. 2025a, arXiv:2503.13062
—. 2025b, arXiv:2504.15833
Pompili, L., Buonanno, A., & Pürrer, M. 2024, arXiv:2410.16859
Pompili, L., et al. 2023, Phys. Rev. D, 108, 124035
Portegies Zwart, S. F., Baumgardt, H., Hut, P., Makino, J., & McMillan, S. L. W. 2004, Nature, 428, 724
Powell, J., & Lasky, P. D. 2025, Publ. Astron. Soc. Austral., 42, e030
Pratten, G., Husa, S., Garcia-Quiros, C., et al. 2020a, Phys. Rev. D, 102, 064001
Pratten, G., Schmidt, P., Buscicchio, R., & Thomas, L. M. 2020b, Phys. Rev. Res., 2, 043096
Pratten, G., et al. 2021, Phys. Rev. D, 103, 104056
Qin, Y., Fragos, T., Meynet, G., et al. 2018, Astron. Astrophys., 616, A28
Rakavy, G., & Shaviv, G. 1967, ApJ, 148, 803
Ramos-Buades, A., Buonanno, A., Estellés, H., et al. 2023a, Phys. Rev. D, 108, 124037
Ramos-Buades, A., Buonanno, A., & Gair, J. 2023b, Phys. Rev. D, 108, 124063
Read, J. S. 2023, Class. Quant. Grav., 40, 135002
Renzo, M., Cantiello, M., Metzger, B. D., & Jiang, Y. F. 2020a, Astrophys. J. Lett., 904, L13
Renzo, M., Farmer, R. J., Justham, S., et al. 2020b, Mon. Not. Roy. Astron. Soc., 493, 4333
Rizzuto, F. P., Naab, T., Spurzem, R., et al. 2022, Mon. Not. Roy. Astron. Soc., 512, 884
Robinet, F., Arnaud, N., Leroy, N., et al. 2020, SoftwareX, 12, 100620
Rodriguez, C. L., Amaro-Seoane, P., Chatterjee, S., & Rasio, F. A. 2018, Phys. Rev. Lett., 120, 151101
Rodriguez, C. L., Zevin, M., Amaro-Seoane, P., et al. 2019, Phys. Rev. D, 100, 043027
Romero-Shaw, I. M., Gerosa, D., & Loutrel, N. 2023, Mon. Not. Roy. Astron. Soc., 519, 5352
Romero-Shaw, I. M., Lasky, P. D., Thrane, E., & Bustillo, J. C. 2020a, Astrophys. J. Lett., 903, L5
Romero-Shaw, I. M., et al. 2020b, Mon. Not. Roy. Astron. Soc., 499, 3295
Ruiz-Rocha, K., Yelikar, A. B., Lange, J., et al. 2025, Astrophys. J. Lett., 985, L37
Sachdev, S., et al. 2019, arXiv e-prints, arXiv:1901.08580
Sakon, S., et al. 2024, Phys. Rev. D, 109, 044066
Salemi, F., Milotti, E., Prodi, G. A., et al. 2019, Phys. Rev. D, 100, 042003
Samsing, J. 2018, Phys. Rev. D, 97, 103014
Santamaria, L., et al. 2010, Phys. Rev. D, 82, 064016
Scheel, M. A., et al. 2025, arXiv:2505.13378
Schmidt, P., Ohme, F., & Hannam, M. 2015, Phys. Rev. D, 91, 024043
Siegel, H., Isi, M., & Farr, W. M. 2025, Phys. Rev. D, 111, 044070
Siemonsen, N., & East, W. E. 2023, Phys. Rev. D, 107, 124018
Singer, L. P., & Price, L. R. 2016, Phys. Rev. D, 93, 024013
Smith, J. R., Abbott, T., Hirose, E., et al. 2011, Class. Quant. Grav., 28, 235005
Smith, L., Ghosh, S., Sun, J., et al. 2024, Phys. Rev. D, 110, 083032
Smith, R. J. E., Ashton, G., Vajpeyi, A., & Talbot, C. 2020, Mon. Not. R. Astron. Soc., 498, 4492
Soni, S., et al. 2025, Class. Quant. Grav., 42, 085016
Speagle, J. S. 2020, Mon. Not. Roy. Astron. Soc., 493, 3132
Spera, M., Mapelli, M., Giacobbo, N., et al. 2019, Mon. Not. Roy. Astron. Soc., 485, 889
Sperhake, U., Berti, E., Cardoso, V., et al. 2008, Phys. Rev. D, 78, 064069
Stevenson, S., Sampson, M., Powell, J., et al. 2019, ApJ, 882, 121
Stone, N. C., Metzger, B. D., & Haiman, Z. 2017, Mon. Not. Roy. Astron. Soc., 464, 946
Sun, L., et al. 2020, Class. Quant. Grav., 37, 225008
—. 2021, arXiv:2107.00129
Szczepańczyk, M., et al. 2021, Phys. Rev. D, 103, 082002
Szczepańczyk, M. J., et al. 2023, Phys. Rev. D, 107, 062002
Tagawa, H., Haiman, Z., & Kocsis, B. 2020, Astrophys. J., 898, 25
Takahashi, R., & Nakamura, T. 2003, Astrophys. J., 595, 1039
Thompson, J., Hoy, C., Fauchon-Jones, E., & Hannam, M. 2025, Phys. Rev. D, 112, 064011. https://link.aps.org/doi/10.1103/ddz7-x9zz
Thompson, J. E., Hamilton, E., London, L., et al. 2024, Phys. Rev. D, 109, 063012
Tsang, K. W., Ghosh, A., Samajdar, A., et al. 2020, Phys. Rev. D, 101, 064012
Tsang, K. W., Rollier, M., Ghosh, A., et al. 2018, Phys. Rev. D, 98, 024023
Tsukada, L., et al. 2023, Phys. Rev. D, 108, 043004

Urban, A. L., et al. 2021, gwdetchar/gwdetchar, Zenodo, doi:10.5281/zenodo.597016

Usman, S. A., Mills, J. C., & Fairhurst, S. 2019, Astrophys. J., 877, 82

Usman, S. A., et al. 2016, Class. Quant. Grav., 33, 215004

Vaccaro, M. P., Mapelli, M., Périgois, C., et al. 2024, Astron. Astrophys., 685, A51

Vajente, G. 2024, aLIGO LHO Logbook, 76459, ,

Vajente, G., Huang, Y., Isi, M., et al. 2020, Phys. Rev. D, 101, 042003

Valencia, J., Tenorio, R., Rosselló-Sastre, M., & Husa, S. 2024, Phys. Rev. D, 110, 124026

van Son, L. A. C., de Mink, S. E., Broekgaarden, F. S., et al. 2020, Astrophys. J., 897, 100

Varma, V., Field, S. E., Scheel, M. A., et al. 2019, Phys. Rev. Research., 1, 033015

Varma, V., Isi, M., & Biscoveanu, S. 2020, Phys. Rev. Lett., 124, 101104

Vazsonyi, L., & Davis, D. 2023, Class. Quant. Grav., 40, 035008

Veitch, J., Pozzo, W. D., Williams, M., et al. 2020, johnveitch/cpnest: v0.9.9, vv0.9.9, Zenodo, doi:10.5281/zenodo.4109271. https://doi.org/10.5281/zenodo.4109271

Venumadhav, T., Zackay, B., Roulet, J., Dai, L., & Zaldarriaga, M. 2020, Phys. Rev. D, 101, 083030

Viets, A., Wade, M., Urban, A., et al. 2018a, Classical and Quantum Gravity, 35, 095015

Viets, A., et al. 2018b, Class. Quant. Grav., 35, 095015

Virgo Collaboration. 2021, PythonVirgoTools, git.ligo.org/virgo/virgoapp/PythonVirgoTools, vv5.1.1, ,

Virtanen, P., et al. 2020, Nature Methods, 17, 261. https://doi.org/10.1038/s41592-019-0686-2

Wadekar, D., Roulet, J., Venumadhav, T., et al. 2023, arXiv e-prints, arXiv:2312.06631

Wang, Y.-Z., Li, Y.-J., Vink, J. S., et al. 2022, Astrophys. J. Lett., 941, L39

Waskom, M., et al. 2021, mwaskom/seaborn: v0.11.2 (August 2021), vv0.11.2, Zenodo, doi:10.5281/zenodo.592845. https://doi.org/10.5281/zenodo.592845

Wette, K. 2020, SoftwareX, 12, 100634

Williams, D. 2025, Class. Quant. Grav., 42, 105012

Williams, D., Veitch, J., Chiofalo, M. L., et al. 2023, J. Open Source Softw., 8, 4170

Woosley, S. E. 2017, Astrophys. J., 836, 244

Woosley, S. E., & Heger, A. 2021, Astrophys. J. Lett., 912, L31

Woosley, S. E., Heger, A., & Weaver, T. A. 2002, Rev. Mod. Phys., 74, 1015

Wright, M., & Hendry, M. 2022, The Astrophysical Journal, 935, 68. https://doi.org/10.3847/1538-4357/ac7ec2

Xu, Y., Rosselló-Sastre, M., Tiwari, S., et al. 2024, Phys. Rev. D, 109, 123034

Yang, Y., et al. 2019, Phys. Rev. Lett., 123, 181101

Zevin, M., Samsing, J., Rodriguez, C., Haster, C.-J., & Ramirez-Ruiz, E. 2019, Astrophys. J., 871, 91

Zhu, H., et al. 2025, Phys. Rev. D, 111, 064052

Zweizig, J. 2006, The Data Monitor Tool Project, labcit.ligo.caltech.edu/~jzweizig/DMT-Project.html, ,